Performance Analysis of Backstepping Control Technique for Magnetically Levitating Train System in the Presence of Time Varying Load

Yeabisra Wubishet Engda

A Thesis Submitted to

The Department of Electrical Power and Control Engineering

School of Electrical Engineering and Computing

Presented in Partial Fulfillment of the Requirement for the Master of Science Degree in Electrical Power and Control Engineering (Control Engineering)

Office of Graduate Studies

Adama Science and Technology University

November 2022

Adama, Ethiopia.

Performance Analysis of Backstepping Control Technique for Magnetically Levitating Train System in the Presence of Time Varying Load

Yeabisra Wubishet Engda

Advisor: Prof. Gang Gyoo Jin

Co-advisor: Mr. Endrias Alemayehu (MSc.)

A Thesis Submitted to

The Department of Electrical Power and Control Engineering

School of Electrical Engineering and Computing

Presented in Partial Fulfillment of the Requirement for the Master of Science Degree in Electrical Power and Control Engineering (Control Engineering)

Office of Graduate Studies

Adama Science and Technology University

November 2022

Adama, Ethiopia.

DECLARATION

I hereby declare that this Master Thesis entitled "Performance Analysis of Backstepping Control Technique for Magnetically Levitating Train System in the Presence of Time Varying Load" is my original work. That is, it has not been submitted for the award of any academic degree, diploma, or certificate in any other university. All sources of materials that are used for this thesis have been duly acknowledged through citation.

Yeabisra Wubishet Engda	_________________	_______________
Name of the student	Signature	Date

RECOMMENDATION

We, the advisors of this thesis, hereby certify that we have read the revised version of the thesis entitled "Performance Analysis of Backstepping Control Technique for Magnetically Levitating Train System in the Presence of Time Varying Load" prepared under our guidance by Yeabisra Wubishet Engda submitted in partial fulfillment of the requirements for the degree of Master of Science in Electrical Power and Control engineering (Control Engineering). Therefore, we recommend the submission of the revised version of the thesis to the department following the applicable procedures.

Prof. Gang Gyoo Jin	______________	____________
Advisor	Signature	Date
Mr. Endrias Alemayehu (MSc.)	______________	____________
Co-advisor	Signature	Date

APPROVAL SHEET

We, the advisors of the thesis entitled "Performance Analysis of Backstepping Control Technique for Magnetically Levitating Train System in the Presence of Time Varying Load" and developed by Yeabisra Wubishet Engda, hereby certify that the recommendation and suggestions made by the board of examiners are appropriately incorporated into the final version of the thesis.

Prof. Gang Gyoo Jin	________________	__________
Advisor	Signature	Date
Mr. Endrias Alemayehu (MSc.)	________________	__________
Co-advisor	Signature	Date

We, the undersigned, members of the Board of Examiners of the thesis by Yeabisra Wubishet Engda have read and evaluated the thesis entitled "Performance Analysis of Backstepping Control Technique for Magnetically Levitating Train System in the Presence of Time Varying Load" and examined the candidate during the open defense. This is, therefore, to certify that the thesis is accepted for partial fulfillment of the requirement of the degree of Master of Science in Electrical Power and Control engineering (Control Engineering).

________________	________________	__________
Chairperson	Signature	Date
Dr Endalew Ayenew		14-11-2022
Internal Examiner	Signature	Date
Dr Beteley Teka		04-11-2022
External Examiner	Signature	Date

Finally, approval and acceptance of the thesis are contingent upon submission of its final copy to the Office of Postgraduate Studies (OPGS) through the Department Graduate Council (DGC) and School Graduate Committee (SGC).

________________	________________	__________
Department Head	Signature	Date
________________	________________	__________
School Dean	Signature	Date
________________	________________	__________
Office of Postgraduate Studies, Dean	Signature	Date

ACKNOWLEDGEMENT

First and foremost, I would like to thank the Almighty God for protecting me and bless his loving heart for giving us St. Mary as our Mother, who gives me the strength to finish this thesis work.

I would also like to thank and appreciate my advisor, Professor Gang Gyoo Jin, for his heartfelt support and guidance. He has given me nice guidance, inspiration and suggestions throughout doing this thesis work.

Besides my advisor, I would like to thank my co-advisor, Mr. Endrias Alemayehu (MSc.), for his insightful comments throughout the writing of this thesis.

Furthermore, I really would like to thank Dr. Endalew Ayenew and Mr. Minyamer Gelaw (MSc.) for their valuable advises, willingness to share their knowledge, and numerous suggestions on all aspects of documentation preparation and writing.

Finally, I want to express my gratitude to my family members and friends for their support and all of their previous sacrifices. Also, I would like to give special thanks to my mother, Wegayehu Biyadiglegn**,** who is my hero and the ideal person for me.

TABLE OF CONTENTS

LIST OF TABLES

LIST OF FIGURES

LIST OF ACRONYMS

ACO	Ant Colony Optimization
BSC	Backstepping Controller
EDS	Electrodynamic suspension
EMS	Electromagnetic suspension
FOPID	Fractional Order Proportional Integral Derivative
GA	Genetic Algorithm
IAE	Integral Absolute Error
ISE	Integral Square Error
ITAE	Integral Time Absolute Error
ITSE	Integral Time Square Error
KVL	Kirchhoff Voltage Law
LHP	Left Half Plane
LIM	Linear Induction Motor
LQG	Linear Quadratic Gaussian
LQR	Linear Quadratic Regulator
LSM	Linear Synchronous Motor
MAGLEV	Magnetically Levitating
MATLAB	Matrix Laboratory
MLS	Magnetic Levitation System
NARMA	Nonlinear Autoregressive Moving Average
PID	Proportional Integral Derivative
PSO	Particle Swarm Optimization
RHP	Right Half Plane
SA	Simulated Annealing

ABSTRACT

Magnetically levitating trains (maglev) are becoming a popular research topic these days since they are a fast mode of public transportation that is environment friendly and requires little maintenance. Because of the maglev train system is a highly nonlinear and unstable system, its efficacy is dependent on a well-designed tracking controller to stabilize the train and follow the desired reference signal. This research work focuses on the performance analysis of a backstepping controller (BSC), which is used for the tracking control of the maglev train with time varying load change and external disturbance. The proposed BSC controller parameters are obtained by minimizing the IAEU using the particle swarm optimization (PSO) algorithm. The LQR controller incorporating with an integral action is also designed for comparison purpose. MATLAB software is used to verify both controllers' tracking performance using different types of reference signals, as well as their performance robustness under the effects of mass change and external disturbance force. The obtained simulation results demonstrate that the backstepping control method outperforms the LQR by reducing peak time by 68% and 30.8%, settling time by 28.8% and 27.7%, rise time by 26% and 26.7%, and IAEU by 26.1% and 25.3%, for upward and downward reference signals, respectively. Similarly, the BSC maintains improved tracking performance by lowering the IAEU value for both multiple step and sinusoidal signals. The performance robustness of both controllers is tested using load variations of up to 40% mass change, time varying load changes, and external disturbance force. In the 40% load change, the proposed control method gives 0.652sec, 0.129sec, 0.193sec, and 0.183 of peak time, rise time, settling time, and IAEU, which are small in comparison to the LQR, respectively. In the external disturbance force rejection test, the BSC settles at 0.193sec with 0.196 IAEU value despite the fact that the overshoot (0.11%) is slightly higher than the LQR controller. For the tracking performance robustness against both time-varying load changes and external disturbance force, the BSC provides 18.993%, 0.124sec, 12.129sec, and 0.317 of overshoot, rise time, settling time, and IAEU, which are all small compared to the LQR. Generally, the simulation results showed that the proposed BSC outperformed the LQR controller in terms of both tracking performance and robustness against load variation and external disturbance force.

Key Words: *BSC, LQR, Maglev train, Particle swarm optimization.*

CHAPTER ONE

INTRODUCTION

1.1 Background of the Study

Levitation is the process of suspending an object in the air in a stable position without any physical contact (Shu'aibu et al., 2017). It can be accomplished through the use of electric or magnetic forces. In a magnetic levitation system, an object (made of nickel, aluminum, iron, etc.) achieves equilibrium in air space under the influence of magnetic field only. The electromagnetic force generated by the electromagnetic coil balances the gravitational pull acting on the object. The force generated should be sufficient to counteract not only gravity but also other accelerations such as disturbance caused by external noise and environmental effects acting on the system (Varshney & Bhushan, 2020).

Magnetic levitation, also known as maglev, is an advanced technology in which an object is suspended or levitated in the midair with no support other than the magnetic field. A medium for levitation is created by the magnetic field produced by a permanent magnet, superconducting magnet, or electromagnet. The maglev system is based on fundamental electromagnetism concepts. The electromagnetic force produced by the electromagnet varies as the current through the coil changes. This is the basic idea behind the levitation of an object (Santhiya & Kishore, 2020). Due to the lack of contact with the levitated object, the magnetic levitation system (MLS) provides no wear and friction. Friction plays a significant role in real world applications as it reduces performance in most cases. MLS is one of the approaches that has made a significant contribution to the reduction of friction (Banerjee et al., 2019). Many applications are interested in maglev technology since it is a non-contact technology that results in zero friction losses and higher energy efficiency. As a result, the cost of maintenance is low. MLS is used in frictionless bearings, high speed ground transportation system, maglev heart pumps, maglev fans, space launching stations, wind turbines, high precision positioning stages, and many other applications (Dalwadi et al., 2021). The most common application of this system is the magnetic levitation train.

The magnetic levitation (maglev) train is a new large-scale transportation system that uses magnetic fields to levitate, provide propulsion and direction. Because of technological advancements, it is becoming more viable to the public transport work, providing faster, more comfortable, and safer transportation than the conventional train (Fernandes et al., 2013).

Figure 1.1 Maglev high speed train (Kumar Tandan et al., 2015)

There are two different approaches for designing maglev train system. The electrodynamic suspension (EDS) system is based on eddy current magnetic repulsive force, while the electromagnetic suspension (EMS) system is based on electromagnetic attractive force (Raj et al., 2019). The majority of these lines use EMS maglev trains, which can be used to implement economical levitation systems due to their relatively simple structure (Kim et al., 2017). EMS maglev train has unstable characteristics. This thesis work is focused on this type of maglev train system. Therefore, designing an excellent tracking controller is required to stabilize the train in the air and follow the desired reference in the presence of external disturbance and load variation.

Several control methods were designed for the suspension air gap tracking control of the maglev system. Some of the designed control techniques are PID controller (Khan et al., 2018)(X. Zhou et al., 2020)(Dey et al., 2020), fuzzy logic controller (Zhao et al., 2019), FOPID controller (Mughees & Mohsin, 2020) and, state feedback controller (Awelewa et al., 2019). The system dynamic characteristics analyses in linear controller designs are based on linearized models, which are implemented in a very small neighborhood near the equilibrium point. So, if the system deviates from equilibrium, the linearized model may become invalid. The high nonlinearity of the magnetic levitation train system makes nonlinear controllers more desirable. Backstepping controller (BSC) is commonly used to solve the nonlinear system control problems. This thesis work proposes it for the suspension air gap tracking control of the magnetically levitating train system in the presence of time varying load. A backstepping control method can ensure improved tracking and transient performance, as well as global asymptotic stability. Conventionally, the control parameters for this controller are selected randomly. An optimization algorithm is required to find the best control parameters. Here, particle swarm optimization technique is used to search the optimal values of the BSC parameters. LQR controller is also designed for comparison purposes. The overall system is implemented and simulated using MATLAB software.

1.2 Statement of the Problem

The need for fast, environmentally friendly, energy-efficient and low-maintenance public transportation is growing all over the world. The maglev train is an efficient and frictionless transportation system that meets these requirements. It exhibits unstable behaviour, which means that the train will attached to the track or may fall down. The system also encounters significant difficulties as a result of external disturbances and load change which varies with time because of passengers get on and off. The aforementioned challenges make clear that a good controller design is required for stable suspension occurrence and improved tracking performance, which affects the safety and comfort of passengers using this mode of transportation. Most previously designed control mechanisms are able to fulfil the requirement of a levitating maglev train. However, they have the following control problem. Different control strategies, such as PID and LQR methods, are implemented using a linearized model of the nonlinear system. During the linearization process, some system behaviours are ignored, and the maglev train does not exactly match the system's nonlinear behaviour. The drawback of using the linearization technique is that, due to the limited operating range, the controller is no longer guaranteed a global running variety. Moreover, nonlinear controllers are also designed in previous works but they lacks robustness in the presence of system parameter uncertainties (like a change in the mass of a maglev train which varies with time) and external disturbances. Thus, the desired tracking performance of the magnetically levitating train cannot be guaranteed when the system's overall operating conditions are altered, and not robust. In view of the above problems, this thesis work proposed the backstepping controller (BSC) to track the desired reference suspension air gap of the magnetically levitating train system in the presence of a change in load mass that varies with time and an external disturbance force.

1.3 Objectives of the Study

1.3.1 General Objective

The general objective of this thesis work is analysing the performance of backstepping control technique for magnetically levitating train system in the presence of time varying load.

1.3.2 Specific Objectives

The specific objectives of this thesis work are:

- To provide better tracking performance of the magnetically levitated train by reducing transient response characteristics of the system such as settling time, rise time, and peak time.
- To test stability of the proposed control system using Lyapunov stability theorem.
- To tune the proposed backstepping controller parameters optimally using PSO algorithm.
- To compare the performance results of the proposed controller with LQR controller from simulation works.
- To test performance robustness by considering time varying load change and external disturbance force.
- To make relevant conclusions and recommendations based on the simulation result.

1.4 Scope of the Study

The scope of this thesis work is to study the detailed mathematical model of the maglev train system. Backstepping controller is designed for desired reference tracking of the system in the presence of external disturbance force and load change which varies with time that are associated with the system. The particle swarm optimization algorithm is used to obtain the optimal parameters of the proposed control method. Simulations are used to validate the effectiveness of the proposed BSC controller by comparing it to that of the LQR controller. The entire system is simulated using MATLAB software.

1.5 Limitation of the Study

This thesis work is limited to the simulation of the magnetic levitation train system using MATLAB software. A real-time simulation is not developed, this is due to the difficulty of materials procurement and additional time and cost incurred for implementing the prototype.

1.6 Motivation of the Study

The Maglev train is regarded as one of the most advanced vehicles currently available in the railway industry. It is a noncontact technology with numerous advantages over conventional rail transportation, including fast speed, low energy consumption, less environmental effect, safety, and reliability. Control algorithm design is vital in the development of this advanced vehicle technology. Thus, this thesis work concentrated on the tracking control of the maglev train system.

1.7 Significance of the Study

As the world continues to expand and cities become more crowded, the demand for convenient and fast public transportation is increasing. The solution to this transportation demand lies in the world of maglev trains, which float on the track rather than being directly on it. This has a lot of potential for developing superfast trains with low maintenance requirements. Because of the unstable nature of the levitation dynamics of this technology, there is a strong need to control the suspension air gap between train and track. In this way, this thesis work has great significance on the tracking control of the suspension air gap of the maglev train system. It can also be used as a source for subsequent researches working on maglev train control systems.

1.8 Thesis Organization

This thesis is organized as follows.

Chapter one: introduces the background of the maglev train system. It also includes the detailed objective, statement of problem, scope, limitation, motivation, and significance of the thesis.

Chapter two: discusses about the theoretical background and related works on the control of maglev train system.

Chapter three: deals with the methodology followed and the nonlinear mathematical model of the system. Moreover, steady state analysis at an operating point, linearization of the nonlinear model and open loop analysis of the proposed system is presented in this chapter.

Chapter four: develop BSC and LQR control techniques for the nonlinear dynamic model and linear model of the maglev train system, respectively. It also describes the particle swarm optimization algorithm, which is used to adjust the proposed controller parameters.

Chapter five: the simulation results and detailed analysis of the results are presented in this chapter.

Chapter six: provides the conclusion and recommendation for future works.

CHAPTER TWO

LITERATURE REVIEW

2.1 Chapter Overview

This chapter discusses two main sections in detail. The first section provides an overview of the maglev train system, including its history, components, working principle, advantages, and disadvantages. The second section is a review of previous related works on the control of the proposed system using various controllers, along with their benefits and drawbacks.

2.2 Maglev Train Overview

2.2.1 Maglev Train

Magnetic levitation (maglev) train is a transport method in which vehicles move without touching the ground using magnetic fields rather than wheels, axels, and bearings. The maglev train uses magnets to lift and propel vehicles along a guideway. It moves smoothly and quietly from origin to destination without ever touching a rail (Jibril et al., 2020).

2.2.2 History of Maglev Train

In 1900, Emile Bachelet and Robert Goddard introduced the concept of a frictionless train, which led to the development of the magnetic levitation theory. Following the recognition of this concept, German inventor Alfred Zehden received patents for a linear motor propelled train in 1905 and 1907 (Ahmad et al., 2020). The basic concept of the electromagnetic suspension was invented in 1922 by German researcher Hermann Kemper, who received patents between 1934 and 1941 for an attractive model of the maglev system (Liu et al., 2022). Maglev transportation system did not make significant advances until the 1960s. Two Americans, Gordan Damby and James Powell, were granted a patent in 1969 for their magnetically levitated train design. Around the same time, Germany and Japan became very interested in a magnetic levitation technology. Both countries began investing money in maglev technology research in the 1970s. Germany built full scale model of maglev train in 1969 and named it the TransRapid. Japan also have developed a maglev prototype model called the ML-500 in 1970 (Tambe, 2018). Today, countries like China, Germany, and Japan use the maglev train system. The world's fastest maglev train, capable of 600 km/hr, is built in China.

2.2.3 Components of a Maglev Train

The five major components of a maglev train system are levitation, guidance, propulsion, input power transfer, and control system (N. Prasad et al., 2019).

2.2.3.1 Levitation

Levitation or Suspension refers to the ability of a train to stay suspended above the track. There are two types of levitation systems: electrodynamic and electromagnetic suspension, which are explained below.

Electrodynamic Suspension (EDS): The EDS system uses a superconducting magnet that generates repulsive magnetic forces. The superconducting magnets are placed on the track bottom or side walls to create mutually repulsive forces that repel the train's superconductive magnet throughout the entire track surface in order to suspend the train. The advantage of this method is that it is extremely stable at high speeds. The suspension gap of EDS is around 100mm (Reddy, R. Lakshman Kumar and Marutheeswar, 2013). So, it is not essential to keep the correct distance between the train and the track (guideway). The disadvantage is that sufficient speed must be built for the train to levitate at all. Furthermore, this system is much more complicated and expensive to implement (Kim et al., 2017). Japan is currently working on this system.

Electromagnetic Suspension (EMS): The EMS system works on the basis of attractive force of electromagnets mounted on the train and on the guideway in order to levitate the train. The suspension gap, or the clearance between the guideway and the train, is very small and should be kept within a limited range to avoid physical contact. In general, an air gap of 8-10mm is maintained for EMS, with a fluctuation range of 4mm from the equilibrium point (Talukdar & Talukdar, 2016)(Leng, Li, et al., 2019). It usually operates with an air gap of 10mm (Reddy, R. Lakshman Kumar and Marutheeswar, 2013). This system has advantages of being easier to implement than the EDS system and maintaining levitation at zero speed. Because of its simple structure, it can also be used to implement cost effective levitation systems (Kim et al., 2017). This system is used by Germanys' TransRapid.

2.2.3.2 Propulsion

Maglev requires a contactless propulsion mechanism in order to move the train forward. Linear motors are the best choice for meeting this requirement hence they produce thrust without any mechanical conversion. Unlike rotary motors, linear motor thrust is independent of any rail to wheel adhesion factor. As a result, these motors are needed to generate both the propulsion and braking forces for maglev train system (N. Prasad et al., 2019). The Linear Induction Motor (LIM) and the Linear Synchronous Motor (LSM) are the two types of linear motors that can be used for maglev propulsion (Thornton, 2006).

2.2.3.3 Guidance

The sideward forces required to make the vehicle follow the guideway are referred to as guidance. The maglev train requires a precise guidance mechanism in order to control the lateral displacement of the maglev train (N. Prasad et al., 2019). A magnetic repulsive force or magnetic attractive force is typically used in guidance mechanisms.

The three components of the maglev train explained above, namely levitation, propulsion, and guidance, are the primary functions of the maglev train system that allow it to travel at high speeds.

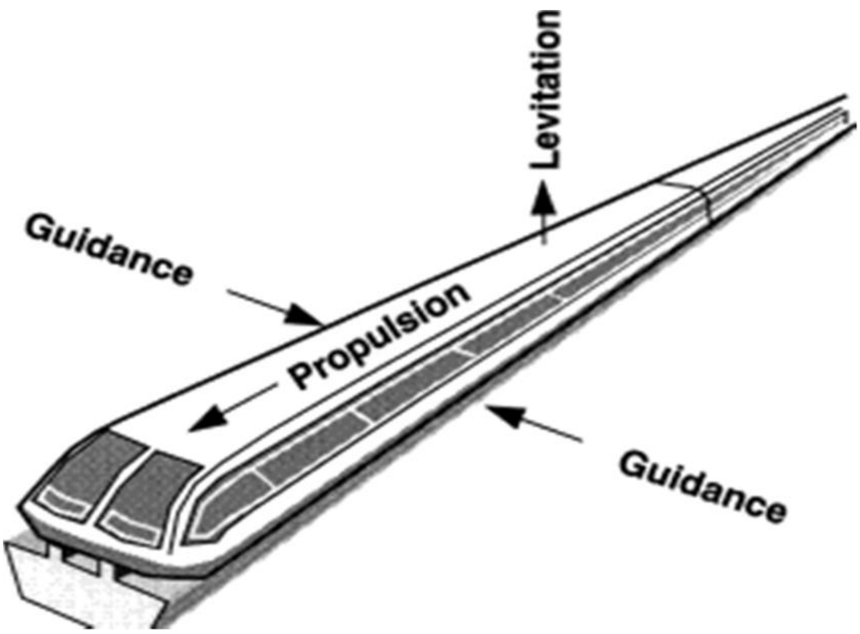

Figure 2.1 Primary functions of maglev train (Nimrad et al., 2015)(Teja et al., 2021)

2.2.3.4 Input Power Transfer

The transfer of electricity from the ground side is essential in a maglev train for powering the levitation and propulsion coils. This system provides the necessary power to the vehicle. An instrument like a pantograph transfers the necessary power at speeds up to 300km/hr (N. Prasad et al., 2019). The contactless power delivery system is made up of linear transformers and linear generators at speeds greater than 300km/hr.

2.2.3.5 Control System

Continuous control and monitoring of air gaps and coil excitations is required for maglev train systems in order to operate reliably and safely. In general, the levitation and guidance forces are regulated to keep the vehicle's position constant with respect to the guideway (N. Prasad et al., 2019). This system maintains a constant air gap, which helps to keep the ride comfortable.

2.2.4 Working Principle of Maglev Train

The operation of maglev train is based on the repelling of similar polar magnets and the attraction of opposite polar magnets. Magnetic force is used to provide magnetic levitation, lateral guiding, and propulsion functions. The magnets are installed along the entire length of the guideway. The magnetic force generated by the magnets creates a distance between the guideway and bottom of the train (YAVUZ & ÖZTÜRK, 2021). Side magnets prevent the train from moving side to side. The magnetic levitation train is stopped and slowed down by generating an opposing magnetic force.

2.2.5 Advantages and Disadvantages of Maglev Train

Maglev trains have some benefits over the conventional high speed rail trains. They allow faster speeds, have no wear and tear, require less maintenance, consume less energy, and produce less vibration and noise (YAVUZ & ÖZTÜRK, 2021). Maglev trains, on the other hand, are more costly to construct and are incompatible with the existing infrastructure (Nimrad et al., 2015).

2.3 Review of Related Works

Since suspension air gap control and following the desired reference signal are essential for the effective operation of the maglev system, several scholars and researchers have proposed a variety of control strategies and optimization techniques. The closely related works are reviewed in this section.

Adaptive backstepping controller is designed in this paper (W. Zhou & Liu, 2013). It does not use the overall system modelling. It tries to improve performance of the system by estimating of unknown parameters such as inductance online. The paper does not test system performance robustness in the presence of external disturbance and load variation.

The LQR controller is designed to suspend and propelled the maglev train on track (Sadaqat et al., 2015). Different realization techniques (minimal realization, observer canonical realization, balanced realization, and modal realization) are used to improve the efficiency of the controller and to make the system highly stable and non-fragile. The observer canonical realization provides the controller with the least error, representing the most optimal and non-fragile controller technique. Even though the designed LQR controller has shown better response to an input disturbance, the effect of load variations associated with the system are not considered in this paper.

The authors (Nayak, 2015) designed adaptive backstepping, 2 DOF PID, and backstepping on Euler approximate of maglev system. These controllers are designed based on nonlinear continuous model, nonlinear discrete model, and linear continuous model, respectively. The paper test mass uncertainty using three different masses that are original, half, and double. The simulation results shows that the adaptive backstepping has undershoot for small mass and overshoot for higher mass and also it has a very high control input. The backstepping on Euler approximate have less control input. The 2DOF PID has less tracking performance than the other two controllers. Even though the paper test tracking performance of different controllers using three different masses it does not consider effects of time varying load or mass and external disturbance.

The authors (Singh & Kumar, 2018) developed two control strategies (PID controller and backstepping approach based controller) for the stabilization and control of a magnetic levitation system. The PID parameters are tuned with a model based tuning algorithm, while

BSC parameters are chosen at random. The BSC approach achieved the desired control objective by providing better response and requiring less control effort than the PID controller. Controller gains of the BSC are determined by a time-consuming method of trial and error. The authors did not test the robustness of the proposed control system.

The focus of (Awelewa et al., 2019) is to stabilize and improve the dynamic performance of a nonlinear magnetic levitation system using compact state feedback controllers. The authors compare the system performance of three nonlinear control laws built using the concept of state feedback linearization; direct state feedback controller, state homogeneity based state feedback controller, and modified homogeneity based controller. Both normal and abnormal operating conditions are used to evaluate performance. The abnormal operating condition occurs when the system is subjected to a unit step disturbance signal for 2 seconds in the ball position from its steady state value. The simulation results in this paper demonstrate that the modified homogeneity based controller reduces the number of controller parameters while maintaining a significantly better dynamic performance than the other two controllers. The effect of parameter uncertainty is not covered in the paper; it only focused on the impact of external disturbance signal on the system.

The authors of (X. Zhou et al., 2020) proposed a PID control strategy for suspension system of a medium speed magnetic levitation train based on an improved particle swarm optimization algorithm. The PSO technique searches the solution space for the optimal PID parameters based on decreasing inertia weight. The proposed control strategy improves the system's efficiency and accuracy. The PID controller is designed based on Taylor's series expansion technique around an operating point, which is not suitable when the system deviates from the operating point.

Supertwisting and Integral Backstepping Sliding Mode controllers are proposed for maglev system (Adil et al., 2020). The authors evaluate the system performance robustness by adding external disturbance. The supertwisting SMC performs better than that of the integral backstepping SMC in terms of dynamic performance and robustness against disturbances. The drawback of this paper is that it does not include effect of load variation on the system.

The authors (Jibril et al., 2020) investigated NARMA-L2, Model reference and Predictive controllers for the nonlinear magnetic levitation train. The step input signal is used to compare the response of the proposed controllers for the magnetic levitation train. The

NARMA-L2 neuro controller eliminates nonlinearities to transform the nonlinear system dynamics in to linear dynamics. The simulation results show that the Magnetic levitation train system with the NARMA-L2 neuro controller has an effective performance with the lowest percentage overshoot compared to the other controllers. The drawback of this paper is that it does not take into account the effect of disturbance and parameter uncertainty.

The authors (Mughees & Mohsin, 2020) present stability control of levitating objects in a maglev plant using fractional order PID controller. The proposed system's stability is determined by Routh Hurwitz's stability criterion. The conventional PID controller are used for comparative analysis. The Ant colony Optimization technique and Ziegler Nicholas method are used to tune the parameters of the both controllers. The aim of the paper is to reduce the settling time of the levitating object in order to reduce oscillations. The FOPID with ACO resulted in the shortest settling time. The maglev system with external disturbance and parameter uncertainty is not analyzed in this paper, and other transient performance characteristics such as rise time and peak time are not improved.

The PID and PSO tuned PID controllers are designed by (Varshney & Bhushan, 2020) for desired path trajectory tracking and position control of the magnetic levitation system. The PSO tuned PID controller performs better than the PID controller in time domain analysis. The paper does not include parameter uncertainties and external disturbances associated to the system in order to define the robustness of the proposed system.

The authors (Pandey & Yadav, 2020) designed robust PID, LQG and optimized robust PID controllers to stabilize the nonlinear maglev mechanism and achieve efficiency to the system's desired design requirements. The Jaya optimization algorithm optimizes the robust PID controller by reducing the system's performance indices ITAE and ITSE. The robust PID controller optimized by Jaya outperformed the other two approaches examined in this paper. The drawback of this paper is that the system performance is evaluated by ignoring effects of external disturbance signal and parameter variation on the system. Furthermore, the linearized model is used to design the controllers, which estimates the system's behavior over a restricted range of operating points.

The authors (Sun et al., 2021) designed backstepping SMC for magnetic levitation system. Gaussian process method is used to obtain a dynamic model with accurate parameters. A bounded known disturbance and load change are considered in this paper. The obtained simulation results verify that the backstepping SMC have better tracking performance. The drawback of this paper is that a time varying load variation is not included in the tracking performance test.

According to the above literature review, various control methods are used in designing a controller for the maglev system. The majority of the literature is concerned with linear controllers, which are based on linear control theory. As a result, it cannot be designed directly for a nonlinear system unless the system is linearized around a certain operating point. Moreover, some of the literature used nonlinear control techniques with considering only the effects of external disturbance and constant load variation on the system. The effects of parameter variation including time varying load change, as well as external disturbance effects, must be considered in order to test and validate the performance of the controllers. Therefore, the backstepping controller is proposed in this thesis work to track the desired reference suspension air gap of the maglev train system in the presence of external disturbance and time varying load change.

CHAPTER THREE

METHODOLOGY AND SYSTEM MODELING

3.1 Chapter Overview

This chapter explains the materials and methods used to complete this thesis work. It also deals with obtaining the mathematical modeling of the maglev train system. In addition, steady state analysis at an operating point, linearization of the nonlinear maglev model, and open loop analysis of the system are all covered in this chapter.

3.2 Materials

In this thesis work, software such as Microsoft office 2016, draw.io, Math Type 6.0 equation, Mendeley Desktop 1.19.8, and MATLAB/2020a are used. Microsoft office 2016 is used to write and edit the thesis documentation. draw.io is drawing software used to draw block diagrams and flowcharts. Math Type 6.0 version is used for writing mathematical formulas and equations in Microsoft offices word and PowerPoint presentation tools. MATLAB is a computing software package that includes technical toolboxes and Simulink. Mendeley Desktop 1.19.8 is used for citation of references in the thesis document body as well as to list the references in the standard style.

3.3 Methods

The following methodologies are used to successfully accomplish this thesis work. The methodology starts with a thorough review of the literature to gain a better understanding of the system; this includes studying the maglev train system, comprehending the design method of the backstepping controller, and reviewing any previous related works in this area. Second, data is collected by reviewing recorded data from varies studies related to this thesis work. Thirdly, the dynamic modeling that describes the system behavior is derived. Fourth, a backstepping control strategy that treats a non-linear system in over large operation regions is designed to improve tracking performance by minimizing rise time, peak time, and settling time. Then, the parameters of the proposed BSC are optimally tuned using the PSO algorithm. Fifthly, the LQR controller is designed to test the effectiveness of the proposed BSC. Sixth, the overall system performance is implemented and simulated using MATLAB software. Then simulation results of the system is analyzed. Finally, the entire thesis work is concluded and suggestions are made for further research in the area. Figure 3.1 summarizes the methodology used for this thesis work.

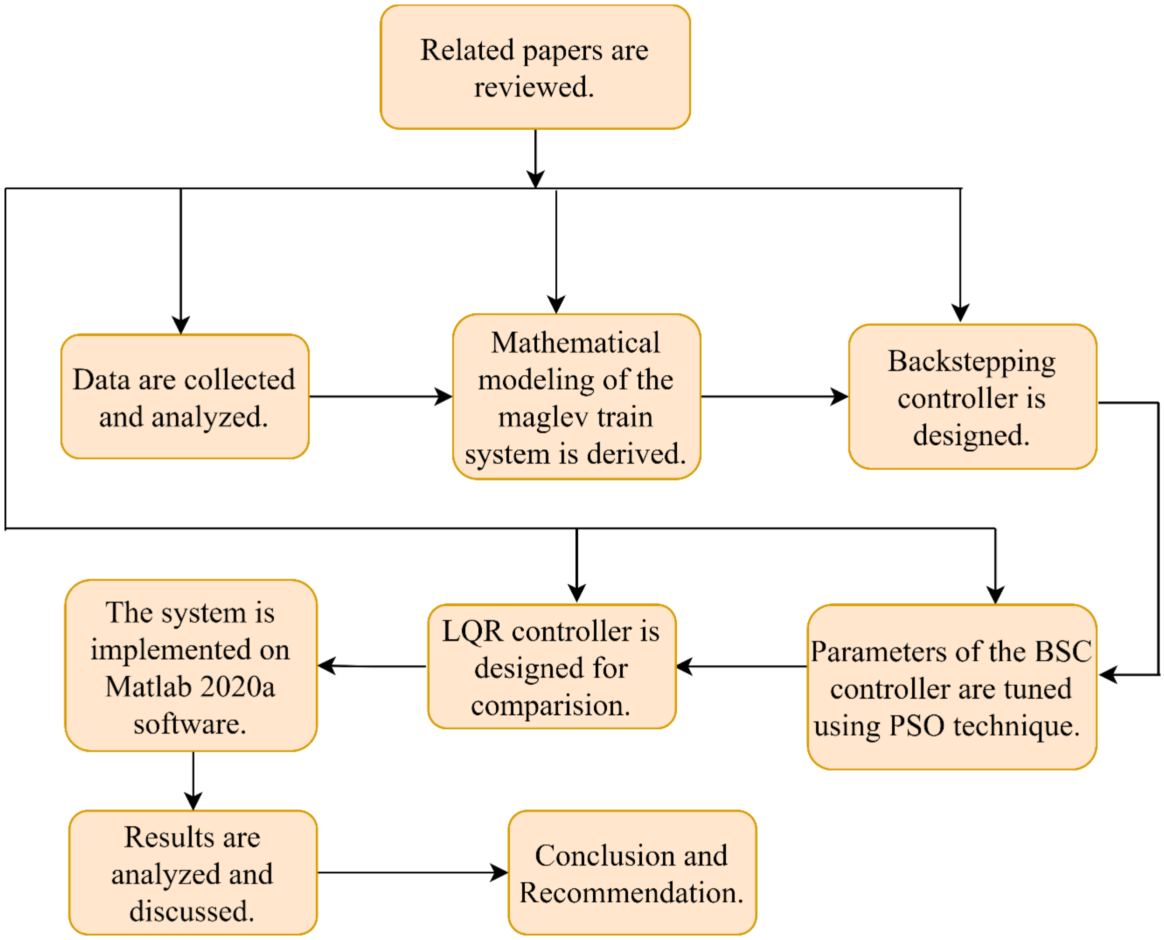

Figure 3.1 Workflow of the research.

3.4 Block Diagram of the Proposed Control System

The block diagram of the proposed backstepping controller for the maglev train system is depicted in Figure 3.2 below. The difference between the reference levitation gap and actual levitation gap is fed in to the backstepping controller, which produces a control input (u) that is used to keep the train in a given levitation or to make it track the desired reference signal. The PSO finds the optimal parameters of the BSC by minimizing the performance index which is the combination of the control and error signals. The external disturbance force and parameter uncertainty (load variation) may cause system instability, making it difficult for the train to maintain the desired levitation gap between the train and the track. The effects of external disturbance force and parameter uncertainty (load variation) associated with the system are considered in the simulation test to validate the robustness of the proposed control method.

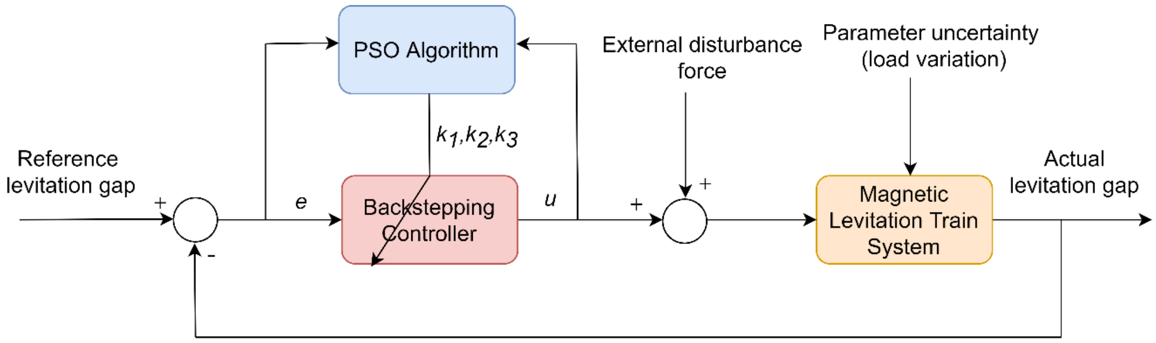

Figure 3.2 Block diagram of the proposed control system

3.5 Mathematical Modeling of the Magnetic Levitation Train System

A mathematical model is the mathematical description of a physical system that is used to explain the behavior of the system using a set of differential equations. It uses fundamental physical laws that govern a specific system, such as Kirchhoff's laws for electrical systems and Newton's law for mechanical systems. The most important task in design and analysis of a control system is to derive a mathematical model (Diran Basmadjian, 2003).

The suspension of a magnetically levitating train system is comprised of three subsystems: an air spring system, a rail system and electromagnetic elements. Since the air spring system doesn't significantly affect the general dynamics in a closed loop formulation, it can be ignored for the purpose of model simplification (Fernandes et al., 2013). The dynamic behavior of the magnetic levitating train system are developed by studying the electrical (electromagnet) and mechanical subsystems of the maglev train (Sharma et al., 2018). Multiple electromagnets suspension system can be deformed in to a single electromagnet suspension system (Dai et al., 2015)(Xu et al., 2018). This thesis work focused on the analysis of a single point suspension of an EMS type maglev train system using a single electromagnet system, which is very helpful in understanding the entire behavior of the levitation system. Figure 3.3 illustrates a simplified model of the single electromagnet suspension system that is used to develop the system mathematical model.

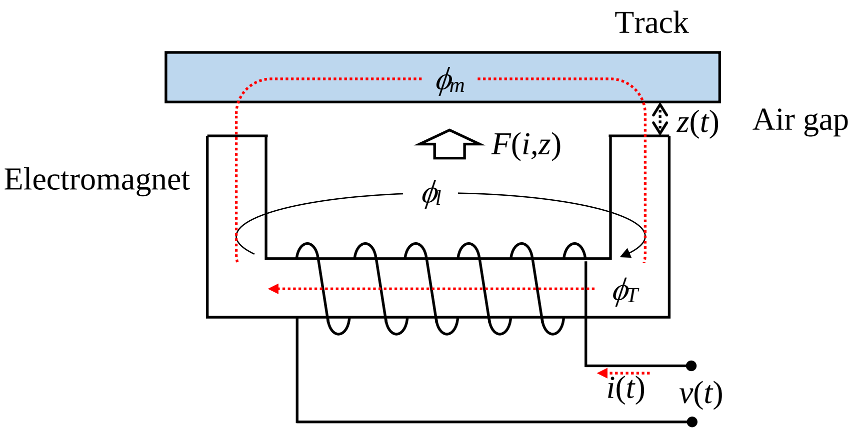

Figure 3.3 Simplified model of the single electromagnet suspension (Ma et al., 2020)

The assumptions considered in the mathematical modeling of the Maglev train system are given as follows (Ma et al., 2020)(Leng, Yu, et al., 2019): Ignore the leakage magnetic flux of the winding (ϕ_l=0) as well as the magnetic resistance in the magnet core and the rail, implies that the magnetic potential is evenly reduced on the air gap. The suspension system has only one degree of freedom, which is vertical; the magnetic saturation characteristics of the track and iron core materials are negligible; the track is regarded as a rigid track; and the mass distribution of the entire system is uniform.

3.5.1 Mathematical Model of the Electrical Subsystem

The electrical subsystem, assumed to be an electromagnetic coil, is adequately represented by a series resistor-inductor combination, as shown in Figure 3.4.

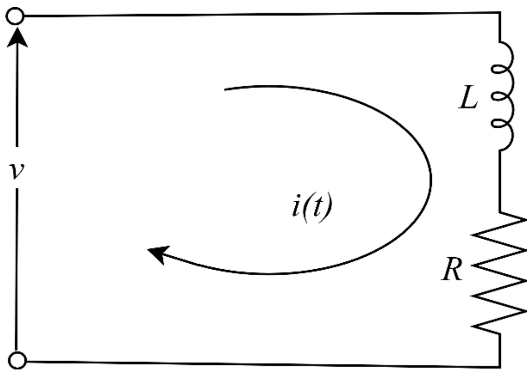

Figure 3.4 Electrical subsystem for the electromagnetic coil (Singh & Kumar, 2018)

The coil inductance of the electromagnet winding is obtained by Biot-Savart law (Zhao et al., 2019):

$$L = \frac{\psi}{i} \tag{3.1}$$

where L is the coil inductance of the electromagnet winding, ψ is the air gap magnetic flux linkage, and i is the coil current of the suspension electromagnet.

The control voltage equation of the suspension electromagnet is obtained by applying Kirchhoff's voltage law (KVL) to the electromagnet winding circuit (Alkurawy, 2019).

$$v = Ri + L\frac{di}{dt} \tag{3.2}$$

Equating i by rearranging Equation 3.1 and substituting it into Equation (3.2) results in

$$u(t) = Ri(t) + \frac{d\psi}{dt} \tag{3.3}$$

where the applied voltage input to the circuit is defined as $u = v$ and R is an electrical resistance of the circuit.

The expression for the magnetic flux linkage (ψ) can be obtained as (Suebsomran, 2014):

$$\psi = \phi N \tag{3.4}$$

First, the mathematical expression for the magnetic flux must be derived in order to get ψ.

$$\phi_T = \phi_m + \phi_l \tag{3.5a}$$

Hence $(\phi_l \cong 0)$,

$$\phi_T \cong \phi_m \tag{3.5b}$$

where ϕ_l is the leakage magnetic flux of the winding, ϕ_m is the air gap flux, and ϕ_T is the main pole flux.

The magnetic flux can be calculated using the magneto motive force. The magneto motive force can be expressed using Hopkinson's law, which is analogous to Ohm's law in magnetic circuits.

$$F_m = \phi R_m \tag{3.6}$$

The magneto motive force can also be expressed as follows:

$$F_m = Ni(t) \tag{3.7}$$

where F_m is the magneto motive across a magnetic element, ϕ is the magnetic flux produced through the electromagnet coil, R_m is the magnetic reluctance of the magnetic circuit, and N is the number of turns of the coil.

The magnetic flux can be expressed as follows using Equations (3.5b) and (3.6):

$$\phi = \phi_T \cong \phi_m = \frac{F_m}{R_m} \tag{3.8}$$

Then, the magnetic reluctance of the magnetic circuit can be expressed as follows (Zhao et al., 2019).

$$R_m = \frac{l}{\mu A_0} + \frac{2z}{\mu_0 A} \tag{3.9a}$$

$$R_m(z) \approx \frac{2z(t)}{\mu_0 A} \tag{3.9b}$$

where l is the length of the magnetic path or core permeability, μ_0 is the permeability of free space (vacuum), μ is the permeability of the magnet core, A is the cross-section area of the magnetic path (the air gap permeability area at the two ends of the electromagnet), A_0 is the effective magnetic pole permeability area of the electromagnet, and $z(t)$ is the levitation gap between the electromagnet and the rail (track).

The total length of magnet core, which is equal to $2z(t)$, is used to express the magnetic reluctance in Equation (3.9b) (Suebsomran, 2014). Substituting Equations (3.7) and (3.9b) in to Equation (3.8) yields:

$$\phi_m = \frac{Ni(t)}{2z(t) / \mu_0 A} = \frac{Ni(t)\mu_0 A}{2z(t)} \tag{3.10}$$

Substituting Equation (3.4) into Equation (3.10) gives:

$$\psi = \frac{\mu_0 N^2 i(t) A}{2z(t)} \tag{3.11}$$

Since the flux linkage is a function of the current and position of the levitated train, partial differentiation relationships can be express it, as shown in Equation (3.12).

$$\frac{d}{dt}\psi = \frac{\partial \psi}{\partial i}\frac{di}{dt} + \frac{\partial \psi}{\partial z}\frac{dz}{dt} \tag{3.12}$$

Substituting Equation (3.12) for Equation (3.3) results in:

$$u(t) = Ri(t) + \frac{\partial \psi}{\partial i}\frac{di}{dt} + \frac{\partial \psi}{\partial z}\frac{dz}{dt} \tag{3.13a}$$

The following equation is obtained when Equation (3.11) is substituted into Equation (3.13a):

$$u(t) = Ri(t) + \frac{\mu_0 N^2 A}{2z(t)}\frac{di(t)}{dt} + \mu_0 N^2 A i(t)\frac{d}{dt}\left(\frac{1}{2z(t)}\right) \tag{3.13b}$$

Therefore, the voltage equation in the electromagnet winding circuit is:

$$u(t) = Ri(t) + \frac{\mu_0 N^2 A}{2z(t)}\frac{di(t)}{dt} - \frac{\mu_0 N^2 A i(t)}{2(z(t))^2}\frac{dz(t)}{dt} \tag{3.14}$$

3.5.2 Mathematical Model of the Mechanical Subsystem

The mechanical subsystem model is used to obtain the train's vertical equation of motion. Newton's second law of motion is used to derive the governing equation. All of the balancing forces acting on the levitated train are taken into account in the equation of motions.

$$f_a = -f_{mag} + f_g \tag{3.15}$$

where f_a is the acceleration force or net force acting on the train , f_{mag} is the suspension force produced by the electromagnet (electromagnetic force generated by the coil), and f_g is the force due to gravity (gravitational force acting on the train).

Figure 3.5 depicts the forces acting on a single electromagnet suspension system. In the figure, $F(i,z)$ represents the electromagnetic force, denoted as f_{mag} in this thesis work.

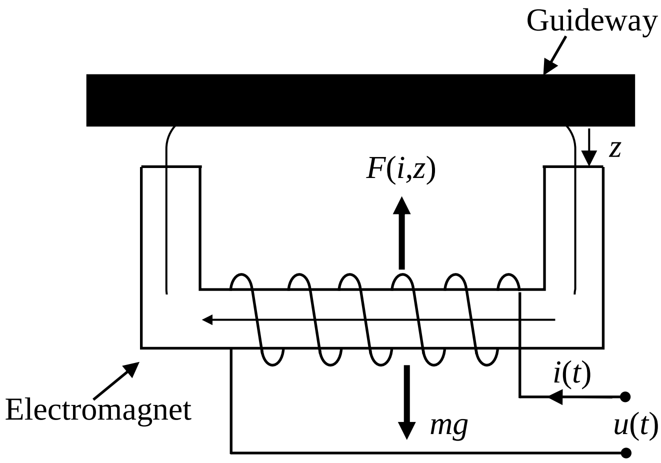

Figure 3.5 Forces acting on the single electromagnet suspension system (Wang et al., 2020)

The magnetic field energy (W_e) generated by the current flowing through the inductor can be expressed as follows (Zhao et al., 2019):

$$W_e = L\int_0^i i\,di = \frac{1}{2}Li^2 \tag{3.16}$$

Substituting Equation (3.1) into Equation (3.16) results in:

$$W_e = \frac{1}{2}\frac{\psi}{i}i^2 = \frac{1}{2}\psi i \tag{3.17}$$

Then, the magnetic field energy can be obtained by substituting Equation (3.11) into Equation (3.17).

$$W_e = \frac{\mu_0 N^2 i^2 A}{4z(t)} \tag{3.18}$$

According to electromagnetic phenomena, power is transferred from one domain to another; no power is dissipated, which means electrical power in equals mechanical power out. The electrical power is the rate at which an electrical energy is transferred by an electric circuit, whereas the mechanical power is a combination of forces and movement that is simply the product of a force on an object and the velocity of the object (Jibril et al., 2020).

$$P_e = \frac{d}{dt} W_e \tag{3.19}$$

$$P_m = -f_{mag} v = -f_{mag} \frac{dz(t)}{dt} \tag{3.20}$$

The negative sign of Equation of 3.20 is due to the fact that the electromagnetic force is directed upward, as illustrated in Figure 3.3.

$$\begin{aligned} P_e &= P_m \\ \frac{d}{dt} W_e &= -f_{mag} \frac{d}{dt} z(t) \end{aligned} \tag{3.21a}$$

where P_e is the power in the electrical system and P_m is the power in the mechanical system.

$$dt\left(\frac{d}{dt} W_e\right) = dt\left(-f_{mag} \frac{d}{dt} z(t)\right) \tag{3.21b}$$

$$dW_e = -f_{mag} dz(t) \tag{3.21c}$$

$$f_{mag} = -\frac{dW_e}{dz(t)} \tag{3.22}$$

Substituting Equation (3.18) into Equation (3.22) yields:

$$f_{mag} = -\frac{d}{dz(t)}\left(\frac{\mu_0 N^2 i^2 A}{4z(t)}\right) \tag{3.23a}$$

$$f_{mag} = \frac{\mu_0 N^2 i^2 A}{4z^2} \tag{3.23b}$$

Substituting Equation (3.23b) into Equation (3.15) results in:

$$m\frac{d^2 z}{dt^2} = -\frac{\mu_0 N^2 i^2 A}{4z^2} + mg \tag{3.24}$$

$$m\ddot{z}(t) = -\frac{\mu_0 N^2 i^2 A}{4z^2} + mg \tag{3.25}$$

In general, Equations (3.14), (3.23b), and (3.25) determine the dynamics of the single electromagnet suspension system. The system’s state variables are position (the levitation gap), velocity, and current through the electromagnet. In addition, the supply voltage across the electromagnet is regarded as the control input variable.

$$x_1(t) = z(t) \tag{3.26a}$$

$$x_2(t) = \dot{z}(t) \tag{3.26b}$$

$$x_3(t) = i(t) \tag{3.26c}$$

The state space representation of the system is obtained by denoting Equations (3.14), (3.23b), and (3.25) by the above state variables.

Substituting the above three Equations (3.26a, 3.26b, and 3.26c) in to Equation (3.14), results in:

$$\begin{aligned} u(t) &= Rx_3(t) + \frac{\mu_0 N^2 A}{2x_1(t)} \frac{dx_3(t)}{dt} - \frac{\mu_0 N^2 A x_3(t)}{2x_1(t)^2} x_2(t) \\ &= Rx_3(t) + \frac{\mu_0 N^2 A}{2x_1(t)} \dot{x}_3(t) - \frac{\mu_0 N^2 A x_3(t)}{2x_1(t)^2} x_2(t) \end{aligned} \tag{3.27}$$

The derivative of the third state variable, represented by Equation (3.28) below, is derived by rearranging Equation (3.27).

$$\dot{x}_3(t) = \frac{-2Rx_3(t)x_1(t)}{\mu_0 N^2 A} + \frac{2x_1(t)}{\mu_0 N^2 A} u(t) + \frac{x_3(t)x_2(t)}{x_1(t)} \tag{3.28}$$

Substituting Equations (3.26a), (3.26b), and (3.26c) into Equation (3.25) yields:

$$m\dot{x}_2(t) = -\frac{\mu_0 N^2 A i(t)^2}{4z(t)^2} + mg \tag{3.29}$$

Multiplying both sides of Equation (3.29) by $\frac{1}{m}$ gives the derivative of the second state variable.

$$\dot{x}_2(t) = -\frac{\mu_0 N^2 A}{4m} \frac{x_3^2(t)}{x_1^2(t)} + g \tag{3.30}$$

Substituting Equations (3.26a), (3.26b), and (3.26c) into Equation (3.23b) results:

$$f_{mag} = -\frac{\mu_0 N^2 A}{4} \frac{x_3^2(t)}{x_1^2(t)} \tag{3.31}$$

Finally, the non-linear state space model of the single electromagnet Maglev train system can be expressed as follows:

$$
\begin{aligned}
\dot{x}_1(t) &= x_2(t) \\
\dot{x}_2(t) &= -a\frac{x_3^2(t)}{x_1^2(t)} + g \\
\dot{x}_3(t) &= \frac{x_3(t)x_2(t)}{x_1(t)} - \frac{Rx_3(t)x_1(t)}{k} + \frac{x_1(t)}{k}u(t) \\
y(t) &= x_1(t)
\end{aligned}
\tag{3.32}
$$

where, $k = \dfrac{\mu_0 N^2 A}{2}$ and $a = \dfrac{k}{2m}$.

Equation (3.32) can be rewritten in the general form:

$$
\begin{aligned}
\dot{\boldsymbol{x}} &= \boldsymbol{f}(\boldsymbol{x},\boldsymbol{u}) \\
y &= g(\boldsymbol{x},\boldsymbol{u})
\end{aligned}
\tag{3.33a}
$$

where

$$
\boldsymbol{f}(\boldsymbol{x},\boldsymbol{u}) = \begin{bmatrix} x_2 \\ -a\dfrac{x_3^2}{x_1^2} + g \\ \dfrac{x_3x_2}{x_1} - \dfrac{Rx_3x_1}{k} + \dfrac{x_1}{k}u \end{bmatrix}, \; g(\boldsymbol{x},\boldsymbol{u}) = x_1
\tag{3.33b}
$$

3.6 Steady State Analysis at an Operating Point

A system is said to be in a steady state when it does not vary over time (Amadi & Nwaoburu, 2020). The steady states for a differential equation of the form $\dot{\boldsymbol{x}} = \boldsymbol{f}(\boldsymbol{x},\boldsymbol{u})$ are the values of x and u that satisfy $\boldsymbol{f}(\boldsymbol{x},\boldsymbol{u}) = 0$. The steady state analysis of the maglev train system at an operating point is discussed below.

If the output y of the maglev train system reaches the set point (or reference input) y_r and the system is operated at that operating point for a long time, Equation (3.32) is written as:

$$
\begin{aligned}
0 = \dot{x}_{10} &= x_{20} \\
0 = \dot{x}_{20} &= -a\frac{x_{30}^2}{x_{10}^2} + g \\
0 = \dot{x}_{30} &= \frac{x_{30}x_{20}}{x_{10}} - \frac{Rx_{30}x_{10}}{k} + \frac{x_{10}}{k}u_0 \\
y &= x_{10}
\end{aligned}
\tag{3.34}
$$

The first equation of Equation (3.34) yields $x_{20} = 0$, rearranging second and third equations results in x_{30} and u_0,which are:

$$x_{30} = x_{10}\sqrt{\frac{g}{a}} \qquad u_0 = Rx_{30} \tag{3.35}$$

Finally, the state variables and the control input at that operating point become

$$\begin{aligned} x_{10} &= y_r \\ x_{20} &= 0 \\ x_{30} &= x_{10}\sqrt{\frac{g}{a}} \\ u_0 &= Rx_{30} \end{aligned} \tag{3.36}$$

3.7 Linearization of the Nonlinear Model

The nonlinear maglev train system model is linearized in order to design the LQR controller that is used for comparison purpose. Furthermore, the linearized model is used to perform the open loop stability analysis using root locus technique, which is not appropriate for the nonlinear model. In this thesis work, the Taylor series expansion method is used to obtain the approximated linear model of the system. This linearization technique linearized the nonlinear equations occur for small deviations of state variables around the operating point.

3.7.1 Linearization of a state space form

Consider the general form of a nonlinear differential equation which is represented by

$$\dot{\boldsymbol{x}} = f(\boldsymbol{x}, \boldsymbol{u}) \tag{3.37a}$$

$$\boldsymbol{y} = \boldsymbol{g}(\boldsymbol{x}, \boldsymbol{u}) \tag{3.37b}$$

where $\boldsymbol{x}\in R^n$ is the state vector, $\boldsymbol{u}\in R^m$ is the control vector, $\boldsymbol{y}\in R^p$ is the output vector, $\boldsymbol{f} \in R^n$ and $\boldsymbol{g}\in R^p$ are smooth vector functions.

Equation (3.37a) satisfies the following relationship at an operating point $(\boldsymbol{x}_0,\boldsymbol{u}_0)$:

$$\dot{\boldsymbol{x}}_0 = f(\boldsymbol{x}_0, \boldsymbol{u}_0) \tag{3.38}$$

Defining Δx and Δu as small deviations from x and u, respectively gives the following relationship (J et al., 2014).

$$\begin{aligned} \boldsymbol{x} &= \boldsymbol{x}_0 + \Delta\boldsymbol{x} \\ \boldsymbol{u} &= \boldsymbol{u}_0 + \Delta\boldsymbol{u} \end{aligned} \tag{3.39}$$

The first-order Taylor series approximation around the operating point $(\boldsymbol{x}_0,\boldsymbol{u}_0)$ can be written as

$$\dot{\boldsymbol{x}}_0 + \dot{\Delta}\boldsymbol{x} = f(\boldsymbol{x}_0 + \Delta\boldsymbol{x}, \boldsymbol{u}_0 + \Delta\boldsymbol{u})$$
$$= f(\boldsymbol{x}_0, \boldsymbol{u}_0) + \frac{\partial \boldsymbol{f}}{\partial x}(\boldsymbol{x}, \boldsymbol{u})\bigg|_{\substack{x=x_0\\u=u_0}} \Delta\boldsymbol{x} + \frac{\partial \boldsymbol{f}}{\partial u}(\boldsymbol{x}, \boldsymbol{u})\bigg|_{\substack{x=x_0\\u=u_0}} \Delta\boldsymbol{u} \tag{3.40}$$

Substituting Equation (3.38) into Equation (3.40) with negligible higher order terms results in

$$\begin{aligned}\Delta\dot{\boldsymbol{x}} &= \frac{\partial \boldsymbol{f}}{\partial x}(\boldsymbol{x}, \boldsymbol{u})\bigg|_{\substack{x=x_0\\u=u_0}} \Delta\boldsymbol{x} + \frac{\partial \boldsymbol{f}}{\partial u}(\boldsymbol{x}, \boldsymbol{u})\bigg|_{\substack{x=x_0\\u=u_0}} \Delta\boldsymbol{u} \\ &= \boldsymbol{A}\Delta\boldsymbol{x} + \boldsymbol{B}\Delta\boldsymbol{u}\end{aligned} \tag{3.41a}$$

where

$$\boldsymbol{A} = \frac{\partial \boldsymbol{f}}{\partial x}(\boldsymbol{x}, \boldsymbol{u})\bigg|_{\substack{x=x_0\\u=u_0}} = \left.\begin{bmatrix} \frac{\partial f_1}{\partial x_1} & \cdots & \frac{\partial f_1}{\partial x_n} \\ \vdots & \cdots & \vdots \\ \frac{\partial f_n}{\partial x_1} & \cdots & \frac{\partial f_n}{\partial x_n} \end{bmatrix}\right|_{(x_0,u_0)} \tag{3.41b}$$

$$\boldsymbol{B} = \frac{\partial \boldsymbol{f}}{\partial u}(\boldsymbol{x}, \boldsymbol{u})\bigg|_{\substack{x=x_0\\u=u_0}} = \left.\begin{bmatrix} \frac{\partial f_1}{\partial u_1} & \cdots & \frac{\partial f_1}{\partial u_n} \\ \vdots & \cdots & \vdots \\ \frac{\partial f_n}{\partial u_1} & \cdots & \frac{\partial f_n}{\partial u_n} \end{bmatrix}\right|_{(x_0,u_0)} \tag{3.41c}$$

Similarly, applying the Taylor series to the output equation in Equation (3.37b) yields the following linear approximation.

$$\boldsymbol{y} = \boldsymbol{C}\Delta\boldsymbol{x} + \boldsymbol{D}\Delta\boldsymbol{u} \tag{3.42a}$$

where

$$\boldsymbol{C} = \frac{\partial \boldsymbol{g}}{\partial x}(\boldsymbol{x}, \boldsymbol{u})\bigg|_{\substack{x=x_0\\u=u_0}} = \left.\begin{bmatrix} \frac{\partial g_1}{\partial x_1} & \cdots & \frac{\partial g_1}{\partial x_n} \\ \vdots & \cdots & \vdots \\ \frac{\partial g_n}{\partial x_1} & \cdots & \frac{\partial g_n}{\partial x_n} \end{bmatrix}\right|_{(x_0,u_0)} \tag{3.42b}$$

$$\boldsymbol{D} = \frac{\partial \boldsymbol{g}}{\partial u}(\boldsymbol{x}, \boldsymbol{u})\bigg|_{\substack{x=x_0\\u=u_0}} = \left.\begin{bmatrix} \frac{\partial g_1}{\partial u_1} & \cdots & \frac{\partial g_1}{\partial u_n} \\ \vdots & \cdots & \vdots \\ \frac{\partial g_n}{\partial u_1} & \cdots & \frac{\partial g_n}{\partial u_n} \end{bmatrix}\right|_{(x_0,u_0)} \tag{3.42c}$$

3.7.2 Linearization of the Nonlinear Maglev Train Model

Now, the nonlinear maglev train model in Equation (3.32) is linearized using the above linearization technique around ($\boldsymbol{x}_0$,$\boldsymbol{u}_0$). Then the matrices $\boldsymbol{A}$, $\boldsymbol{B}$, and $\boldsymbol{C}$ in Equations (3.41) and (3.42) are obtained as

$$\boldsymbol{A} = \left.\begin{bmatrix} \frac{\partial f_1}{\partial x_1} & \frac{\partial f_1}{\partial x_2} & \frac{\partial f_1}{\partial x_3} \\ \frac{\partial f_2}{\partial x_1} & \frac{\partial f_2}{\partial x_2} & \frac{\partial f_2}{\partial x_3} \\ \frac{\partial f_3}{\partial x_1} & \frac{\partial f_3}{\partial x_2} & \frac{\partial f_3}{\partial x_3} \end{bmatrix}\right|_{(x_0,u_0)} = \begin{bmatrix} 0 & 1 & 0 \\ \frac{2ax_{30}^2}{x_{10}^3} & 0 & \frac{-2ax_{30}}{x_{10}^2} \\ -\frac{Rx_{30}}{k}+\frac{u_0}{k} & \frac{x_{30}}{x_{10}} & -\frac{Rx_{10}}{k} \end{bmatrix} \tag{3.43a}$$

$$\boldsymbol{B} = \left.\begin{bmatrix} \frac{\partial f_1}{\partial u} \\ \frac{\partial f_2}{\partial u} \\ \frac{\partial f_3}{\partial u} \end{bmatrix}\right|_{(x_0,u_0)} = \begin{bmatrix} 0 \\ 0 \\ \frac{x_{10}}{k} \end{bmatrix} \tag{3.43b}$$

$$\boldsymbol{C} = \left.\begin{bmatrix} \frac{\partial g}{\partial x_1} & \frac{\partial g}{\partial x_2} & \frac{\partial g}{\partial x_3} \end{bmatrix}\right|_{(x_0,u_0)} = \begin{bmatrix} 1 & 0 & 0 \end{bmatrix} \tag{3.43c}$$

As a result, the linearized model of the maglev train system can be presented using the following general representation:

$$\Delta\dot{\boldsymbol{x}} = \boldsymbol{A}\Delta\boldsymbol{x} + \boldsymbol{B}\Delta\boldsymbol{u} \tag{3.44a}$$

$$\boldsymbol{y} = \boldsymbol{C}\Delta\boldsymbol{x} \tag{3.44b}$$

where

$$\boldsymbol{A} = \begin{bmatrix} 0 & 1 & 0 \\ \frac{2ax_{30}^2}{x_{10}^3} & 0 & \frac{-2ax_{30}}{x_{10}^2} \\ -\frac{Rx_{30}}{k}+\frac{u_0}{k} & \frac{x_{30}}{x_{10}} & -\frac{Rx_{10}}{k} \end{bmatrix},\ \boldsymbol{B} = \begin{bmatrix} 0 \\ 0 \\ \frac{x_{10}}{k} \end{bmatrix},\ \boldsymbol{C} = \begin{bmatrix} 1 & 0 & 0 \end{bmatrix}, \tag{3.44c}$$

$$\begin{aligned} \boldsymbol{x} &= \boldsymbol{x}_0 + \Delta\boldsymbol{x} \\ \boldsymbol{u} &= \boldsymbol{u}_0 + \Delta\boldsymbol{u} \end{aligned} \tag{3.44d}$$

3.8 Open Loop Analysis

The maglev train system's open-loop control operates entirely on the basis of an input, and the output has no effect on the control action. Figure 3.6 depicts the maglev train's open loop response to a step signal in the absence of a controller. The open loop response in Figure 3.6 illustrates the system's diverging free response in which the levitation gap of the maglev train system increases continuously, showing that there is an obvious instability phenomena.

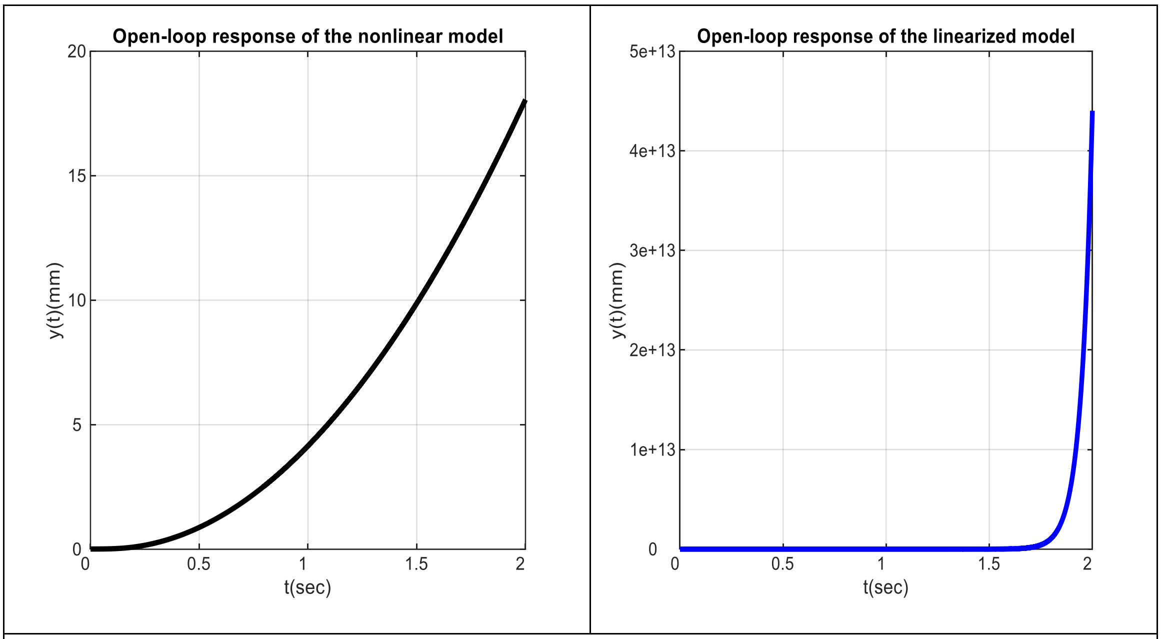

Figure 3.6 Open loop response of the maglev train system

In this thesis work, the root locus method, which requires the linearized model of the system, is also used to perform an open loop analysis of the system. As shown in Figure 3.7 below, the given system has two poles (-11.2+17j and -11.2-17j) in the left-half of the s-plane (LHP) and one pole (18.6) in the right-half of the s-plane (RHP). As a result of the single pole in the RHP, the system becomes unstable.

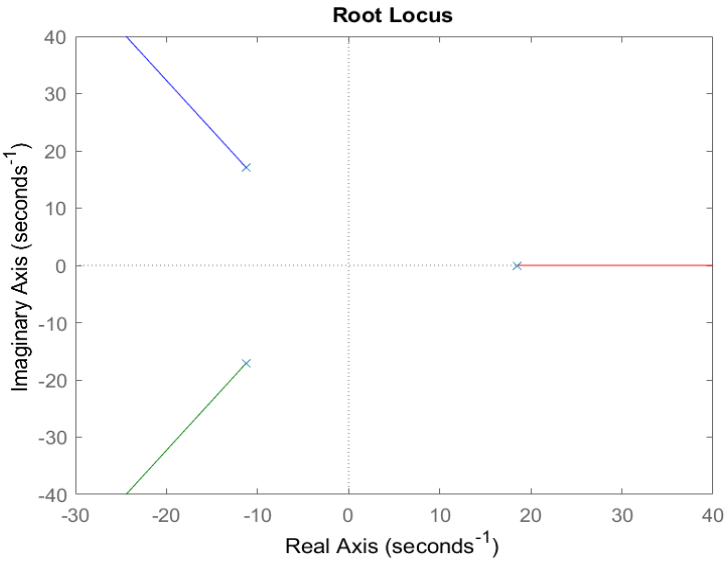

Figure 3.7 Root locus of the maglev train system

Both responses emphasize that the system requires closed loop control. The controller design is discussed in the following chapter.

CHAPTER FOUR

CONTROLLER DESIGN

4.1 Chapter Overview

The proposed backstepping controller, which is based on the Lyapunov function, is briefly explained in this chapter. In addition, the particle swarm optimization (PSO) algorithm based on minimizing the proposed objective function (IAEU) is discussed. Finally, LQR controller is designed for comparison purposes.

4.2 Lyapunov Stability Theory

The Lyapunov stability theory is used to determine whether or not the system is stable. The direct and indirect methods of Lyapunov, established by Russian mathematician Lyapunov, are used to analyze stability of the dynamical system. Lyapunov's direct method determine system stability using an energy function, whereas Lyapunov's indirect method uses system linearization to determine the stability of a system (Nicaise, 2003). This thesis work focused with the direct method of Lyapunov, hence the proposed controller is designed based on it.

The stability theorem using the Lyapunov direct method consists of two steps. The first step is to find a suitable continuously differentiable, positive definite function which is known as Lyapunov function $V(x)$ (Meigoli & Nikravesh, 2012). It is often helpful to think of $V(x)$ as some form of energy which is never negative and can only be zero in the zero state. Second, compute the first order time derivative of the candidate Lyapunov function, which is denoted by $\dot{V}(x)$.

Consider the following system dynamics

$$\dot{\boldsymbol{x}} = f(\boldsymbol{x}) \tag{4.1}$$

where $\boldsymbol{x} \in \mathrm{R}^n$ is the state vector and $\boldsymbol{f} \in \mathrm{R}^n$ is smooth vector functions.

Let $V(x)$ be the candidate Lyapunov function. Then,

$$\dot{V}(x) = \frac{\partial V(x)}{\partial t} = \frac{\partial V(x)}{\partial t}\frac{\partial x}{\partial t} = \frac{\partial V(x)}{\partial t} f(x) \tag{4.2}$$

According to the stability theory of Lyapunov (Jackreece, 2018),

- The system is stable if $\dot{V}(x)$ is negative semidefinite.

- The system is asymptotically stable if $\dot{V}(x)$ is negative definite.
- The system is globally asymptotically stable if $V(x)$ is positive definite and radially unbounded for all which means if $V(x) \to \infty$ for $\|x\| \to \infty$, and if $\dot{V}(x)$ is negative definite for all.

4.3 Backstepping Controller Design

Backstepping control is a method developed in the 1990s by Peter V.Kokotovic and others for constructing stabilizing controls for a specific type of nonlinear systems (T. Rasheed & K. Hamzah, 2021). A backstepping control is a recursive technique that employs a systematic design procedure and the Lyapunov function to a certain type of nonlinear dynamical system made of subsystems radiating from an irreducible component. Its recursive structure allows the controller designer to start with the system that is known to be stable and then back out new controllers to gradually stabilize each outer subsystem. The process is completed when the last external feedback control is obtained (Singh & Kumar, 2018). As a result, this control method is known as backstepping control. This controller ensures asymptotic convergence for regulation and tracking properties. It uses the distinction between the desired reference and actual output to begin the design process for tracking problems. Backstepping controller has the advantages of flexibility in the controller design which is due to its recursive use of Lyapunov functions, handling all system nonlinearities and ensuring all desired dynamics' properties (Bai et al., 2013)(Basri et al., 2018).

The backstepping controller (BSC) design is restricted by the requirement that the system model is provided in a strict feedback form. The derived nonlinear state space model of the maglev train system in Equation (3.32) is in strict feedback form. The BSC is designed in the following ways to make the system's actual output track the desired reference, $y \to y_r$ as $t \to \infty$, such that the tracking error approaches zero $(e \to 0)$.

A new definition of state variables is required for the backstepping control algorithm, so the error of each state is defined as follows.

$$e_1 = y_r - y \tag{4.3}$$

Hence, $y = x_1$ Equation (4.3) becomes:

$$e_1 = y_r - x_1 \tag{4.4}$$

where y_r represents the desired reference levitation gap of the maglev train.

$$e_2 = x_2 - w_1 \tag{4.5}$$

$$e_3 = x_3 - w_2 \tag{4.6}$$

where x_2 and x_3 are given by

$$x_2 = e_2 + w_1 \tag{4.7}$$

$$x_3 = e_3 + w_2 \tag{4.8}$$

where w_1 and w_2 are the virtual control input for e_1 and e_2, respectively.

The backstepping design procedure can be developed using the subsystems (4.4-4.8). The following steps is used to derive the control law based on the Lyapunov function.

Step 1

Consider the following subsystem e_1 of the system (4.4-4.8), and the time derivative of the tracking error in Equation (4.4) can be represented as:

$$\dot{e}_1 = \dot{y}_r - \dot{x}_1 \tag{4.9a}$$

Substituting Equation (3.32), which represents the nonlinear model of the system discussed in section 3.5.2, into Equation (4.9a) results in

$$\dot{e}_1 = \dot{y}_r - x_2 \tag{4.9b}$$

x_2 is regarded as virtual controller for e_1. Let w_1 represents the virtual control input.

$$\dot{e}_1 = \dot{y}_r - w_1 \tag{4.10}$$

The first candidate Lyapunov function for this subsystem is chosen as:- $V(e_1) = V_1$

$$V_1 = \frac{1}{2} e_1^2 \tag{4.11}$$

Compute the time derivative of the candidate Lyapunov function (V_1) in order to define w_1 which is the virtual control input for e_1.

$$\dot{V}_1 = e_1 \dot{e}_1 \tag{4.12}$$

Substituting Equation (4.10) into Equation (4.12) results in

$$\dot{V}_1 = e_1(\dot{y}_r - w_1) \tag{4.13}$$

The virtual control input w_1 is selected in such a way that the above time derivative of the candidate Lyapunov function is negative definite.

$$w_1 = \dot{y}_r + k_1 e_1 \tag{4.14}$$

where k_1 is user defined positive constant parameter. Then substituting Equation (4.14) into

(4.13) results in

$$\begin{aligned}\dot{V}_1 &= e_1(\dot{y}_r - \dot{y}_r - k_1 e_1) \\ &= -k_1 e_1^2 < 0\end{aligned} \tag{4.15}$$

$\dot{V}_1$ is clearly quadratic and negative definite. Thus, according to Lyapunov stability theory discussed in section 4.2, the closed loop subsystem is globally asymptotically stable by the action of the control law (w_1).

Step 2

Consider the subsystem (e_1, e_2) of the system (4.4-4.8), and substituting Equation (4.14) into (4.5) results

$$\begin{aligned}e_2 &= x_2 - w_1 \\ &= x_2 - \dot{y}_r - k_1 e_1\end{aligned} \tag{4.16}$$

Then, the time derivative of the error of the second state in Equation (4.16) can be written as:

$$\dot{e}_2 = \dot{x}_2 - \ddot{y}_r - k_1 \dot{e}_1 \tag{4.17}$$

Substituting Equation (3.32), which represents the nonlinear model of the system discussed in section 3.5.2, into Equation (4.17) yields

$$\dot{e}_2 = -a\frac{x_3^2}{x_1^2} + g - \ddot{y}_r - k_1 \dot{e}_1 \tag{4.18}$$

Equation (4.4) and (4.16) are rearranged to give the following equations.

$$x_1 = y_r - e_1 \tag{4.19}$$

$$x_2 = e_2 + \dot{y}_r + k_1 e_1 \tag{4.20}$$

Then substituting Equation (4.20) into (4.9b) results in

$$\begin{aligned}\dot{e}_1 &= \dot{y}_r - \left(e_2 + \dot{y}_r + k_1 e_1\right) = \dot{y}_r - e_2 - \dot{y}_r - k_1 e_1 \\ &= -e_2 - k_1 e_1\end{aligned} \tag{4.21}$$

The following equation is obtained when Equations (4.19) and (4.21) are substituted into (4.18):

$$\begin{aligned}\dot{e}_2 &= -a\frac{x_3^2}{\left(y_r - e_1\right)^2} + g - \ddot{y}_r - k_1(-e_2 - k_1 e_1) \\ &= -a\frac{x_3^2}{\left(y_r - e_1\right)^2} + g - \ddot{y}_r + k_1(e_2 + k_1 e_1)\end{aligned} \tag{4.22}$$

x_3 is regarded as virtual controller for e_2. Let w_2 represent the virtual control input.

$$\dot{e}_2 = \frac{-a}{\left(y_r - e_1\right)^2} w_2^2 + g - \ddot{y}_r + k_1(e_2 + k_1 e_1) \tag{4.23}$$

The second candidate Lyapunov function for this subsystem is chosen as:- $V(e_1, e_2) = V_2$

$$V_2 = V_1 + \frac{1}{2}e_2^2 = \frac{1}{2}(e_1^2 + e_2^2) \tag{4.24}$$

Compute the time derivative of the candidate Lyapunov function (V_2) in order to define w_2 which is the virtual control input for e_2.

$$\dot{V}_2 = e_1\dot{e}_1 + e_2\dot{e}_2 \tag{4.25}$$

Substituting Equation (4.21) and (4.23) into (4.25) yields:

$$\begin{aligned} \dot{V}_2 &= e_1(-e_2 - k_1 e_1) + e_2\left(-\frac{a}{(y_r - e_1)^2} w_2^2 + g - \ddot{y}_r + k_1(e_2 + k_1 e_1) \right) \\ &= -k_1 e_1^2 + e_2\left(-e_1(1 - k_1^2) - \frac{a}{(y_r - e_1)^2} w_2^2 + k_1 e_2 + g - \ddot{y}_r \right) \end{aligned} \tag{4.26}$$

The virtual control input w_2 is selected in such a way that $\dot{V}_2$ is negative definite.

$$w_2 = (y_r - e_1)\sqrt{\frac{1}{a}\left(g - \ddot{y}_r + e_2(k_1 + k_2) - e_1(1 - k_1^2)\right)} \tag{4.27}$$

where k_2 is user defined positive constant parameter. Then substituting Equation (4.27) into (4.26) gives

$$\begin{aligned} \dot{V}_2 &= e_2\left(-\frac{a}{(y_r - e_1)^2}\left((y_r - e_1)\sqrt{\frac{1}{a}\left(g - \ddot{y}_r + e_2(k_1 + k_2) - e_1(1 - k_1^2)\right)} \right)^2 \right) \\ &\quad + e_2\left(-e_1(1 - k_1^2) + k_1 e_2 + g - \ddot{y}_r\right) - k_1 e_1^2 \\ &= -k_1 e_1^2 + e_2\left(-e_1 + k_1^2 e_1 - g + \ddot{y}_r - e_2(k_1 + k_2) + e_1 - k_1^2 e_1 + k_1 e_2 + g - \ddot{y}_r\right) \end{aligned} \tag{4.28a}$$

$$\begin{aligned} \dot{V}_2 &= -k_1 e_1^2 + e_2\left(-e_2(k_1 + k_2) + k_1 e_2\right) \\ &= -k_1 e_1^2 - k_2 e_2^2 < 0 \end{aligned} \tag{4.28b}$$

$\dot{V}_2$ is negative definite. Thus, according to Lyapunov stability theory, the above subsystem is globally asymptotically stable by the action of the control law (w_2).

Step 3

Consider the whole system (e_1, e_2, e_3), and the time derivative of the error of the third state in Equation (4.6) can be written as:

$$\dot{e}_3 = \dot{x}_3 - \dot{w}_2 \tag{4.29}$$

Substituting Equation (3.32), which represents the nonlinear model of the system discussed in section 3.5.2, into Equation (4.29) yields

$$\dot{e}_3 = \frac{x_3 x_2}{x_1} - \frac{R x_3 x_1}{k} + \frac{1}{k} x_1 u - \dot{w}_2 \tag{4.30}$$

The following equation is obtained when Equation (4.27) is substituted into (4.8):

$$\begin{aligned} x_3 &= e_3 + (y_r - e_1)\sqrt{\frac{1}{a}\left(g - \ddot{y}_r + e_2(k_1 + k_2) - e_1(1 - k_1^2)\right)} \\ &= e_3 + (y_r - e_1)\sqrt{q} \end{aligned} \tag{4.31}$$

where, $q = \frac{1}{a}\left(g - \ddot{y}_r + e_2(k_1 + k_2) - e_1(1 - k_1^2)\right)$ (4.32)

Therefore, Equation (4.27) becomes

$$w_2 = (y_r - e_1)\sqrt{q} \tag{4.33}$$

The following equation is obtained when Equations (4.8), (4.19), and (4.21) are substituted into (4.18).

$$\begin{aligned} \dot{e}_2 &= -a\frac{(e_3 + w_2)^2}{(y_r - e_1)^2} + g - \ddot{y}_r - k_1(-e_2 - k_1 e_1) \\ &= -a\frac{(e_3 + w_2)^2}{(y_r - e_1)^2} + g - \ddot{y}_r + k_1(e_2 + k_1 e_1) \end{aligned} \tag{4.34}$$

Substituting Equations (4.19), (4.20) and (4.31) into Equation (4.30) yields:

$$\begin{aligned} \dot{e}_3 = &\frac{\left(e_3 + (y_r - e_1)\sqrt{q}\right)\left(e_2 + \dot{y}_r + k_1 e_1\right)}{(y_r - e_1)} - \frac{\mathrm{R}\left(e_3 + (y_r - e_1)\sqrt{q}\right)(y_r - e_1)}{k} \\ &+ \frac{1}{k}(y_r - e_1)u - \dot{w}_2 \end{aligned} \tag{4.35}$$

The total candidate Lyapunov function for the whole system is chosen as:- $V(e_1, e_2, e_3) = V$

$$V = V_1 + V_2 + \frac{1}{2}e_3^2 = \frac{1}{2}(e_1^2 + e_2^2 + e_3^2) \tag{4.36}$$

Compute the time derivative of the total candidate Lyapunov function (V) in order to define u which is the final control law of the whole system.

$$\dot{V} = e_1\dot{e}_1 + e_2\dot{e}_2 + e_3\dot{e}_3 \tag{4.37}$$

Substituting Equations (4.21), (4.34), and (4.35) into (4.37) yields:

$$\dot{V}=e_1\left(-e_2-k_1e_1\right)+e_2\left(-a\frac{(e_3+w_2)^2}{\left(y_r-e_1\right)^2}+g-\ddot{y}_r+k_1\left(e_2+k_1e_1\right)\right)$$
$$+e_3\left(\frac{\left(e_3+(y_r-e_1)\sqrt{q}\right)\left(e_2+\dot{y}_r+k_1e_1\right)}{\left(y_r-e_1\right)}\right) \tag{4.38a}$$
$$+e_3\left(-\frac{\mathrm{R}\left(e_3+(y_r-e_1)\sqrt{q}\right)\left(y_r-e_1\right)}{k}+\frac{1}{k}\left(y_r-e_1\right)u-\dot{w}_2\right)$$

Substituting Equation (4.33) into (4.38a) yields

$$\dot{V}=e_1\left(-e_2-k_1e_1\right)+e_2\left(\frac{-a}{(y_r-e_1)^2}\left(e_3^2+2e_3(y_r-e_1)\sqrt{q}+(y_r-e_1)^2q\right)+g-\ddot{y}_r\right)$$
$$+\mathrm{e}_2\left(k_1(e_2+k_1e_1)\right)+e_3\left(\frac{\left(e_3+(y_r-e_1)\sqrt{q}\right)\left(e_2+\dot{y}_r+k_1e_1\right)}{\left(y_r-e_1\right)}\right) \tag{4.38b}$$
$$+e_3\left(-\frac{\mathrm{R}\left(e_3+(y_r-e_1)\sqrt{q}\right)\left(y_r-e_1\right)}{k}+\frac{1}{k}\left(y_r-e_1\right)u-\dot{w}_2\right)$$

$$\dot{V}=-k_1e_1^2+e_2\left(-e_1-\frac{a}{(y_r-e_1)^2}\left((y_r-e_1)^2q\right)-\frac{a}{(y_r-e_1)^2}\left(e_3^2+2e_3(y_r-e_1)\sqrt{q}\right)\right)$$
$$+e_2\left(g-\ddot{y}_r+k_1(e_2+k_1e_1)\right)+e_3\left(\frac{\left(e_3+(y_r-e_1)\sqrt{q}\right)\left(e_2+\dot{y}_r+k_1e_1\right)}{\left(y_r-e_1\right)}\right) \tag{4.38c}$$
$$+e_3\left(-\frac{\mathrm{R}\left(e_3+(y_r-e_1)\sqrt{q}\right)\left(y_r-e_1\right)}{k}+\frac{1}{k}\left(y_r-e_1\right)u-\dot{w}_2\right)$$

Substituting Equation (4.32) into Equation (4.38c) yields:

$$\dot{V}=-k_1e_1^2-k_2e_2^2+e_2\left(-\frac{a}{(y_r-e_1)^2}\left(e_3^2+2e_3(y_r-e_1)\sqrt{q}\right)\right)$$
$$+e_3\left(\frac{\left(e_3+(y_r-e_1)\sqrt{q}\right)\left(e_2+\dot{y}_r+k_1e_1\right)}{\left(y_r-e_1\right)}\right) \tag{4.38d}$$
$$+e_3\left(-\frac{\mathrm{R}\left(e_3+(y_r-e_1)\sqrt{q}\right)\left(y_r-e_1\right)}{k}+\frac{1}{k}\left(y_r-e_1\right)u-\dot{w}_2\right)$$

$$\dot{V} = -k_1 e_1^2 - k_2 e_2^2 + e_3\left(-\frac{a e_2}{(y_r - e_1)^2}\left(e_3 + 2(y_r - e_1)\sqrt{q}\right)\right)$$
$$+ e_3\left(\frac{\left(e_3 + (y_r - e_1)\sqrt{q}\right)\left(e_2 + \dot{y}_r + k_1 e_1\right)}{\left(y_r - e_1\right)}\right) \tag{4.38e}$$
$$+ e_3\left(-\frac{\mathrm{R}\left(e_3 + (y_r - e_1)\sqrt{q}\right)\left(y_r - e_1\right)}{k} + \frac{1}{k}\left(y_r - e_1\right)u - \dot{w}_2\right)$$

The final control law u is selected in such a way that $\dot{V}$ is negative definite.

$$u = \frac{k}{(y_r - e_1)}\left(\frac{a e_2}{(y_r - e_1)^2}\left(e_3 + 2(y_r - e_1)\sqrt{q}\right) - \frac{\left(e_3 + (y_r - e_1)\sqrt{q}\right)\left(e_2 + \dot{y}_r + k_1 e_1\right)}{\left(y_r - e_1\right)}\right)$$
$$+ \frac{k}{(y_r - e_1)}\left(\dot{w}_2 - k_3 e_3\right) + \mathrm{R}\left(e_3 + (y_r - e_1)\sqrt{q}\right) \tag{4.39}$$

where $\dot{w}_2$ is computed as follows.

$$\dot{w}_2 = \frac{d}{dt}(y_r - e_1)\sqrt{q} \tag{4.40a}$$

$$w_2 = \left(\dot{y}_r - \dot{e}_1\right)\sqrt{q} + (y_r - e_1)\frac{\dot{q}}{2\sqrt{q}} \tag{4.40b}$$

where , $$\dot{q} = \frac{1}{a}\left(-\dddot{y}_r + \dot{e}_2(k_1 + k_2) - \dot{e}_1\left(1 - k_1^2\right)\right) \tag{4.41}$$

Substituting Equation (4.39) into Equation (4.38e) results in:

$$\dot{V} = -k_1 e_1^2 - k_2 e_2^2 - k_3 e_3^2 \tag{4.42}$$

$\dot{V}$ is negative definite. Thus, according to Lyapunov stability theory, the whole closed loop system is globally asymptotically stable by the action of the final control law u . As a result of the above steps, the system in Equation (3.32) becomes globally asymptotically stable.

4.4 Optimal Tuning of the Backstepping Controller

The proposed backstepping controller has three design parameters namely k_1, k_2, and k_3, which have a direct impact on the performance of the system. The optimal parameters are important for enhancing system performance. Particle swarm optimization (PSO) technique is used in this thesis work for tuning the three design parameters of the proposed controller. Section 4.4.2 goes through the PSO algorithm in detail.

4.4.1 Objective Function

An objective function must be carefully selected in order to achieve acceptable system performance characteristics with minimizing the control input. Moreover, selection of the appropriate objective function is the most crucial step in the optimization technique. In the realm of control, an objective function is often referred to as a performance index. Integral Absolute Error, Integral Time Absolute Error, Integral Square Error, and Integral Time Square Error are the most widely used performance indicators (Tsai et al., 2021). These performance indices are explained in the following way.

Integral Absolute Error (IAE) integrates the absolute error across time without adding weight to any of the errors in system response. The Integral Time Absolute Error (ITAE) method integrates the absolute error multiplied by the time over time and gives significantly greater weight to errors that occur over long periods of time than to those that occur at the beginning of the response. The Integral Square Error (ISE) integrates the square error over time and penalizes huge errors strongly than minor ones, while the Integral Time Square Error (ITSE) integrates the squared error weighted by over time (J.Jebakumar et al., 2014).

The drawback of the performance indices discussed in the above paragraph is that IAE has a slower response than that of ISE, ISE performs quickly with low amplitude and oscillation while both ITAE and ITSE result in a system that has a slow initial response (Chen et al., 2017). This thesis work uses the Integral of Absolute Error and Control Signal (IAEU) as the objective function to provide acceptable dynamic characteristics in the transition process while avoiding an excessive control input when the setpoint changes abruptly. It provides information on both setpoint tracking and control effort (Durand et al., 2014). It is defined in the following way:

$$IAEU = \int_0^t |e(t)| + w|\Delta u|\, dt \tag{4.43}$$

where $e(t)$ is the error, that is, the difference between the reference signal and actual output with $e(t) = y_r - y$, and $\Delta u = u - u_0$ which is the deviation of the control input. u is the final value of the control signal. u_0 denotes the control input at an operating point as shown in Equation (3.35). The proposed performance index (IAEU) can satisfy the designer's various requirements by changing the weighting factor. Selecting a suitable value for the weighting factor w in Equation (4.47) is a crucial task in the design procedure of controller. Decreasing the weighting factor ensures a faster system response, while increasing the weighting factor reduces unnecessary control effort at the expense of a delayed response. Thus, the following weighting factor of , $w = 2\times10^{-4}$, is used in this thesis work to achieve a good compromise between the speed of the closed-loop response and the control effort.

4.4.2 Particle Swarm Optimization as an Optimization Tool

The Particle swarm optimization (PSO) is a swarm-based stochastic algorithm proposed by Kennedy and Eberhart in 1995. This algorithm makes use of animal social behavior concepts such as school of fish and flock of birds (Imran et al., 2013). PSO depicts each possible solution to a given problem as a particle with a specific velocity moving through the problem space like a bird swarm searching for food sources. After that, each particle combines some aspects of its previous best position and present location, as well as those of one or more swarm agents, with certain random disturbances to determine its next path through the search space. The next iteration begins once all particles have been moved. The whole swarm (for example, birds flock looking for food) will most likely approach the optimum objective function over time (Gad, 2022). Each particle is represented by its position (a set of coordinates defining a point in the search space), velocity, and best prior position.

In PSO, the particles are randomly distributed in the search area and each particle, which represents a solution, attempts to find an optimal or nearly optimal solution by generating new ones. Each particle is represented by its position (a set of coordinates defining a point in the search space), its best previous position, and its velocity. Particles in their current position are evaluated using a fitness function at each iteration of the process, and if the value of the fitness function is better than any previously obtained, it is saved as the best position p_{best}. The particle that is closest to the goal receives the best fitness function value and is saved as p_{best} (Nakisa et al., 2014). After that, the following formula is used to calculate the particle's next position as well as its velocity (Li et al., 2019);

$$v_i^{t+1} = \omega v_i^t + c_1 r_1 (p_{best} - x_i^t) + c_2 r_2 (g_{best} - x_i^t) \tag{4.44}$$

$$x_i^{t+1} = v_i^{t+1} + x_i^t \qquad i = 1, 2, ..., n \tag{4.45}$$

where, t is the iteration time, x_i is the particle position in the search space at i^{th} iteration, v_i is the velocity of particle at i^{th} iteration, p_{best} is the personal best position of the particle, g_{best} is the global best position for the PSO, c_1, c_2 are the acceleration coefficients, ω is the weight inertia, and r_1, r_2 are random numbers between 0 and 1.

PSO, like other swarm intelligence or evolutionary computing approaches, has several parameters that influence the performance of the algorithm such as inertia weight ω, swarm size, number of iterations, and acceleration coefficients (He et al., 2016)(Piotrowski et al., 2020). The selection of the acceleration coefficients and inertia weight of the PSO algorithm have a significant impact on optimization performance (Martínez-Ledesma & Jaramillo Montoya, 2020).

Acceleration coefficients: The importance of cognitive and social influence is determined by the acceleration coefficients c_1 and c_2, respectively. The cognitive component c_1 depicts each particle's individual knowledge as it moves towards its best-known position and the social or cooperative component c_2 symbolizes the swarm's collaborative knowledge and directs the particle towards the global solution (Martínez-Ledesma & Jaramillo Montoya, 2020). Both parameters are positive constants and are known as learning factors. In most cases, c_1 and c_2 have the same value, thus the social and cognitive searches are weighted equally. If $c_1 >> c_2$,each particle is significantly more attracted to its own optimal position, resulting in excessive roaming and on the other hand, if $c_1 << c_2$, particles are more strongly attracted to the global optimal position, forcing them to rush there before they should (He et al., 2016). The cognitive and social components most commonly used are those proposed by Kennedy and Eberhart i.e. $c_1 = c_2 = 2$ (Sahu et al., 2012)(Wang et al., 2018).

Inertia weight : It is used to balance the global and local searches, with the higher inertia weighting favoring global searches and the lower inertia weighting preferring local searches (Wang et al., 2018). So the value of inertia weight ω should gradually reduce with time (Li et al., 2019). Numerical experiments illustrated the impact of ω, and 0.9 for the upper value $\omega_{\max}$ and 0.4 for the lower value $\omega_{\min}$ are suggested (Huang et al., 2016)(He et al., 2016).

Swarm size: It is the number of particles in the swarm. Although the PSO technique is not very sensitive to the size of the swarm, an inadequate number of particles may prevent convergence to the optimal solution (Martínez-Ledesma & Jaramillo Montoya, 2020). A larger swarm will cover more of the search space per iteration. However, as the number of particles increases, so does the computing complexity per iteration. Several empirical studies have shown that the PSO can find optimal solutions even with small swarm sizes. The size of the swarm is commonly selected as 20 to 50 particles (Wang et al., 2018)(Piotrowski et al., 2020).

Number of iterations: The number of iterations must be properly determined. Too few iterations may cause the search to stop prematurely. A large number of iterations, on the other hand, results in excessive computing complexity if the number of iterations is the only condition for stopping (Martínez-Ledesma & Jaramillo Montoya, 2020).

Particle swarm optimization (PSO) is a population-based optimization tool that can be simply constructed and used to solve a wide range of function optimization problems or problems that can be turned into function optimization problems. It has been employed in a broad range of application including dynamic tracking problems, control systems, power systems, and others (Shabir, 2016). The main advantage of PSO is its swift convergence, which compares well to other global optimization techniques such as Genetic Algorithm (GA), Simulated Annealing (SA), and others (Aote et al., 2013). Furthermore, the PSO has advantage of good robustness and quickly converges to the optimal value with small number of parameters and correspondingly fewer iterations (Shabir, 2016)(Wang et al., 2018).

In this thesis work, the commonly used parameter configuration suggested by Kennedy and Eberhart, $c_1 = c_2 = 2$ and a linearly decreasing ω from 0.9 to 0.4 are used.

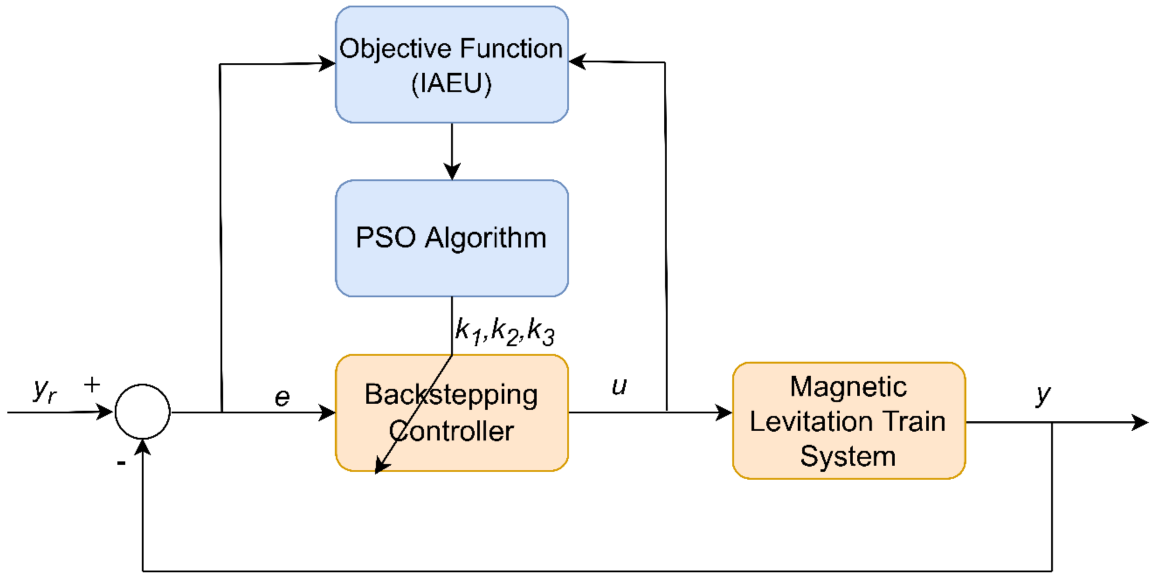

Figure 4.1 Block diagram of the proposed backstepping controller with PSO algorithm

The block diagram of the proposed BSC controller with the PSO tuner is shown in Figure

4.1 above. The particle swarm optimization is implemented to obtain the optimal parameters of the proposed BSC and it is carried out by minimizing the objective function (IAEU) which is discussed in section 4.4.1. In this thesis work, 9-12 iterations are done by varying the upper and lower bounds until the least function value of the proposed performance index and the required tracking response are attained. Both the upper and lower bounds are greater than zero since the proposed system is stable if all three parameters of the BSC controller are positive, as explained in section 4.3.

4.5 LQR Controller Design

In this section, the linear quadratic regulator is designed for comparison with the controller proposed in the previous section. Linear quadratic regulator (LQR) is an optimal control technique that considers the states of the dynamical system as well as the control input to make the optimal control decisions (L. B. Prasad et al., 2014). It is a state space model based controller that compares system output to setpoint value and provides feedback to the system through the controller gain *K*.

Consider the linearized equation in Equation (3.44) in state variable form:

$$\begin{aligned} \Delta\dot{\boldsymbol{x}} &= \boldsymbol{A}\Delta\boldsymbol{x} + \boldsymbol{B}\Delta\boldsymbol{u} \\ \boldsymbol{y} &= \boldsymbol{C}\Delta\boldsymbol{x} \end{aligned} \tag{4.46a}$$

where

$$\Delta\boldsymbol{x} = \boldsymbol{x} - \boldsymbol{x}_0 \tag{4.46b}$$

$$\Delta\boldsymbol{u} = u - u_0 \tag{4.46c}$$

An integral action is incorporated into the LQR controller to track a reference input, where the integrator is implemented to remove steady state error and ensure tracking (Malkapure & Chidambaram, 2014)(Ghaffar & Richardson, 2015). In this thesis work, an integral action has been added to the LQR controller to ensure tracking. The control formulation is achieved by incorporating a new state that computes the integral of the error signal to the linear system matrices. As a result, the following new state variable is added to the linearized state space model of the maglev train system discussed in section 3.7.2 in order to make the system output follows the desired reference.

$$z = \int (y - y_r)\,dt \tag{4.47}$$

where z is the integral of the system output minus the reference.

Differentiating both sides of the Equation (4.47) and substituting the second equation of

Equation 4.46a yields

$$\dot{z} = y - y_r = C\Delta x - y_r \tag{4.48}$$

Equations (4.46a) and (4.48) are combined to form the following linear augmented state space model.

$$\Delta\dot{\tilde{x}} = \tilde{A}\Delta\tilde{x} + \tilde{B}\Delta u + \begin{bmatrix} 0 \\ -1 \end{bmatrix} y_r \tag{4.49}$$

where

$$\Delta\tilde{\boldsymbol{x}} = \begin{bmatrix} \Delta\boldsymbol{x} \\ z \end{bmatrix},\ \tilde{A} = \begin{bmatrix} A & 0 \\ C & 0 \end{bmatrix} \text{ and } \tilde{B} = \begin{bmatrix} B \\ 0 \end{bmatrix} \tag{4.50}$$

Then, the feedback control law designed from the new augmented matrices is represented as follows.

$$\Delta u = -\tilde{K}\Delta\tilde{\boldsymbol{x}} \tag{4.51a}$$

where

$$\tilde{K} = [\boldsymbol{K}_1 \quad k_i] \tag{4.51b}$$

where $\boldsymbol{K}_1$ is the state feedback control gain vector and k_i is the integral error gain.

Substituting Equations (4.47), (4.50), (4.51b) into (4.51a) results in

$$\begin{aligned} \Delta u &= -\boldsymbol{K}_1\Delta\boldsymbol{x} - k_i z \\ &= -\boldsymbol{K}_1\Delta\boldsymbol{x} - k_i \int y - y_r \end{aligned} \tag{4.51c}$$

Equation (4.51c) can be rewritten as

$$\Delta u = -\boldsymbol{K}_1\Delta\boldsymbol{x} - k_i \int y - y_r \tag{4.52}$$

The block diagram of the LQR controller which is incorporated with an integral action is shown in Figure 4.2.

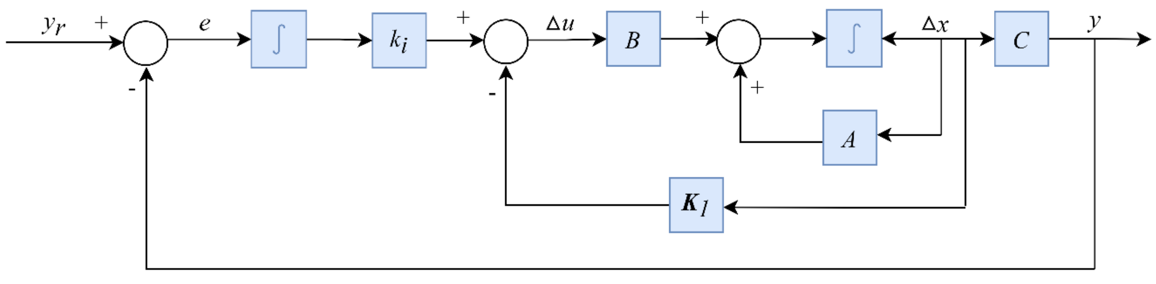

Figure 4.2 Block diagram of the LQR controller with an integral action

The final control law is given by substituting Equation (4.52) into (4.46c)

$$-\boldsymbol{K}_1\Delta\boldsymbol{x} + k_i\int y_r - y = u - u_0 \tag{4.53}$$

Rewriting Equation (4.53) yields

$$u = u_0 - \boldsymbol{K}_1\Delta\boldsymbol{x} + k_i\int y_r - y \tag{4.54}$$

The elements of the matrix $\tilde{K}$ are selected in such a way that the quadratic cost function, also known as the quadratic performance index (*J*), is minimized (Fernaza, 2014).

$$J = \int_0^\infty (\Delta\tilde{\boldsymbol{x}}^T Q \Delta\tilde{\boldsymbol{x}} + u^T R u) dt \tag{4.55}$$

where $\boldsymbol{Q}\in\Re^{4\times4}$ is a semi-positive definite and symmetric matrix and $\boldsymbol{R}\in\Re^{1\times1}$ is a symmetric and positive definite matrix. Here *J* is always a scalar.

The following equation represents the optimal state feedback gain $\tilde{K}$ (Herrera et al., 2017).

$$\tilde{K} = R^{-1}B^T P \tag{4.56}$$

where *P* is the solution of the Algebraic Ricatti Equation (ARE) given below (L. B. Prasad et al., 2014).

$$\tilde{A}^T P + P\tilde{A} - P\tilde{B}R^{-1}\tilde{B}^T P + Q = 0 \tag{4.57}$$

The proper selection of the weighting matrices is required for a successful controller design. ***Q*** is used to penalize the bad performance by minimizing the system states, while ***R*** is used for penalizing the control effort.

CHAPTER FIVE

SIMULATION RESULT AND DISCUSSIONS

5.1 Chapter Overview

The simulation results of the proposed backstepping controller and LQR controller for the maglev train system are discussed and compared in this chapter. To verify the effectiveness of the proposed control algorithm, the simulation is divided into two sections. The first section evaluates the tracking capability of both controllers under the single step signal, multiple step signal, and sinusoidal signal. The second section is used to verify robustness under the effect of load change and external disturbance force. The proposed performance index (IAEU) and the transient response characteristics of the system such as rise time, peak time, and settling time are used to compare the tracking performance. The overall simulation is carried out using MATLAB software.

5.2 Parameter Settings of the Maglev Train system

The parameters and their values of the magnetically levitating train system model used for the simulation works are based on the test maglev train at the national maglev center of Tongji university which is collected from other related references.

Table 5.1 Physical parameter values of the magnetically levitating train system (Xu et al., 2017)(Xu et al., 2018)

Parameters with symbol	Values with unit
Mass of the EMS train(m)	700 [kg]
Pole area of the suspension electromagnet (A)	0.024 [m^2]
Number of turns of the coil (N)	450
Magnetic reluctance of the magnetic circuit (R)	1.2 [Ω]
Permeability of free space (μ_0)	$4\pi \times 10^{-7}$ [$H.m^{-1}$]

The initial position of the suspension air gap taken in this thesis work is 10mm that is selected based on the operating range of the maglev train system which is explained in section 2.2.3.1. With this selection, the other initial conditions and the nominal control input are calculated by inserting the parameter values mentioned in Table 5.1 into Equation (3.36). Then, the obtained results are expressed as follows:

$$\begin{aligned} x_{20} &= 0 \\ x_{30} &= 21.21 \\ u_0 &= 25.45 \end{aligned} \tag{5.1}$$

5.3 Controller Parameter Settings

5.3.1 Parameter Settings for the Proposed Backstepping Controller

The three design parameters of the BSC represented as k_1, k_2, and k_3 are determined using the particle swarm optimization algorithm. The details of the PSO technique parameter settings which are used in the simulation are illustrated in Table 5.2.

Table 5.2 Parameter settings of the PSO

Parameter		Value
Swarm size		20
Maximum iteration		30
Number of the parameters		3
Inertia weight	ω_{min}	0.4
	ω_{max}	0.9
Acceleration constant	c_1	2
	c_2	2
Lower bounds		[0.0001 0.0001 0.0001]
Upper bounds		[38 75 75]

The graphical result of the PSO technique with its best function value is shown in Figure 5.1. The minimum best function value is 0.020271 at iteration 30.

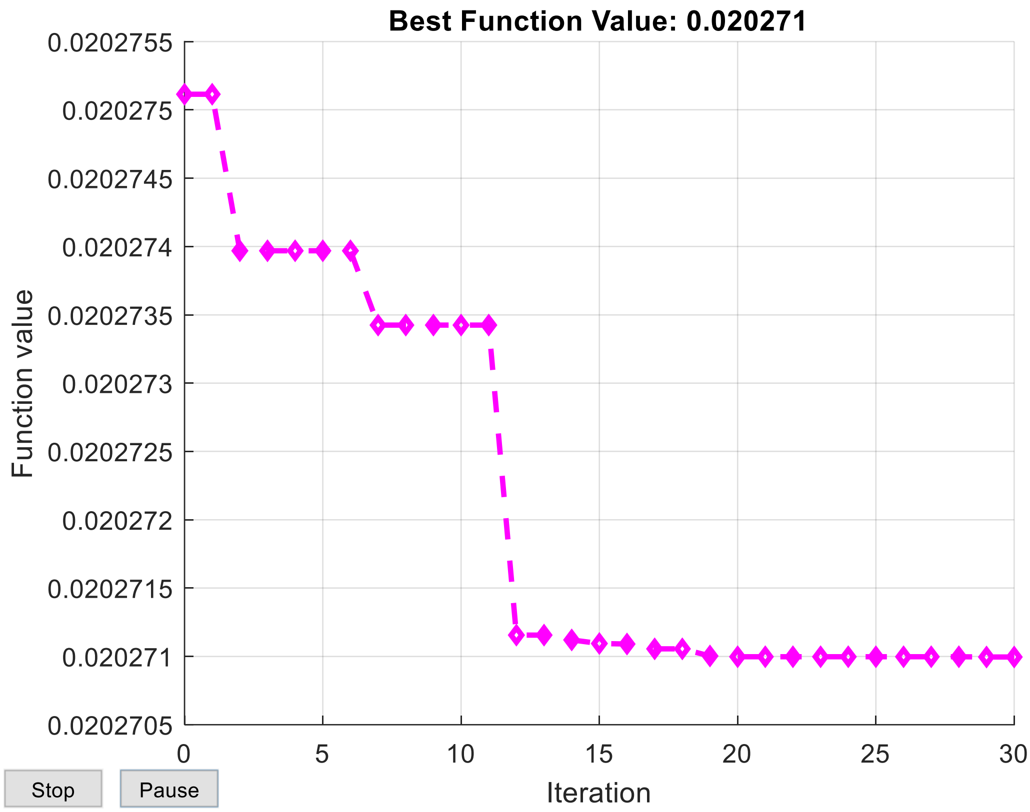

Figure 5.1 Convergence curve of the PSO algorithm

The optimization algorithm runs for 30 iterations to find a minimum value for the proposed objective function in Equation (4.43) using the algorithm settings given in Table 5.2. Figure 5.1 illustrates a graph of the objective function vs. a number of iterations. The PSO reaches the best solution at the 19th iteration. The PSO optimized tuned parameter values of the proposed BSC are shown in Table 5.3.

Table 5.3 Optimal values of the BSC gains

Optimization Technique	BSC gains		
	k_1	k_2	k_3
PSO	33.5416	33.6734	31.1596

5.3.2 Parameter Settings for the LQR controller

The primary design parameters of the LQR controller state (Q) and control (R) weighting matrices are selected by the designer. The proper selection of these weighting matrices is required for a successful LQR design. In this thesis work, the weighting matrices that are given below are selected after many times of trial and error method.

$$Q = \begin{bmatrix} 0.1 & 0 & 0 & 0 \\ 0 & 0.1 & 0 & 0 \\ 0 & 0 & 0.1 & 0 \\ 0 & 0 & 0 & 8\times 10^{7} \end{bmatrix} \text{ and } R = 1\times 10^{-4} \tag{5.2}$$

The feedback gain matrix is obtained using the MATLAB "$\tilde{K} = lqr(\tilde{A}, \tilde{B}, Q, R)$" command with these Q and R values.

Where $\tilde{A} = \begin{bmatrix} A & 0 \\ C & 0 \end{bmatrix} = \begin{bmatrix} 0 & 1 & 0 & 0 \\ 1962 & 0 & -0.9 & 0 \\ 0 & 2121 & -3.9 & 0 \\ 1 & 0 & 0 & 0 \end{bmatrix}$ and $\tilde{B} = \begin{bmatrix} B \\ 0 \end{bmatrix} = \begin{bmatrix} 0 \\ 0 \\ 3275.5 \\ 0 \end{bmatrix}$ are obtained by inserting the system parameter values mentioned in Table 5.1 into Equation (4.50) which is discussed in section 4.5.

5.4 Tracking Performance Tests

In this section, the tracking performance of the backstepping controller is compared to that of the LQR controller. Step signal, multiple step signal, and sinusoidal signal are used as the tracking references. The controllers performance is evaluated by plotting the actual output of the system with that of the reference signals. Moreover, the tracking performance of the controllers is evaluated in the presence of external disturbance force and load variation.

5.4.1 Tracking performance under normal condition

This section discusses the tracking performance of the proposed BSC and LQR controllers for single step, multiple step, and sinusoidal signals under normal conditions, that is, without considering the effect of external disturbance and load variation.

5.4.1.1 Single step signal

The tracking performance of the proposed and LQR controllers in tracking the single step signals is evaluated using two different constant reference signals. These test signals are used to demonstrate the stationary suspension, which is one the benefits of the EMS maglev train system. They are also used to test straight path terrain tracking ability of the system.

A. Upward test case

This test case represents the tracking response when the initial position of the suspension air gap is 10mm, and the target position is 12mm. The simulation results of the proposed BSC and LQR controllers to this test case for 2 seconds are illustrated in Figures 5.2 and 5.4. It is shown in Figure 5.2 (a) that both control methods follow the reference signal satisfactorily. The result shows that the proposed backstepping controller responds more quickly to the suspension air gap position change than the LQR controller.

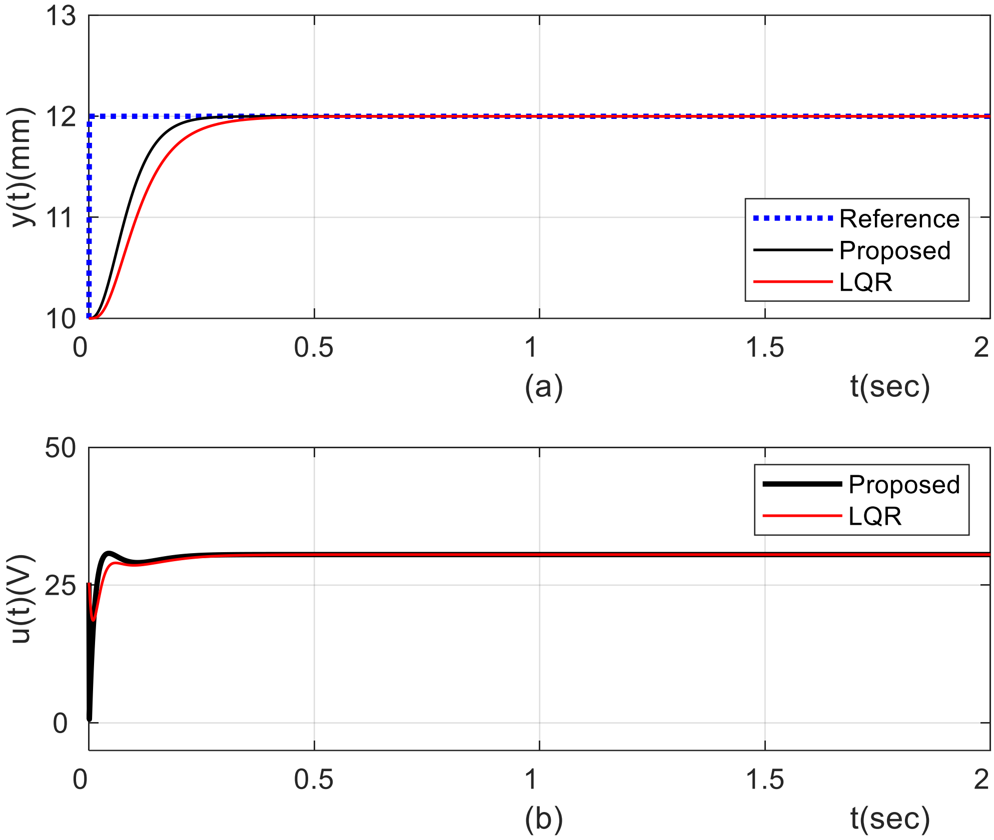

Figure 5.2 Upward test case tracking response of the proposed BSC and LQR controllers with their control input signals

Figure 5.2 (b) shows the control input response maglev train system using the proposed BSC and LQR controllers. The train was forced to follow the desired position by applying a small control input voltage of about 30.54 V. The tracking performance of the proposed BSC and LQR control methods is given in terms of IAEU and transient response characteristics, namely settling time, overshoot, rise time, and peak time, as shown in Table 5.4 below.

Table 5.4 Tracking performance specifications for Upward test case

Tracking controller	Performance characteristics				
	M_p	t_p	t_r	t_s	*IAEU*
Proposed BSC	0	0.639	0.128	0.190	0.181
LQR	0	2.0	0.173	0.267	0.245

Table 5.4 which summarizes the step reference performance characteristics of the LQR and backstepping controller, even though both controllers have 0 overshoot value, the proposed backstepping controller achieves better performance by reducing the peak time by 68.05%, the rise time by 26.01%, the settling time by 28.84% and the IAEU value by 26.12% as compared to the LQR controller. So, it is clear from these numerical performance indicators that the proposed controller has better tracking performance for the given reference signal. Figure 5.3 depicts the graphical representation which compares the transient performance characteristics of both controllers for the upward test case. The graph demonstrates that the BSC controller has better tracking performance than the LQR.

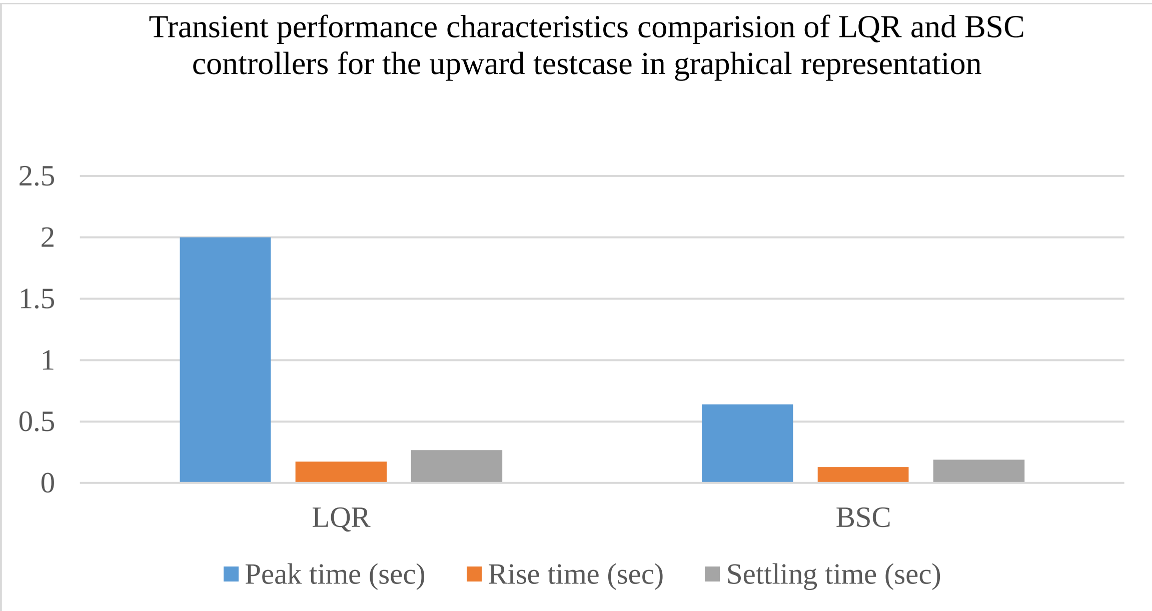

Figure 5.3 Graphical representation of LQR and BSC controllers for the upward test case tracking performance based on transient performance characteristics

Figure 5.4 depicts the tracking error, which is the difference between the actual output and the desired references.

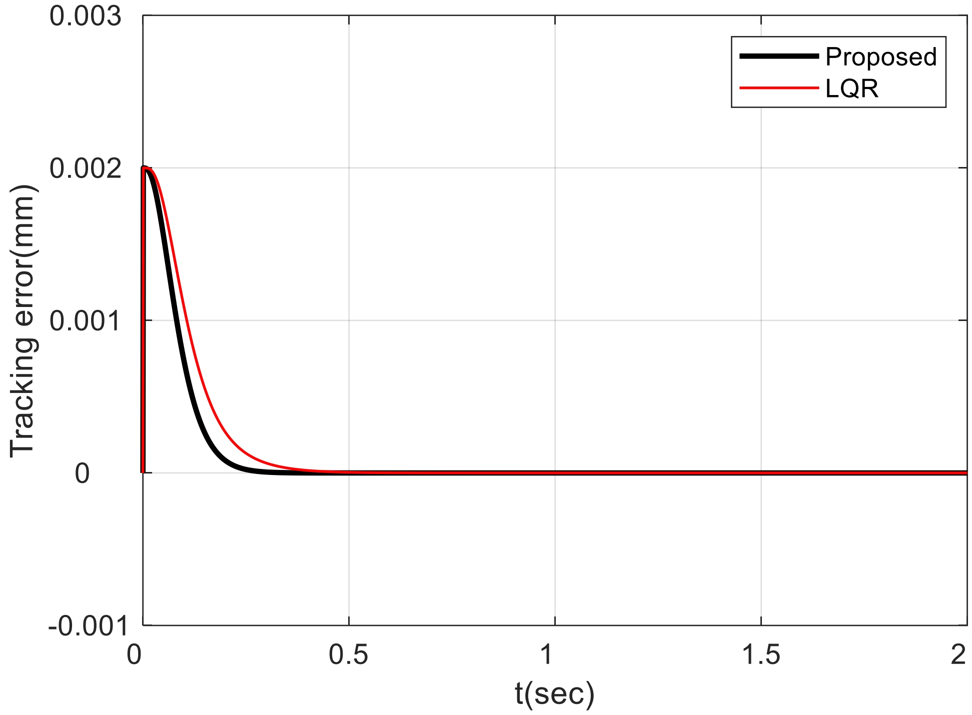

Figure 5.4 Tracking error for Upward test case

From Figure 5.4 above, the tracking error converges to zero and remains close to zero for both control strategies. However the proposed controller's tracking error drops to zero faster than that of the LQR controller.

B. Downward test case

This test case represents the tracking response when the maglev train system is levitated from 10mm to 8mm. Figures 5.5 and 5.7 show the simulation results of the proposed BSC and LQR controllers for this test case. The simulation is run for 2 seconds. Figure 5.5 (a) illustrates how well both control mechanisms track the desired reference signal. The input control signal of the system using the proposed BSC and LQR controllers due to the given reference step input is shown in Figure 5.5 (b). A control input voltage of about 20.36 V is used to force the train to follow the desired reference signal.

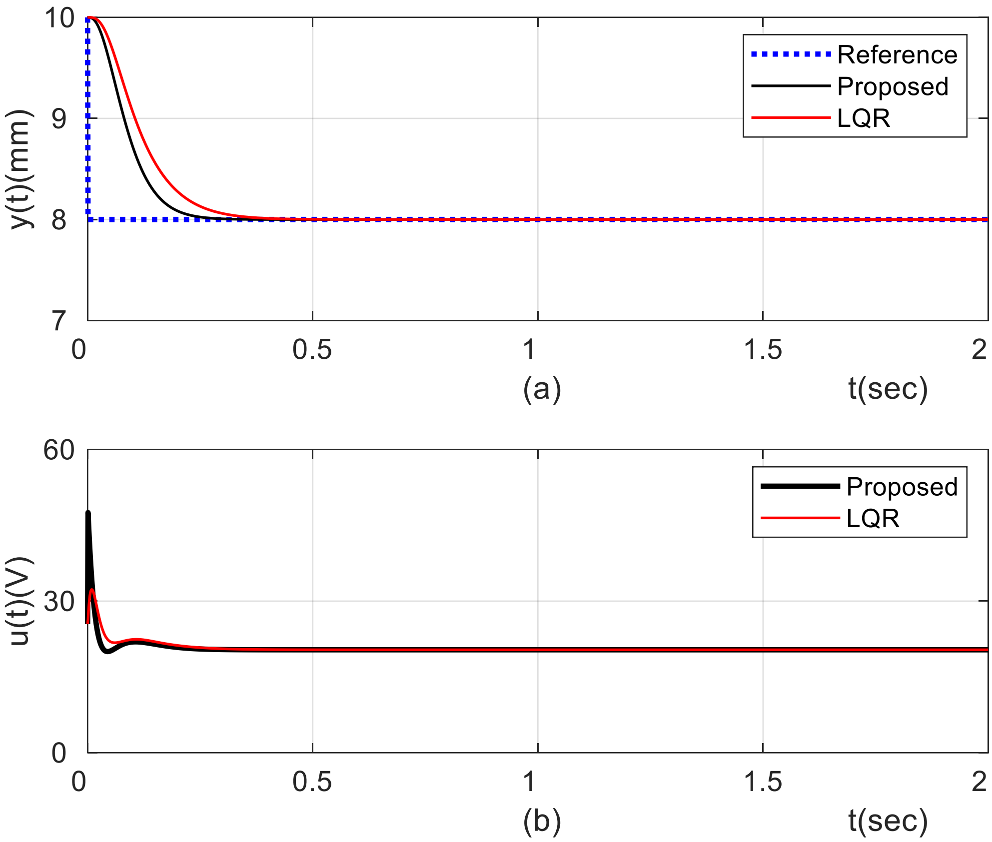

Figure 5.5 Downward tracking response of the proposed BSC and LQR controllers with their control input signals

The tracking performance of the proposed BSC and LQR methods is compared in terms of peak time, rise time, overshoot, settling time, and IAEU in Table 5.5.

Table 5.5 Tracking Performance Specifications for Downward test case

Tracking controller	Performance characteristics				
	M_p	t_p	t_r	t_s	$IAEU$
Proposed BSC	0	0.651	0.129	0.193	0.183
LQR	0	0.941	0.176	0.267	0.245

Table 5.5 shows that the backstepping controller has lower values for peak time, rise time, settling time, and IAEU, with 0.651 seconds, 0.129 seconds, 0.193 seconds, and 0.183, respectively.

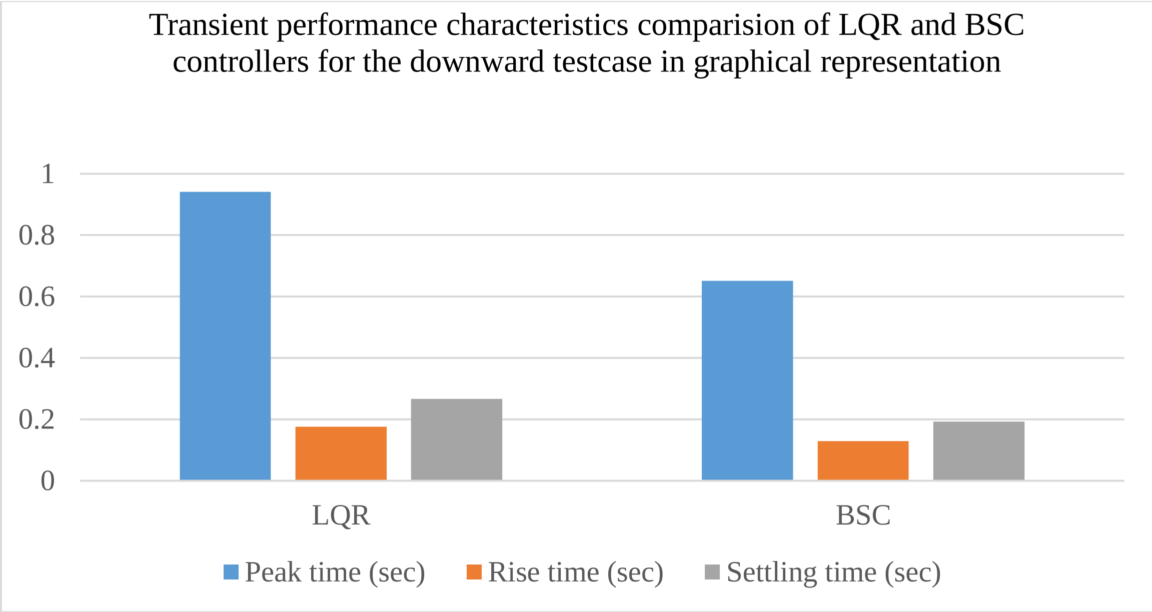

Figure 5.6 Graphical representation of LQR and BSC controllers for the downward test case tracking performance based on transient performance characteristics

Figure 5.6 depicts the graphical representation which compares the transient performance characteristics of both controllers for the downward test case. The graph demonstrates that the BSC controller has better tracking performance than the LQR.

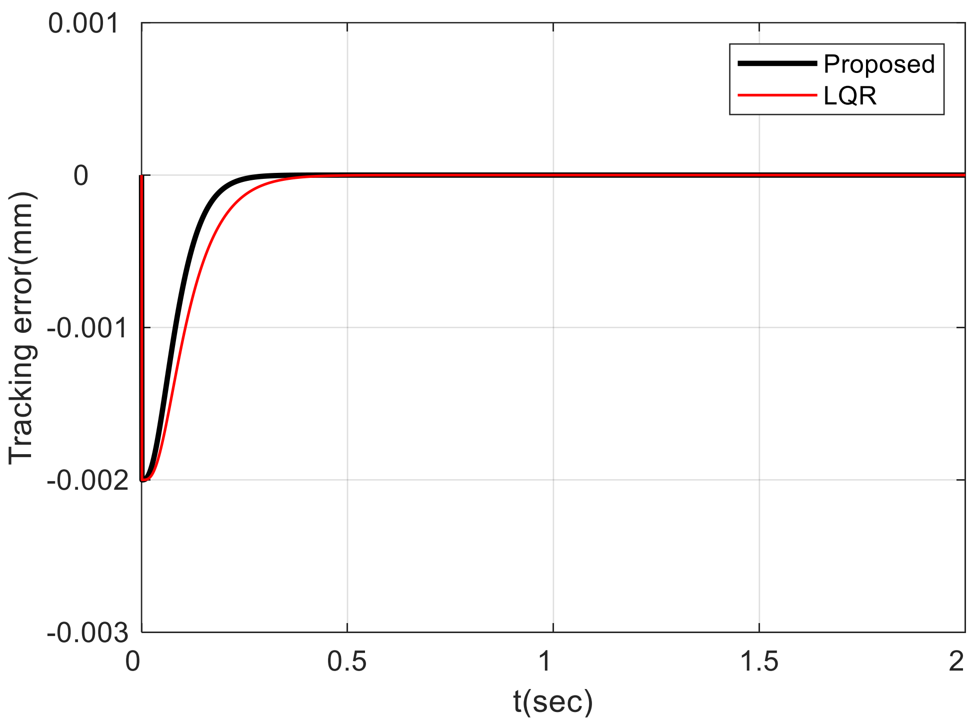

Figure 5.7 Tracking error for Downward test case

The simulation result of the tracking error is depicted in Figure 5.7 above. The tracking error of LQR controller takes longer time to approach to zero than the BSC controller.

5.4.1.2 Multiple step signal

In this research work, multiple step signal references are used to evaluate the controller's performance in tracking terrains with a straight path and a curb lane. It is also used to analyze the tracking ability of both control methods in a given range of desired height. Two different multiple step signal testing scenarios are used to analyze the tracking performance of both controllers. The tracking ability of both controllers for these reference signals is compared by using the value of IAEU.

A. Up-Down-Down-Up signal scenario

In this scenario, the tracking response is tested when the suspension air gap is increased from 10mm to 12mm (Up) initially, then decreased from 12mm to 10mm (Down) at a time of 3 seconds, decreased from 10mm to 8mm (Down) at the time of 6 seconds, and finally increased from 8mm to 10mm (Up) at the time of 9 seconds. The simulation results of the BSC and LQR controllers for this scenario over a time period of 12 seconds are shown in Figures 5.8 and 5.9. The control parameters of both algorithms are consistent with the single step signal tracking. From the tracking responses below, both controllers are able to track the given reference signal satisfactorily, but the LQR has a delay tracking compared with the BSC, as shown in the zoom portions of Figure 5.8 (a). The backstepping and LQR controllers have 0.724 and 0.974 values of IAEU, respectively. The IAEU values indicate that the backstepping controller maintains better tracking for the given reference signal by reducing it by 25.67% as compared to the LQR controller. As can be seen from Figure 5.8 (b) a fluctuating control effort is required to track the given reference signal.

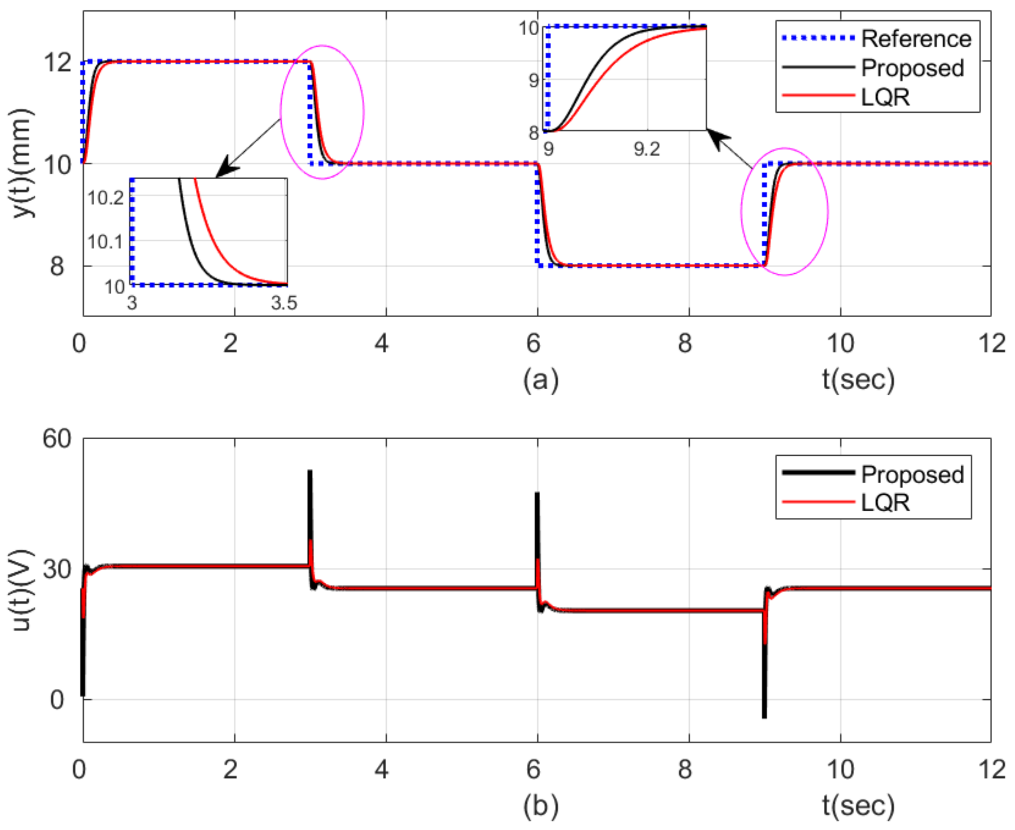

Figure 5.8 Up-Down-Down-Up signal tracking response of the proposed BSC and LQR controllers with their control input signals

The tracking error of both control strategies , which was close to zero before the variation of the reference signals, re-converges to zero after short transience, as shown in Figure 5.9. However, the zoom portions illustrate that the proposed controller's tracking error re-converges to zero faster than the LQR controller's. The zoom portions also indicated that the error of the BSC changes faster, while LQR takes some time, which demonstrates that the proposed backstepping controller has a faster tracking performance.

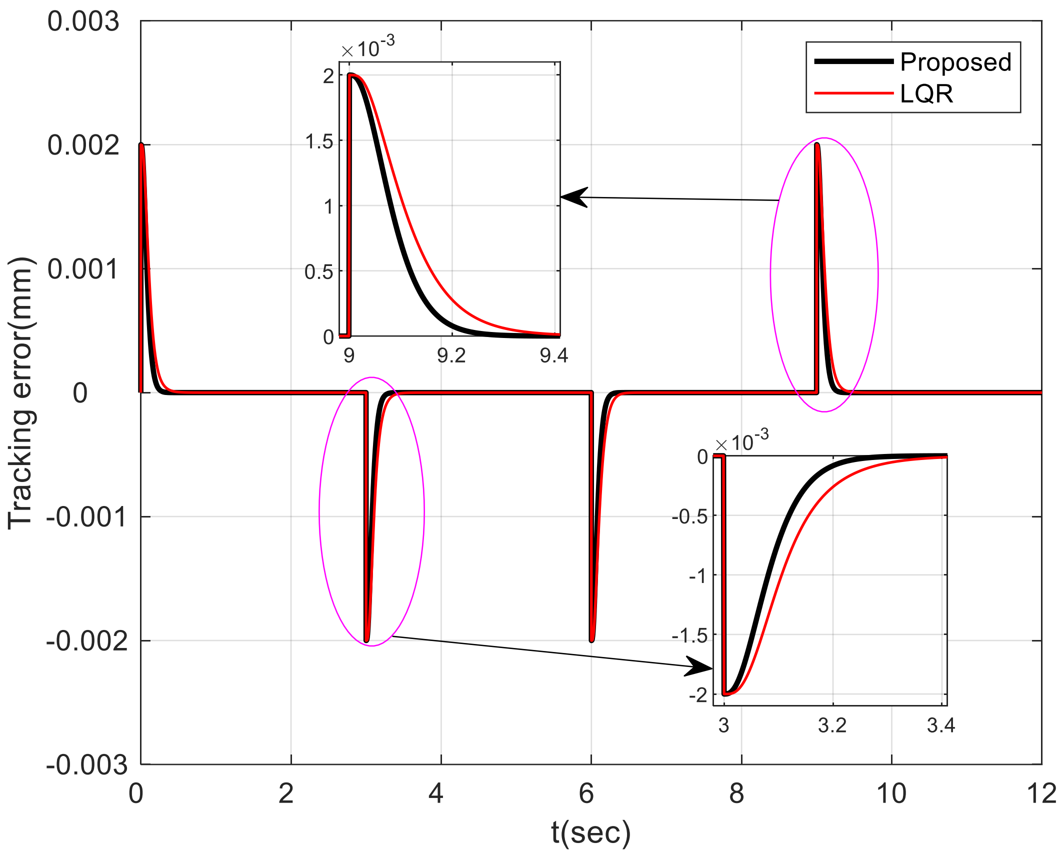

Figure 5.9 Tracking error of both controllers for Up-Down-Down-Up signal

B. Down-Up-Up-Down signal scenario

In this scenario, the tracking response is tested by decreasing the suspension air gap from 10mm to 8mm (Down) initially, increasing from 8mm to 10mm (Up) after three seconds, increasing from 10mm to 12mm (Up) after six seconds, and then decreasing from 12mm to 10mm (Down) after nine seconds.

Figures 5.10 and 5.11 show the simulation results of the BSC and LQR controllers for this scenario. The simulation is run for 12 seconds to see the clear difference between the tracking responses of the system with both control strategies. Figure 5.10 (a) clearly shows that the tracking response of both controllers is almost consistent with the given reference signal. However the proposed BSC control technique reaches to the desired reference signal faster than the LQR controller, as illustrated in the zoom portions of Figure 5.10 (a).

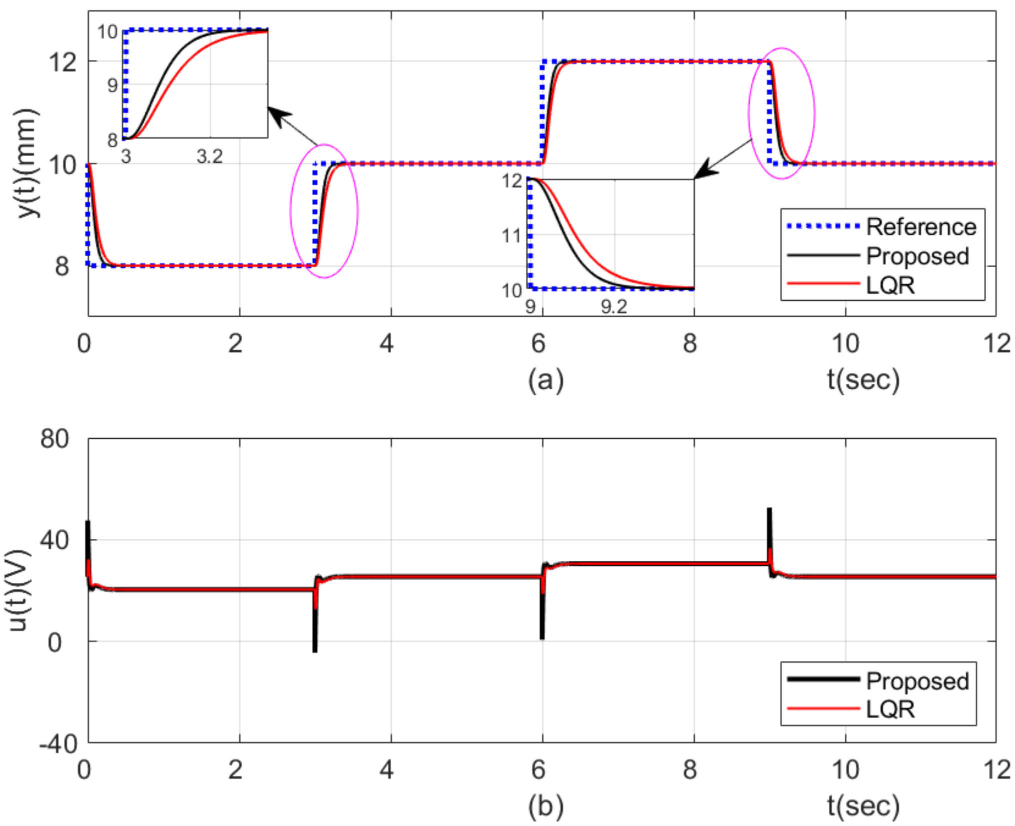

Figure 5.10 Down-Up-Up-Down signal tracking response of the proposed BSC and LQR controllers with their control input signals

The BSC and LQR have 0.724 and 0.974 values of IAEU, respectively. The IAEU values indicate that the backstepping controller maintains better tracking for the given reference signal by reducing it by 25.67% as compared to the LQR controller. Figure 5.10 (b) depicts the fluctuating control effort required to track the given reference multiple step signal. As shown in Figure 5.11 below, the tracking error of both control strategies, which was close to zero before the variation of the reference signals, re-converges to zero after short transience. The zoom portions illustrate that the tracking error of the proposed controller re-converges to zero faster than that of the LQR controller.

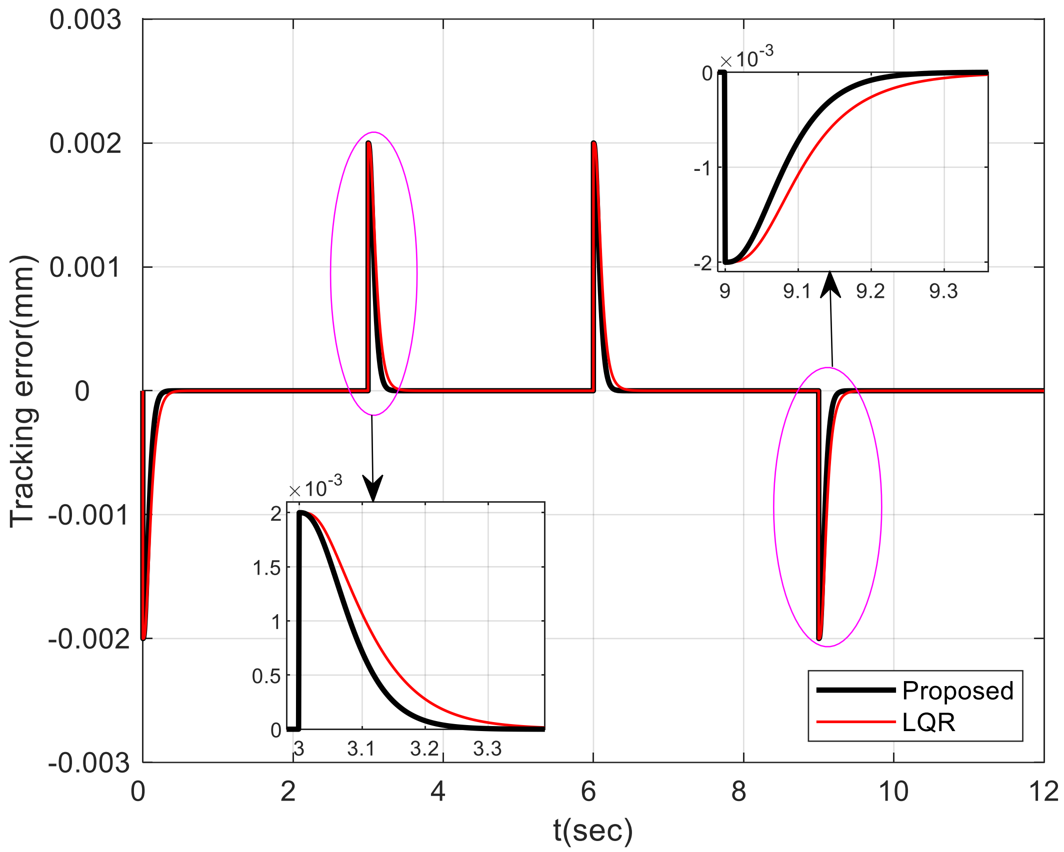

Figure 5.11 Tracking error for Down-Up-Up-Down signal

5.4.1.3 Sinusoidal signal

The tracking performance of the maglev train using the BSC and LQR controllers with a sinusoidal signal is analyzed in this section. The sinusoidal signal $(10+2\times\sin(5t))$ is used in this thesis work. The reason behind the choice of the sinusoidal signal is to test both controllers' ability to track terrains such as curved lanes, turn lanes, and climbing lanes. The sinusoidal signal can test the rapidity of the control algorithms, as it varies smoothly and changes rapidly. The simulation results of both controllers to this signal for 2 seconds are illustrated in Figures 5.12 and 5.13. Figure 5.12 (a) demonstrates that the proposed BSC nicely tracks the desired sinusoidal signal while the LQR controller fails to track the desired sinusoidal reference signal at all.

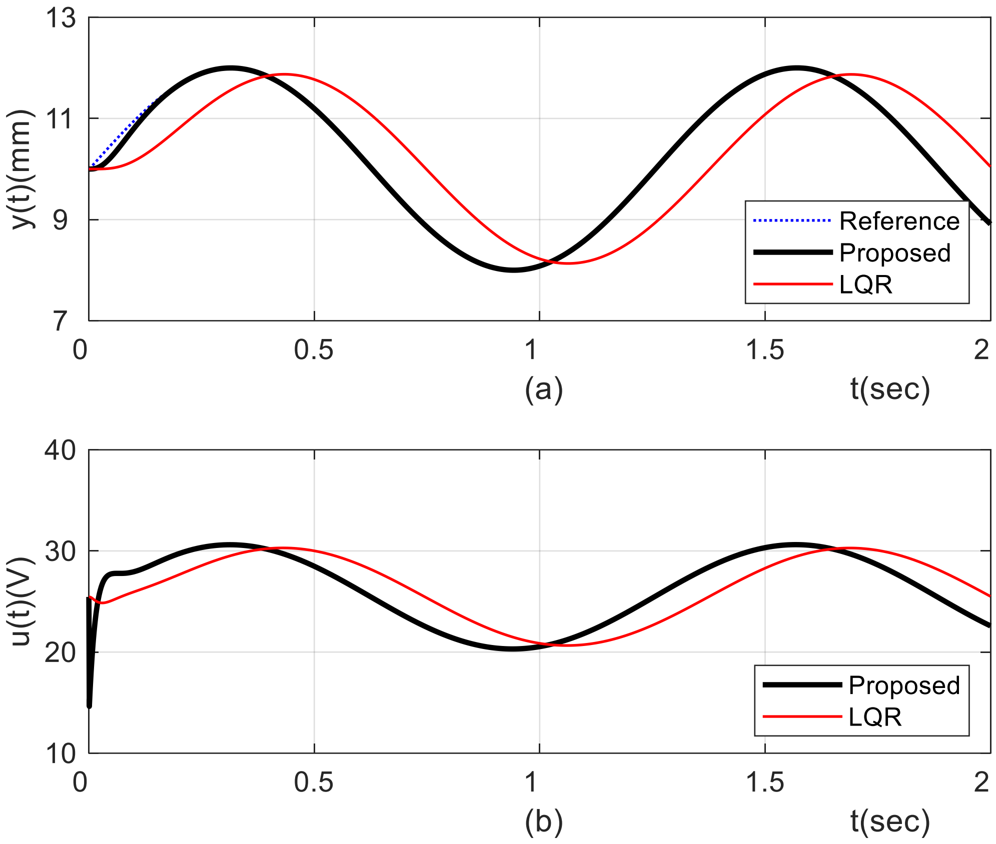

Figure 5.12 Tracking response of the proposed BSC and LQR controllers for sinusoidal reference with their control input signals

The backstepping and LQR controllers have 0.037 and 1.411 value of IAEU, respectively. The proposed controller achieves better tracking performance by reducing the IAEU by 97.38% as compared to the LQR. The IAEU values and the above tracking response shows that the proposed controller can satisfactorily track the given sinusoid reference. Figure 5.12 (b) depicts that a fluctuated control effort is required to force the train to follow the desired sinusoidal signal. The tracking error of both control strategies is depicted in Figure 5.13. The response clearly shows that the tracking error of the proposed controller is stable around zero, whereas the LQR controller has a large amount of tracking error that does not converge to zero.

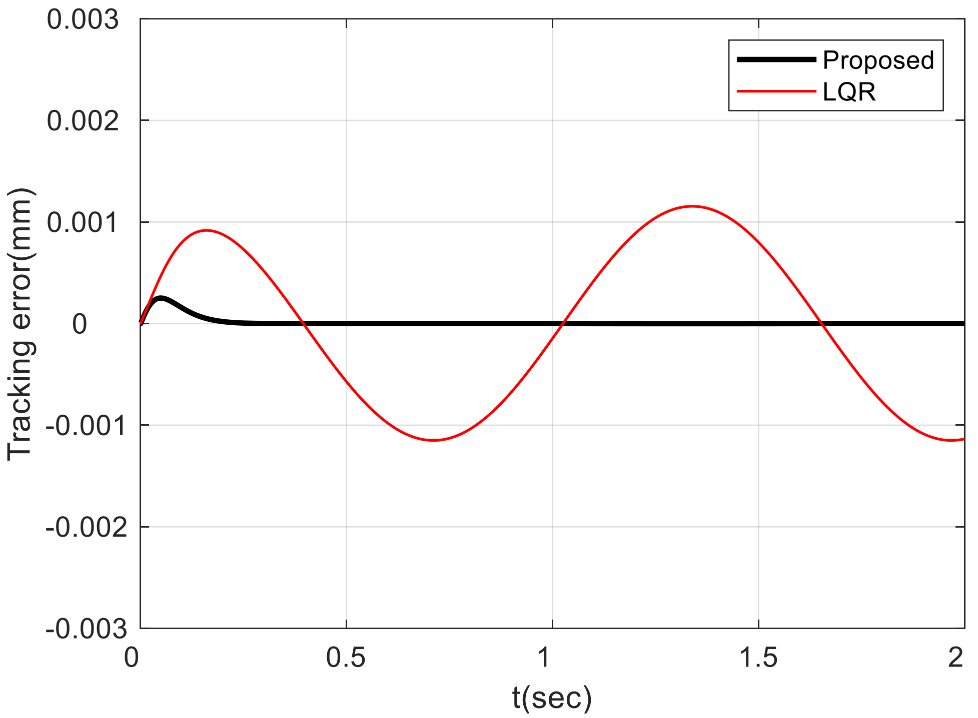

Figure 5.13 Tracking error for the sinusoidal reference

Figure 5.14 depicts the graph which represents the tracking performance comparison of LQR and BSC controllers based on IAEU values for different types of reference signals explained in the above sections. The graph shows that the BSC has a lower IAEU value for all the given references.

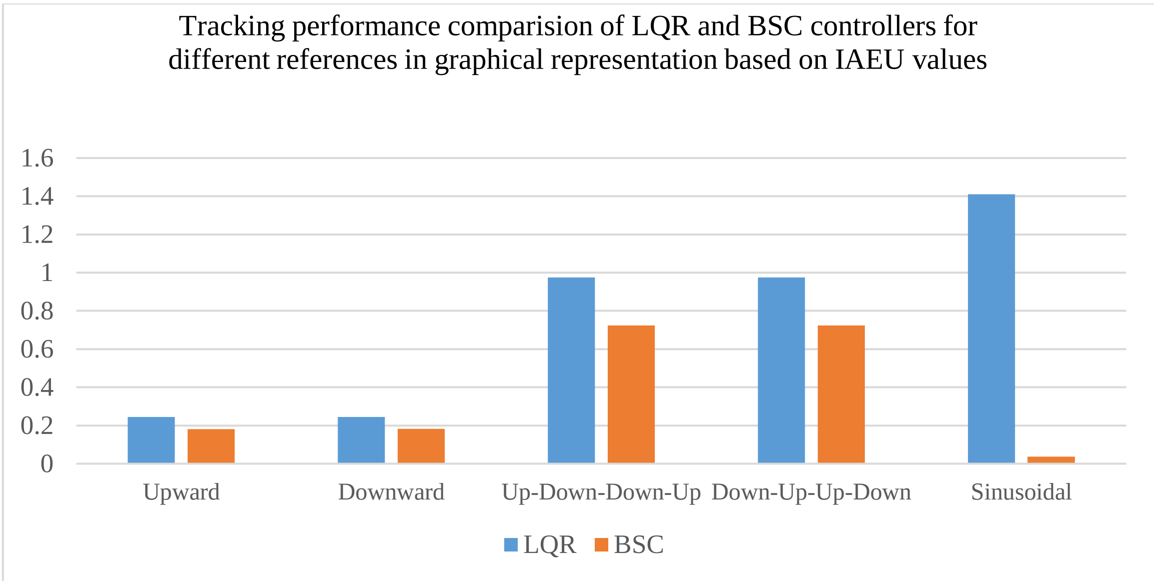

Figure 5.14 Graphical representation of LQR and BSC controllers for different references tracking performance based on based on IAEU values

5.4.2 Robust tracking performance

It is necessary for the maglev train system to be robust and to have a fast response time so that the train does not fall. In this section, the performance robustness of the backstepping and LQR controllers is evaluated. This thesis work considers two different conditions to test the tracking performance robustness of the system. The first one is load variation (mass change in the vehicle) and the other is external disturbance force.

5.4.2.1 Robustness against load variation

This section focuses on the load variation of the maglev train, which is regarded as an internal disturbance of the system. The suspension must support the total mass of the train which includes both the vehicle’s mass and the load (weight of passengers). In this thesis work, the load variations up to 40% of the train mass are taken in to account. This section has two parts. In the first part of this section, the robustness of both control strategies in the presence of 10%, 20%, and 40% of mass change is tested. Because of the frequent and significant load changes in the maglev train system, the tracking performance robustness of both control strategies with time-varying load change is tested in the second part of this section.

A. Constant load variations

In this section, the system’s robustness is tested when the original mass of the train is increased by load mass of 70kg, 140kg, and 280kg, which correspond to 10%, 20%, and 40% of the train's actual mass, respectively. Thus, the total mass will increase to 770 kg, 840kg, and 980 kg.

Figures 5.15 and 5.16 illustrate the simulation response of the magnetic suspension air gap and the tracking error when the train mass is increased to 770kg using the LQR and BSC control strategies.

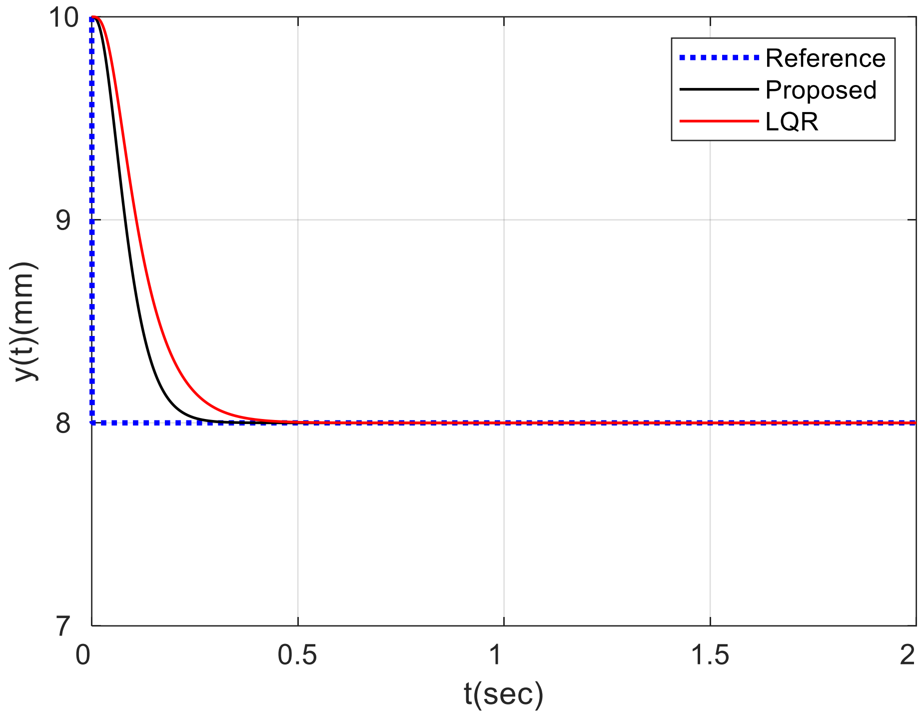

Figure 5.15 Tracking response with a 10% increment in the train mass

According to the figure above, both control methods satisfactorily follow the reference signal with an internal disturbance of a 70kg load mass. The result clearly shows that the proposed backstepping controller settles faster than the LQR controller. The tracking performance of both control strategies with a 10% increase in load mass is compared in Table 5.6 in terms of peak time, rise time, overshoot, settling time, and IAEU.

Table 5.6 Transient performance measures with a 10% increment in the mass of the train

Tracking controller	Performance characteristics				
	M_p	t_p	t_r	t_s	*IAEU*
Proposed BSC	0	0.651	0.129	0.193	0.183
LQR	0	1.597	0.184	0.278	0.252

Table 5.6 clearly shows that the proposed BSC achieves better performance by reducing the peak time by 59.24%, the rise time by 29.89%, the settling time by 30.57% and the IAEU value by 27.38% as compared to the LQR controller. As a result, the BSC has better

robustness against the given mass change than that of the LQR controller.

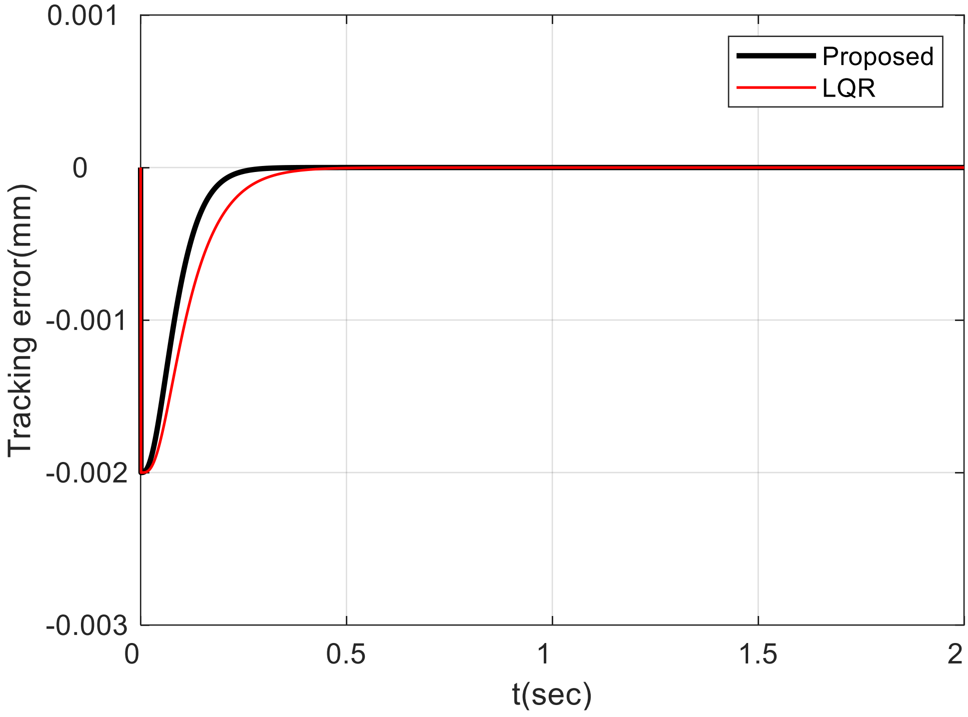

Figure 5.16 Tracking error response with a 10% increment in the train mass

The simulation result of the tracking error, presented in Figure 5.16, shows that the tracking error of the proposed controller approaches to zero faster than that of the LQR controller.

Figures 5.17 and 5.18 illustrate the simulation response of the magnetic suspension air gap and tracking error when the total mass of the train is increased to 840kg using the LQR and BSC control strategies, respectively. Both control methods nicely follow the given reference signal with an internal disturbance of 140kg load mass, as shown in Figure 5.17 below. The results demonstrate that the proposed backstepping controller settles to the desired reference faster than the LQR controller.

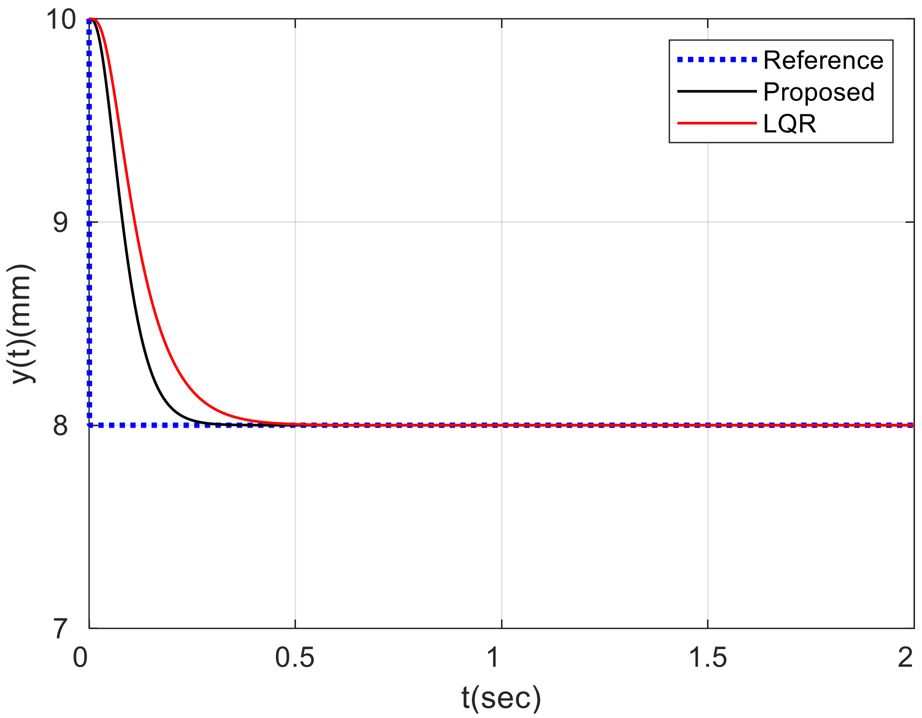

Figure 5.17 Tracking response with a 20% increment in the train mass

Table 5.7 summarizes the transient performance characteristics and IAEU values of both control methods in the presence of 20% increase in the train mass.

Table 5.7 Transient performance measures with a 20% increment in the mass of the train

Tracking controller	Performance characteristics				
	M_p	t_p	t_r	t_s	*IAEU*
Proposed BSC	0	0.651	0.129	0.193	0.183
LQR	0	2.228	0.191	0.289	0.261

The numerical performance indicators in Table 5.7 depicted that the proposed backstepping controller has stronger robustness under the given load increment than that of the LQR controller. The proposed BSC achieves better performance by reducing the peak time by 70.78%, the rise time by 32.46%, the settling time by 33.22% and the IAEU value by 29.88% as compared to the LQR controller. Thus, the proposed controller has better robustness against the given 20% mass change than the LQR controller.

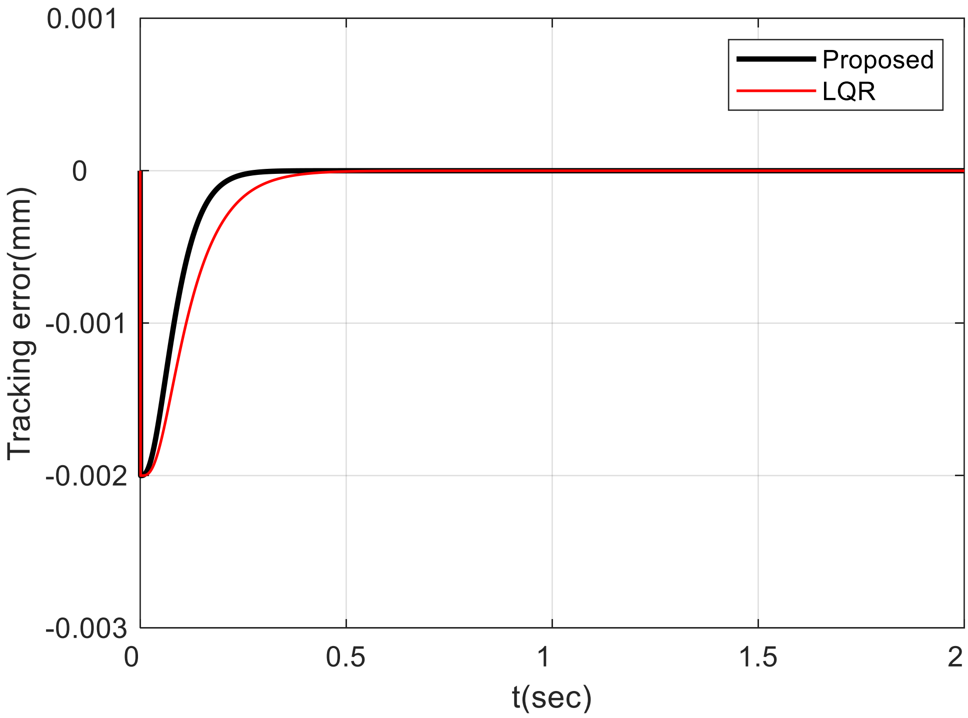

Figure 5.18 Tracking error response with a 20% increment in the train mass

Even though the tracking error of both control strategies converges to zero and remains close to zero, the tracking error of the proposed control method drops to zero quickly, while the tracking error of LQR controller takes longer time to approach to zero.

Figures 5.19 and 5.20 illustrate the simulation response and the tracking error of the LQR and proposed backstepping control strategies for the maglev train when the train load mass is changed to 980kg which indicates 40% increment in the train mass, respectively. Both control schemes follow the reference signal nicely in the presence of an internal disturbance of 280kg load mass, as shown in the figure below. The simulation result shows that the proposed backstepping controller settles to the desired reference suspension air gap faster than the LQR controller.

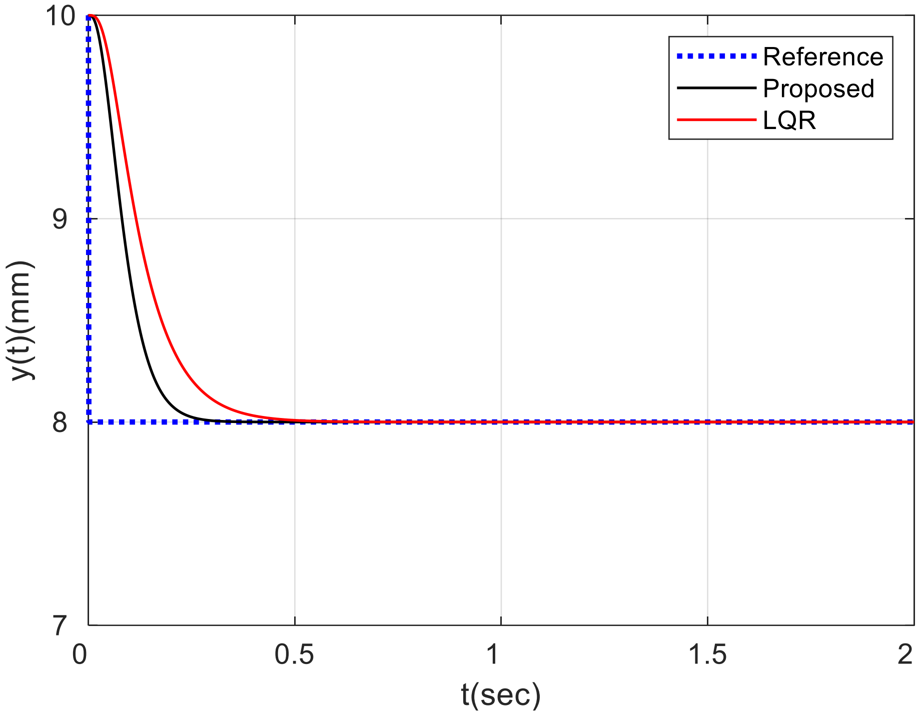

Figure 5.19 Tracking response with a 40% increment in the train mass

The transient performance characteristics and IAEU values of both control methods in the presence of 40% increase in the train mass is summarized in Table 5.8.

Table 5.8 Transient performance measures with a 40% increment in the mass of the train

Tracking controller	Performance characteristics				
	M_p	t_p	t_r	t_s	*IAEU*
Proposed BSC	0	0.652	0.129	0.193	0.183
LQR	0	2.524	0.205	0.308	0.273

Table 5.8 shows that the proposed backstepping controller achieves better performance by reducing the peak time by 74.17%, the rise time by 37.07%, the settling time by 37.34% and the IAEU value by 32.97% as compared to the LQR controller. The performance indicators in the Table 5.8 above verifies the robustness of the proposed control strategy under a 40% increase in train mass, which ensures that the system remains in a stable suspension state when the load mass is changed over a wide range.

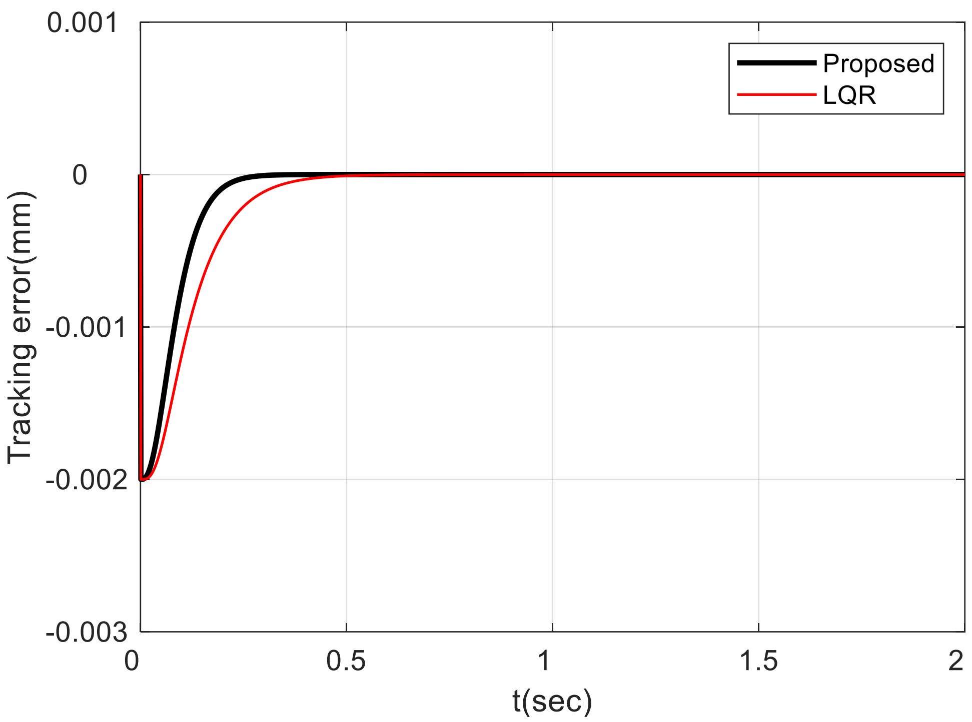

Figure 5.20 Tracking error response with a 40% increment in the train mass

The simulation result of the tracking error is depicted in Figure 5.20 above. The figure shows that the tracking error of the proposed control method drops to zero quickly, while the tracking error of LQR controller takes longer time to approach to zero.

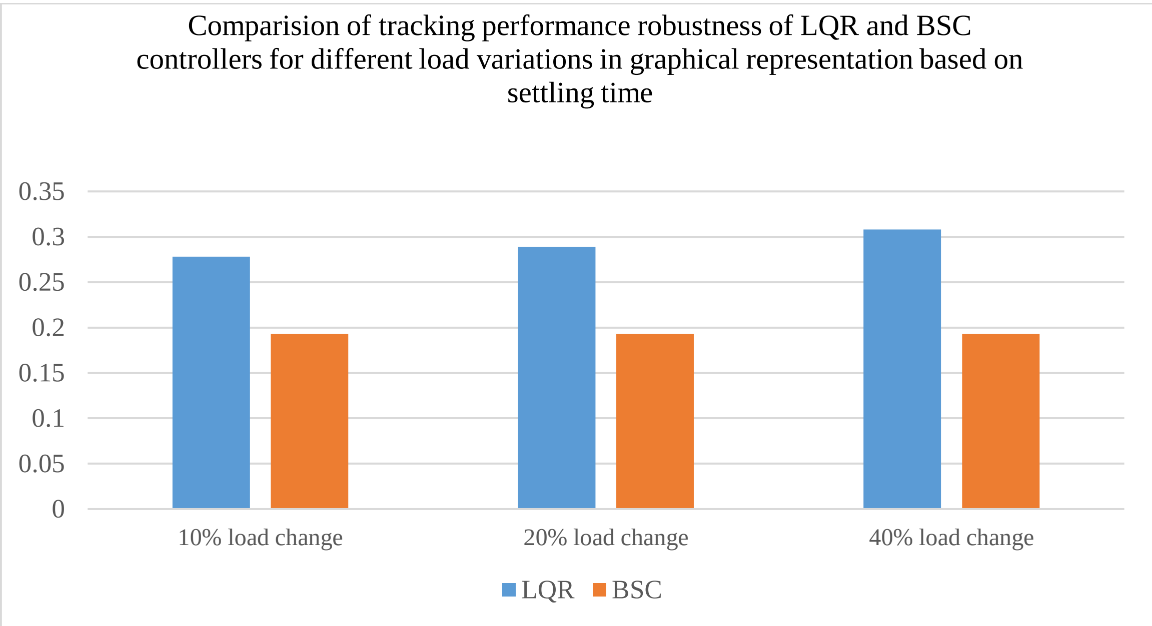

Figure 5.21 Graphical representation of tracking performance robustness of LQR and BSC controllers under different load variations based on settling time

Figure 5.21 compares the tracking performance robustness of LQR and BSC controllers for different load variations based on settling time. The graph verifies that the BSC controller has better tracking performance robustness than the LQR under the taken load variations.

B. Time-varying load variations

It should be noted that the number of passengers at each station varies greatly. During rush hour, the train is heavy and full, but it is empty during non-peak times. As can be seen, the load mass varies significantly in this system. In this part of section 5.4.2.1, the system's robustness is tested as the train's mass increases and varies throughout the simulation. The following varying load changes is considered in this thesis work. The robust tracking performance is tested when the train remains empty until 4 second, then the mass of the train is increased by 40% until 8 second, a 20% decrement is considered from 8 to 12 second, and a 10% decrement is considered from 12 second to the end of the simulation. The simulation responses of the magnetic suspension air gap and the tracking error for this varying load changes are shown in Figures 5.22 and 5.23, respectively.

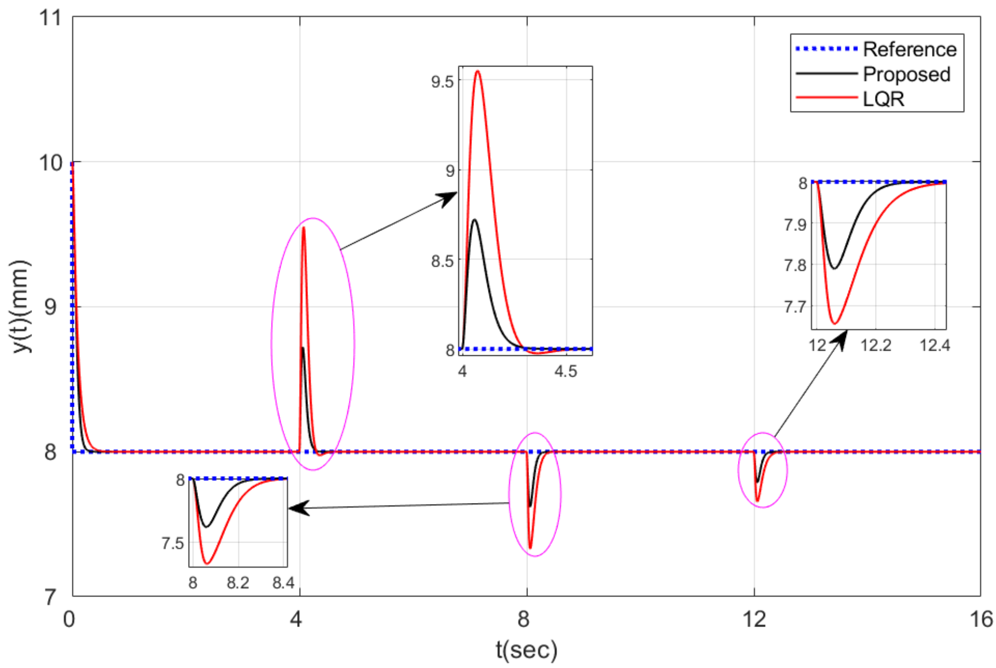

Figure 5.22 Tracking response under sudden increment and drop in the train mass

According to Figure 5.22, in the case of the BSC control scheme, a load of 280kg is increased on the train mass in 4 second, and the air gap distance between the train and the track is increased from 8mm to about 8.72mm at 4.06 second. In about 4.4 second the air gap distance is maintained at 8mm. In 8 second, a load of 140kg is retained from the initial added load of 280kg, and the air gap distance between the train and the track is reduced from 8mm to 7.62mm at 8.06 second. The air gap distance is maintained at 8mm in 8.37 second. A load of 70kg is remained from the total 350 kg increment in 12second, and the air gap distance between the train and the track is reduced from 8mm to 7.79mm at 12.06 second. In 12.36 second, the air gap distance is maintained at 8mm. The minimum and maximum air gap distance variations are 7.62mm and 8.72mm, respectively.

On the other hand, the LQR controller increases the air gap distance between the train and the track from 8mm to 9.55mm at 4.07 second when a load of 280kg is applied to the train mass at 4 second, as shown in Figure 5.22. The air gap distance is kept at 8mm in 4.58 second. The air gap distance between the train and the track decreased from 8mm to 7.33mm at 8.06 second when a load of 140kg is remained from the initial added load of 280kg at 8 second. The air gap distance is kept at 8mm in about 8.46 second. A load of 70kg is kept out of the total 280kg increment at 12 second, and the air gap distance between the train and the track is immediately reduced from 8mm to 7.65mm at 12.06 second. The air gap distance is maintained at 8mm in 12.55 second. The minimum and maximum variations of the air gap distance are 7.33mm and 9.55mm, respectively.

The above analysis shows that when the load mass changes significantly, the BSC controller reduces the fluctuation of the suspension air gap while maintaining tracking performance when compared to the LQR controller. Table 5.9 summarizes the quantitative comparison of the two control algorithms.

Table 5.9 Performance measures under sudden increment and drop in the train mass

Tracking controller	Performance characteristics				
	M_p	t_p	t_r	t_s	*IAEU*
Proposed BSC	19.044	8.059	0.124	12.128	0.303
LQR	33.496	8.062	0.198	12.201	0.556

Table 5.9 above illustrates that the backstepping controller performs better on all numerical performance indicators. The proposed BSC achieves better performance by reducing the

overshoot by 43.14%, the peak time by 0.037%, the rise time by 37.37%, the settling time by 0.61%, and the IAEU value by 45.5% as compared to the LQR controller. As a result, the BSC has better robustness against the given time varying mass change than that of the LQR controller.

Figure 5.23 below depicts the tracking error when the train mass increases and decreases abruptly. The tracking error which was nearly zero prior to the mass change re-converges to zero after a short time, demonstrating the robustness of the proposed controller. That is, the tracking error stabilizes around zero and remains there except for a brief period of time following a change in load mass.

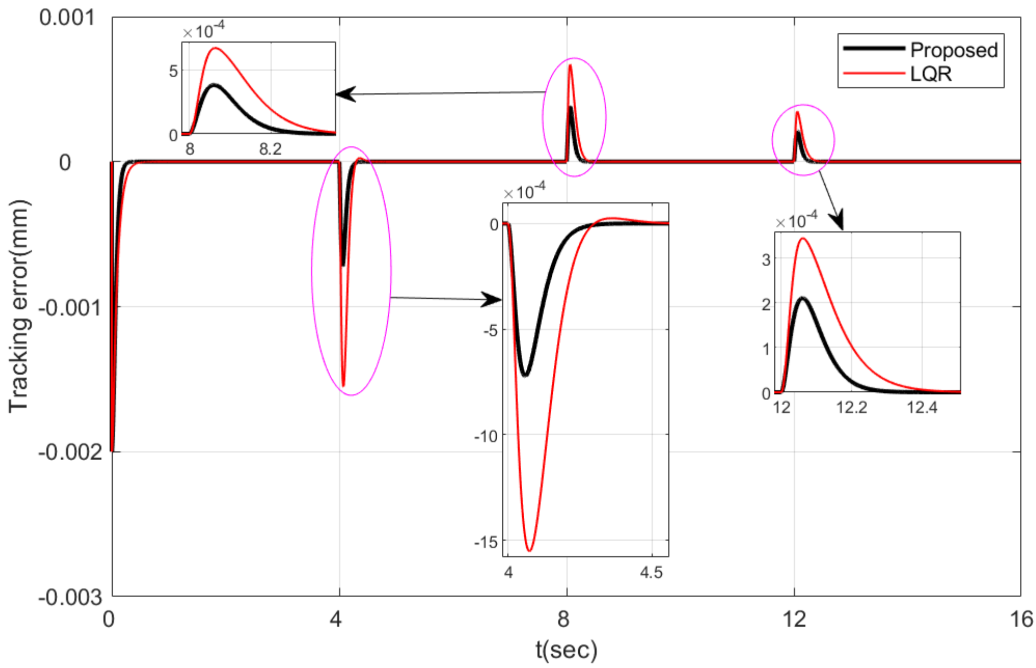

Figure 5.23 Tracking error response under sudden increment and drop in the train mass

According to zoom portions of Figure 5.23 above, the maximum tracking error of the BSC and LQR control schemes in the case of the first load change of 40% increment in the train's mass is -0.00072mm and -0.0015mm, respectively. The BSC and LQR control algorithms has a maximum tracking error value of 0.00038mm and 0.00067mm, respectively in the case of the next load variation of 20% increment in the train mass. The maximum tracking error of the BSC and LQR control methods in the case of the last load change of 10% increment in the train mass is 0.00021mm and 0.00034mm, respectively. The maximum tracking error value of the backstepping and LQR controller are 0.00038mm and 0.00067mm, respectively.

5.4.2.2 Robustness against external disturbance

The maglev train is influenced by an external disturbance force in addition to the load variation. The train moves in an unbalanced region due to environmental disturbances such as an external disturbance force produced by wind. In this thesis work a dynamic external disturbance force is added to the proposed system in order to evaluate the anti-disturbance performance of both control algorithms.

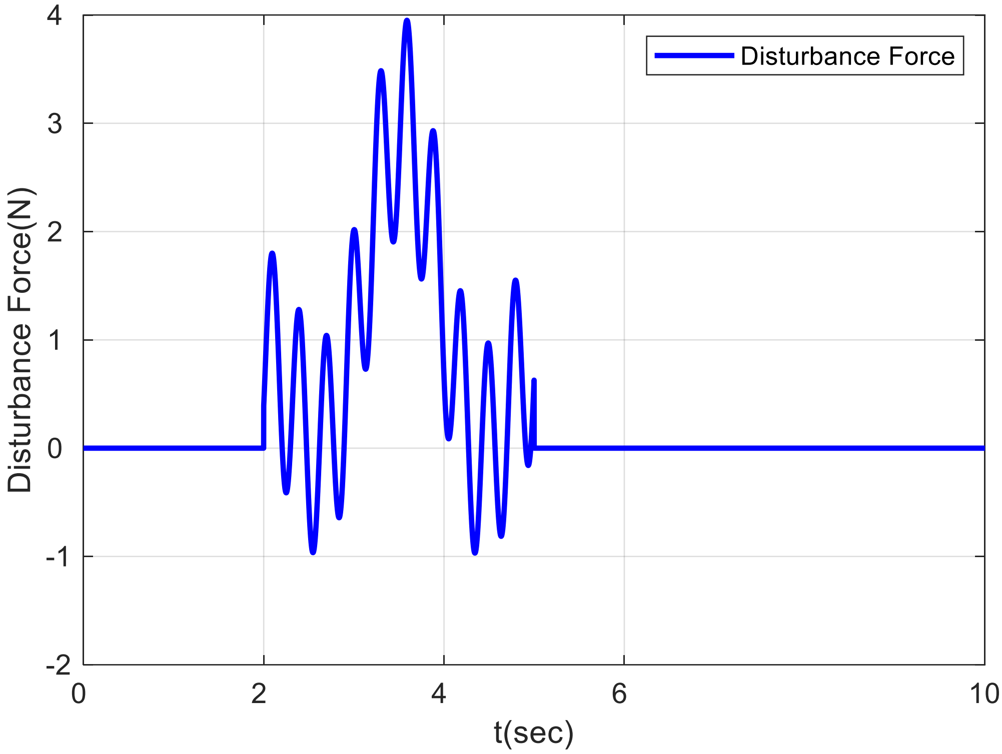

Figure 5.24 Dynamic disturbance force

The dynamic disturbance force introduced to the proposed system at a time of 2 second for a duration of 3 seconds is depicted in Figure 5.24 above. Figures 5.25 shows the tracking response of the system with both control strategies when the dynamic disturbance force discussed above is added to the system. From Figure 5.25 below depicts that both control methods keep tracking the given reference with some fluctuation due to the existence of the dynamic disturbance force. Even though the LQR has less fluctuation than that of the proposed backstepping controller, it has a delay tracking compared with the BSC, as shown in the zoom portions of Figure 5.25.

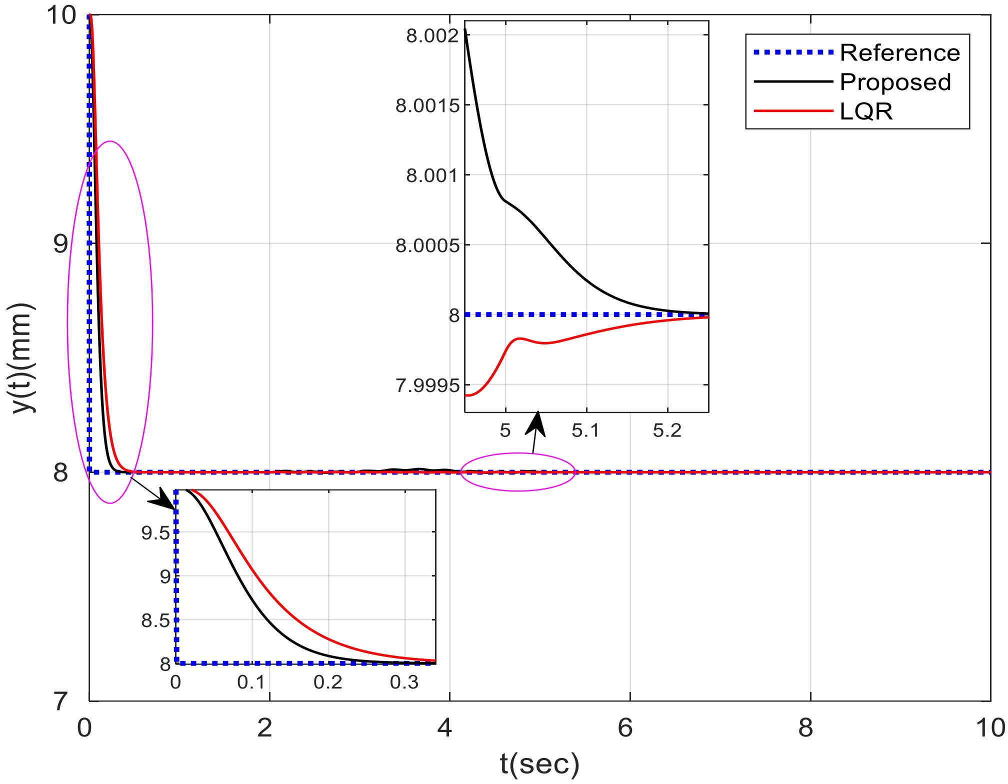

Figure 5.25 Tracking response under the effect of dynamic disturbance force

The quantitative comparison of both control algorithms under the existence of a dynamic disturbance force is shown in Table 5.10.

Table 5.10 Performance measures under the existence of a dynamic disturbance force.

Tracking controller	Performance characteristics				
	M_p	t_p	t_r	t_s	*IAEU*
Proposed BSC	0.110	2.618	0.129	0.193	0.196
LQR	0.058	4.055	0.176	0.267	0.246

Even though the BSC has large overshoot, it has lower values for the rest of performance measures as shown in Table 5.9. To be more specific, the proposed backstepping controller achieves better performance by reducing the peak time by 35.44%, the rise time by 26.7%, the settling time by 27.71% and the IAEU value by 20.32% as compared to the LQR controller. The above tabular result has verified that the proposed control method is more robust of against the dynamic external disturbance force than that of the LQR controller. Figure 5.26 depicts the tracking error response of both controller under the existence of dynamic external disturbance force.

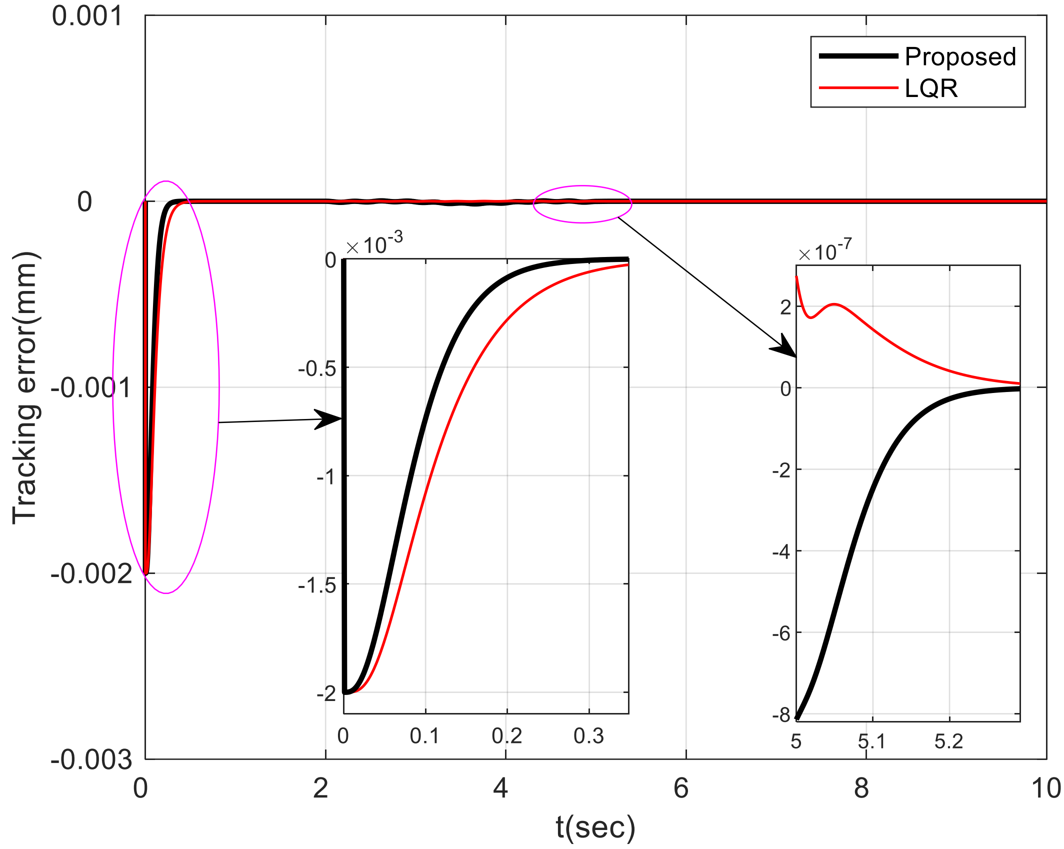

Figure 5.26 Tracking error response under the effect of dynamic disturbance force

Even though the tracking error of the BSC control strategies fluctuates more than that of the LQR controller, it re-converges to zero faster than the tracking error of the LQR controller.

5.4.2.3 Robustness against both load variations and wind disturbance

The above two preceding sections verify that the tracking performance of the proposed system is affected by both load variations and external disturbance. So, the tracking performance robustness of the proposed system using backstepping and LQR control algorithms under the existence of both dynamic external disturbance force and mass change is analyzed in this section. The time varying load variation is used here as it contains different mass changes. Figure 5.27 shows the tracking response of both controllers when the dynamic external disturbance force discussed in section 5.4.2.2 is added to the system that have a sudden increase and drop in train mass which is discussed in section 5.4.2.1 (B).

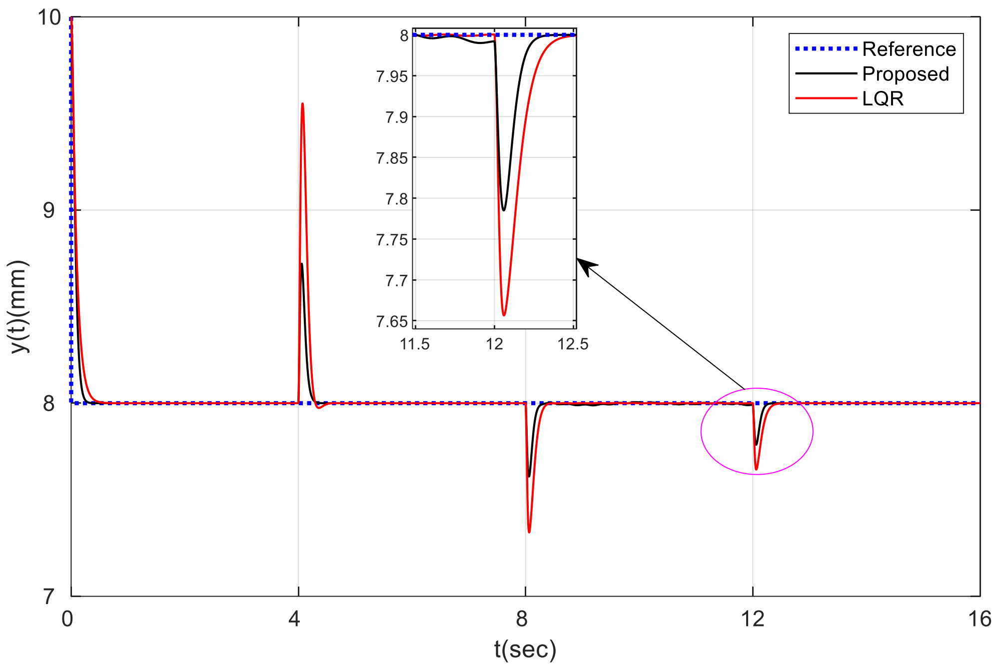

Figure 5.27 Tracking performance of both controllers with the effect of both sudden increase and drop in train mass and dynamic disturbance force

As shown in Figure 5.27 the dynamic external disturbance force is introduced at a time of 8 second for a duration of 4 seconds. The tracking performance of both controllers fluctuates due to the existence of both mass changes and a dynamic external disturbance force as depicted in the figure above. The added disturbance fluctuates the tracking performance between 7.989mm to 8.005mm and between 7.999mm to 8.001mm for the case of BSC and LQR, respectively. Even though the LQR has less fluctuation than the proposed backstepping controller, it has a delay tracking compared with the BSC, as shown in the zoom portions of Figure 5.27. The quantitative comparison of both control algorithms under the existence of both time varying load variations and a dynamic external disturbance force is shown in Table 5.10. The table depicts that the backstepping controller has lower values for peak time (t_p), rise time (t_r), overshoot (M_p), settling time (t_s), and integral absolute error and control signal (IAEU), with values of 8.059 seconds, 0.124 seconds, 18.993%, 12.129 seconds, and 0.317, respectively.

Table 5.11 Performance measures with the effect of both sudden increase and drop in train mass and dynamic disturbance force

Tracking controller	Performance characteristics				
	M_p	t_p	t_r	t_s	*IAEU*
Proposed BSC	18.993	8.059	0.124	12.129	0.317
LQR	33.471	8.062	0.187	12.201	0.558

The above tabular result has verified that the proposed control method is more robust of against both dynamic external disturbance force and load variations than that of the LQR controller. To be more specific, the proposed BSC achieves better performance by reducing the overshoot by 43.25%, the peak time by 0.037%, the rise time by 33.69%, the settling time by 0.59%, and the IAEU value by 43.19% as compared to the LQR controller. Figure 5.28 shows the tracking error response of both controller under the existence of dynamic external disturbance force and time-varying load variations.

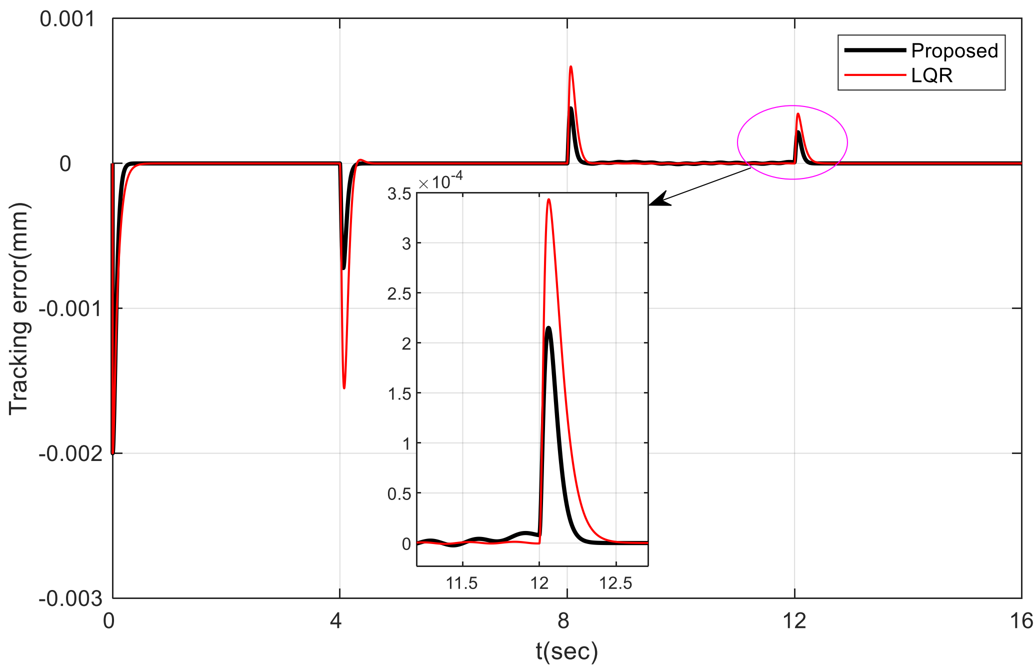

Figure 5.28 Tracking error of both controllers under the effect of both time varying load variation and dynamic disturbance force

The tracking error of both controllers fluctuates due to the existence of both time varying mass changes and the dynamic external disturbance force as depicted in Figure 5.28 above. Even though the tracking error of the proposed backstepping controller fluctuates more than that of the LQR controller, it re-converges near to zero faster than the tracking error of the LQR controller as it is clearly shown in the zoom portion of Figure 5.28. As a result, the BSC has better robustness against the existence of both time varying mass changes and the dynamic external disturbance force.

Figure 5.29 compares the tracking performance robustness of LQR and BSC controllers under the effect of time varying load variations and dynamic external disturbance force based on the value of IAEU. The graph shows that the BSC has a lower IAEU value than that of the LQR in all cases.

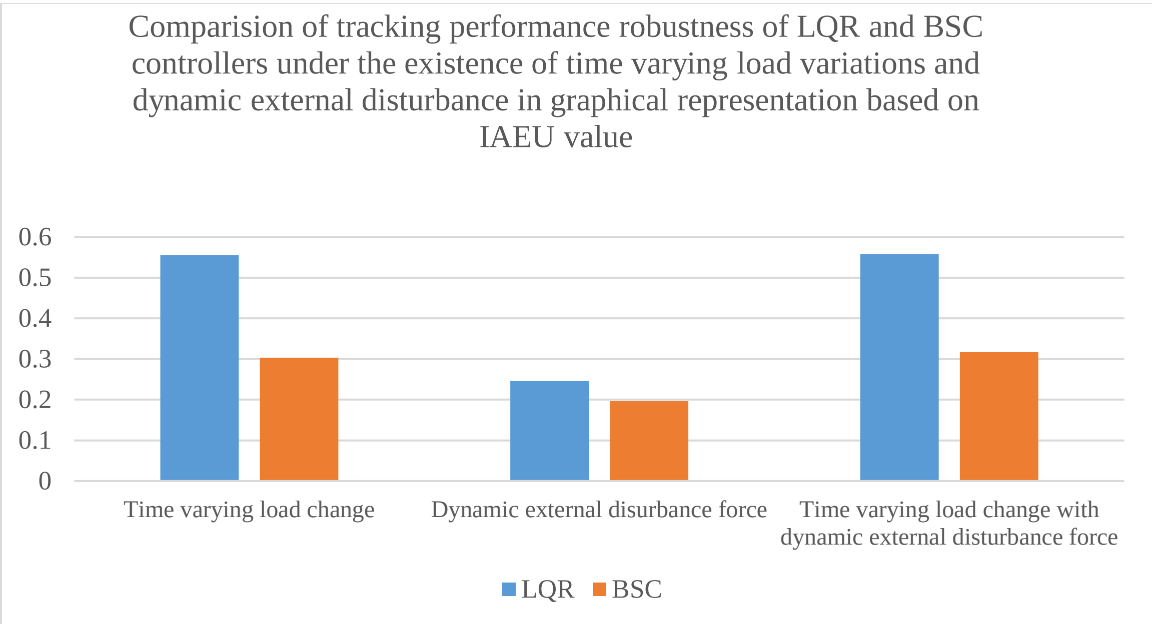

Figure 5.29 Graphical representation of tracking performance robustness of LQR and BSC controllers under the existence of time varying load variations and dynamic external disturbance based on IAEU value

CHAPTER SIX

CONCLUSION AND RECOMMENDATION

6.1 Conclusion

Hence the maglev train is nonlinear and unstable system, the backstepping controller is designed in this thesis work. First the mathematical model of the maglev train is derived. Then, based on the Lyapunov function, the backstepping control scheme is designed for the tracking control of the maglev train. The particle swarm optimization technique is used to obtain the optimal value of the designed backstepping controller parameters. In addition, to compare the performance of the proposed BSC method, the LQR controller incorporating with the integral action is designed. The Taylor series expansion method is used to obtain the linearized model of the system which is required to design this controller. The integral action is added to the LQR controller to ensure tracking. The comparison was done by evaluating the tracking capability of both controllers using different references and by testing the tracking performance robustness under the effect of mass change and external dynamic disturbance force. The proposed performance index (IAEU) and the transient performance characteristics namely, overshoot, peak time, settling time, and rise time are used to compare the tracking performance.

For the tracking capability test using different references, the proposed BSC has lower values of settling time, rise time, peak time, and IAEU value in the case of all references used in this research work, which verifies that the proposed backstepping control scheme has better tracking performance ability.

In this thesis work, the tracking performance robustness against the load change is tested up to 40% increment of the train mass. It also evaluates the robustness against time varying load changes that contains different load change increment of the train mass. The proposed controller outperformed the LQR controller.

A dynamic external disturbance force is also used in this thesis work in order to test the tracking performance robustness of both controllers under the effect of this disturbance. In the tracking performance robustness against this disturbance force, the BSC has got more fluctuation than that of the LQR controller. Even though the proposed control strategy fluctuates more than the LQR, it settles to the desired reference faster than the LQR controller.

At the end, the tracking robustness is tested when both time varying load variations and external dynamic force have effect on the system at the same time. The BSC achieves better performance by reducing the overshoot by 43.25%, the peak time by 0.037%, the rise time by 33.69%, the settling time by 0.59%, and the IAEU value by 43.19% as compared to the LQR controller.

Generally, it can be concluded from the overall simulation results of this research work that the BSC controller provides better tracking performance and has better ability to handle the effects of load variations and external disturbance force.

6.2 Recommendation

The maglev train needs to be stable and able to track any reference signal under the effect of parameter uncertainty of mass variation and sudden external disturbance force. So, this research work can be further improved by using an adaptive backstepping control strategy that can provides the best solution during the existence of wide range of time varying load and sudden disturbance force.

In addition, this research work is done only in MATLAB simulation software to validate the tracking performance of the proposed controller on the system. So, it is recommended to implement the hardware of the proposed system in CTVE (Center of Excellence for Transport and Vehicle Engineering) in ASTU in order to check the exact validation of the proposed controller with enough time and sufficient resources.

Research fund Acknowledgment

This research thesis was funded by Adama Science and Technology University under the grant number **ASTU/SM-R/540/22**, Adama, Ethiopia.

REFERENCES

Adil, H. M. M., Ahmed, S., & Ahmad, I. (2020). Control of MagLev System Using Supertwisting and Integral Backstepping Sliding Mode Algorithm. IEEE Access, 8, 51352–51362. https://doi.org/10.1109/ACCESS.2020.2980687

Ahmad, Z., Umar, M., Shaukat, S., Hassan, S., & Lupin, S. (2020). Design and Performance Enhancement of a Single Axis Magnetic Levitation System Using Fuzzy Supervised PID. Proceedings of the 2020 IEEE Conference of Russian Young Researchers in Electrical and Electronic Engineering, EIConRus 2020, 2340–2345.https://doi.org/10.1109/EIConRus49466.2020.9039153

Alkurawy, L. E. J. (2019). Simulation of Robust Control of Magnetic Levitation System. Journal of Engineering and Applied Sciences, 14(13), 4523–4531.https://doi.org/10.36478/jeasci.2019.4523.4531

Amadi, C. P., & Nwaoburu, A. O. (2020). Numerical Simulation of Steady-State Analysis to Predict Population Size over Time Using Linear Differential Equation Model. February, 6–11.

Aote, S. S., Raghuwanshi Principal, M. M., & Latesh Malik HOD, R. (2013). A Brief Review on Particle Swarm Optimization: Limitations & Future Directions. International Journal of Computer Science Engineering, 2(05), 2319–7323.

Awelewa, A. A., Popoola, O., & Ademola, A. (2019). Nonlinear dynamic simulation of a magnetic levitation system using MATLAB/Simulink. International Journal of Engineering Research and Technology, 12(12), 2143–2158.

Bai, R., Tong, S., & Karimi, H. R. (2013). Modeling and backstepping control of the electronic throttle system. Mathematical Problems in Engineering, 2013. https://doi.org/10.1155/2013/871674

Banerjee, S., Mukherjee, R., Mukheriee, M., Sengupta, S., & Pandey, S. (2019). Operating Frequency Enhancement of Magnetic levitation system using fractional order PIλDμ Controller: Design and Tuning. 2019 IEEE International Conference on Distributed Computing, VLSI, Electrical Circuits and Robotics, DISCOVER 2019 - Proceedings. https://doi.org/10.1109/DISCOVER47552.2019.9008060

Basri, M. A. M., Abidin, M. S. Z., & Subha, N. A. M. (2018). Simulation of Backstepping-based Nonlinear Control for Quadrotor Helicopter. Applications of Modelling and Simulation, 2, 34–40.

Chen, J., Omidvar, M. N., Azad, M., & Yao, X. (2017). Knowledge-based particle swarm optimization for PID controller tuning. 2017 IEEE Congress on Evolutionary Computation, CEC 2017 - Proceedings, 1819–1826.https://doi.org/10.1109/CEC.2017.7969522

Dai, G., Sun, Y., Dong, D., & Qiang, H. (2015). Nonlinear Control for Electromagnetic Suspension Systems on Elastic Guideway. Mathematical Modelling of Engineering Problems, 2(4), 7–12. https://doi.org/10.18280/mmep.020402

Dalwadi, N., Deb, D., & Muyeen, S. M. (2021). A reference model assisted adaptive control structure for maglev transportation system. Electronics (Switzerland), 10(3), 1–16. https://doi.org/10.3390/electronics10030332

Dey, S., Dey, J., & Banerjee, S. (2020). Optimization Algorithm Based PID Controller Design for a Magnetic Levitation System. 2020 IEEE Calcutta Conference, CALCON 2020 - Proceedings, 258–262. https://doi.org/10.1109/CALCON49167.2020.9106522

Diran Basmadjian. (2003). Mathematical Modeling of Physical Systems. January, 1–19. https://doi.org/10.9790/1676-09325764

Durand, S., Boisseau, B., Martinez-Molina, J. J., Marchand, N., & Raharijaona, T. (2014). Event-based LQR with integral action. 19th IEEE International Conference on Emerging Technologies and Factory Automation, ETFA 2014, 1. https://doi.org/10.1109/ETFA.2014.7005067

Fernandes, G., Junior, B., Augusto, J., & Barreiros, L. (2013). PID Control Design for a Maglev Train System. 389, 425–429. https://doi.org/10.4028/www.scientific.net/AMM.389. 425

Fernaza, O. (2014). Study of Linear Quadratic Regulator (LQR) Control Method and Its Application to Automatic Voltage Regulator (AVR) System. 5(10), 50–58.

Gad, A. G. (2022). Particle Swarm Optimization Algorithm and Its Applications: A Systematic Review. In Archives of Computational Methods in Engineering (Issue 0123456789). Springer Netherlands. https://doi.org/10.1007/s11831-021-09694-4

Ghaffar, A. A., & Richardson, T. (2015). Model Reference Adaptive Control and LQR

Control for Quadrotor with Parametric Uncertainties. 9(2), 244–250.

He, Y., Ma, W. J., & Zhang, J. P. (2016). The Parameters Selection of PSO Algorithm influencing On performance of Fault Diagnosis. MATEC Web of Conferences, 63(2016), 02019. https://doi.org/10.1051/matecconf/20166302019

Herrera, M., Leica, P., Chavez, D., & Camacho, O. (2017). A blended sliding mode control with linear quadratic integral control based on reduced order model for a VTOL system. ICINCO 2017 - Proceedings of the 14th International Conference on Informatics in Control, Automation and Robotics, 1(Icinco), 606–612. https://doi.org/10.5220/0006429606060612

Huang, S., Tian, N., Wang, Y., & Ji, Z. (2016). Particle swarm optimization using multi-information characteristics of all personal-best information. SpringerPlus, 5(1). https://doi.org/10.1186/s40064-016-3244-8

Imran, M., Hashim, R., & Khalid, N. E. A. (2013). An overview of particle swarm optimization variants. Procedia Engineering, 53(1), 491–496. https://doi.org/10.1016/j.proeng.2013.02.063

J.Jebakumar, K.Mishra, & B.MISHRA. (2014). Controller Selection and Sensitivity Check on the Basic of Performance Index Calculation. International Journal of Electrical, Electronics and Data Communication, 2(1), 91–93.

J, J., T, S., & Babu T, H. (2014). Analysis of Modelling Methods of Quadruple Tank System. International Journal of Advanced Research in Electrical, Electronics and Instrumentation Engineering, 03(08), 11552–11565. https://doi.org/10.15662/ijareeie.2014.0308070

Jackreece, P. C. (2018). Lyapunov - Krasovskii stability analysis of nonlinear integro - differential equation. 7(2), 53–55. https://doi.org/10.14419/ijamr.v7i2.

Jibril, M., Tadese, E. A., Tadese, M., Dawa, D., & Dawa, D. (2020). Comparison of Neural Network Based Controllers for Nonlinear EMS Magnetic Levitation Train. Control Theory and Informatics, 10, 13–18. https://doi.org/10.7176/cti/10-02

Khan, M. K. A. A., Manzoor, S., Marais, H., Aramugam, K., Elamvazuthi, I., & Parasuraman, S. (2018). PID Controller design for a Magnetic Levitation system. 2018 IEEE 4th International Symposium in Robotics and Manufacturing Automation, ROMA 2018, 3. https://doi.org/10.1109/ROMA46407.2018.8986710

Kim, M., Jeong, J. H., Lim, J., Kim, C. H., & Won, M. (2017). Design and control of levitation and guidance systems for a semi-high-speed maglev train. Journal of Electrical Engineering and Technology, 12(1), 117–125. https://doi.org/10.5370/JEET.2017.12.1.117

Kumar Tandan, G., Sen, P. K., Sahu, G., Sharma, R., & Bohidar, S. (2015). A Review on Development and Analysis of Maglev Train. International Journal of Research in Advent Technology, 3(12), 2321–9637. www.ijrat.org

Leng, P., Li, Y., Zhou, D., Li, J., & Zhou, S. (2019). Decoupling Control of Maglev Train Based on Feedback Linearization. IEEE Access, 7, 130352–130362. https://doi.org/10.1109/ACCESS.2019.2940053

Leng, P., Yu, P., Gao, M., Li, J., & Li, Y. (2019). Optimal control scheme of maglev train based on the disturbance observer. Chinese Control Conference, CCC, 2019-July, 1935–1940. https://doi.org/10.23919/ChiCC.2019.8866319

Li, X.-L., Serra, R., & Olivier, J. (2019). Effects of Particle Swarm Optimization Algorithm Parameters for Structural Dynamic Monitoring of Cantilever Beam. Surveillance, Vishno and AVE Conferences, 1–7. https://www.semanticscholar.org/paper/Effects-of-Particle-Swarm-Optimization-Algorithm-of-Xiao-lin-Serra/0d7a6c8cd6467e6182299e9ad7bcf567d715b054#paper-header

Liu, Z., Stichel, S., & Berg, M. (2022). Overview of Technology and Development of Maglev and Hyperloop Systems (Vol. 1, Issue 60).

Ma, D., Song, M., Yu, P., & Li, J. (2020). Research of rbf-pid control in maglev system. Symmetry, 12(11), 1–15. https://doi.org/10.3390/sym12111780

Malkapure, H. G., & Chidambaram, M. (2014). Comparison of two methods of incorporating an integral action in linear quadratic regulator. In IFAC Proceedings Volumes (IFAC-PapersOnline) (Vol. 3, Issue PART 1). IFAC. https://doi.org/10.3182/20140313-3-IN-3024.00105

Martínez-Ledesma, M., & Jaramillo Montoya, F. (2020). Performance evaluation of the particle swarm optimization algorithm to unambiguously estimate plasma parameters from incoherent scatter radar signals. Earth, Planets and Space, 72(1).

https://doi.org/10.1186/s40623-020-01297-w

Meigoli, V., & Nikravesh, S. K. Y. (2012). Stability analysis of nonlinear systems using higher order derivatives of Lyapunov function candidates. Systems and Control Letters, 61(10), 973–979. https://doi.org/10.1016/j.sysconle.2012.07.005

Mughees, A., & Mohsin, S. A. (2020). Design and Control of Magnetic Levitation System by Optimizing Fractional Order PID Controller Using Ant Colony Optimization Algorithm. IEEE Access, 8, 116704–116723. https://doi.org/10.1109/ACCESS.2020.3004025

Nakisa, B., Nazri, M. Z. A., Rastgoo, M. N., & Abdullah, S. (2014). A survey: Particle swarm optimization based algorithms to solve premature convergence problem. Journal of Computer Science, 10(10), 1758–1765. https://doi.org/10.3844/jcssp.2014.1758.1765

Nayak, A. (2015). System Department of Electrical Engineering Dedicated to my family and my friends.

Nicaise, S. (2003). Stability and Controllability of. Mathematica, 60(0), 51–60. https://doi.org/10.9734/ARJOM/2020/v16i230175

Nimrad, A. R., Dhangar, N. Y., Naik, G. L., & Madhavi, R. H. (2015). Maglev Monorail. 22, 109–113.

Pandey, T., & Yadav, S. (2020). Optimal control design for trajectory control of magnetic levitation system using jaya algorithm. 2020 IEEE Students' Conference on Engineering and Systems, SCES 2020. https://doi.org/10.1109/SCES50439.2020.9236772

Piotrowski, A. P., Napiorkowski, J. J., & Piotrowska, A. E. (2020). Population size in Particle Swarm Optimization. Swarm and Evolutionary Computation, 58(March 2019), 100718. https://doi.org/10.1016/j.swevo.2020.100718

Prasad, L. B., Tyagi, B., & Gupta, H. O. (2014). Optimal control of nonlinear inverted pendulum system using PID controller and LQR: Performance analysis without and with disturbance input. International Journal of Automation and Computing, 11(6), 661–670. https://doi.org/10.1007/s11633-014-0818-1

Prasad, N., Jain, S., & Gupta, S. (2019). Electrical Components of Maglev Systems:

Emerging Trends. Urban Rail Transit, 5(2), 67–79. https://doi.org/10.1007/s40864-019-0104-1

Raj, R., Swain, S. K., & Mishra, S. K. (2019). Optimal Control for Magnetic Levitation System Using H-J-B Equation Based LQR. 2nd International Conference on Energy, Power and Environment: Towards Smart Technology, ICEPE 2018, 1–6. https://doi.org/10.1109/EPETSG.2018.8658765

Reddy, R. Lakshman Kumar and Marutheeswar, G. V. (2013). Different Controlling Methods And PID Controller Design For Magnetic Levitation System. Nternational Journal of Advanced Research in E Lectrical, Electronics and Instrumentation Engineering, Vol 2(12), 6210–6217.

Sadaqat, E., Rehman, U., Junaid, E. M., Obaid, E., & Rehman, U. (2015). Linear Quadratic Regulator controller for Magnetic Levitation System. January 2019.

Sahu, A., Panigrahi, S. K., & Pattnaik, S. (2012). Fast Convergence Particle Swarm Optimization for Functions Optimization. Procedia Technology, 4, 319–324. https://doi.org/10.1016/j.protcy.2012.05.048

Santhiya, M., & Kishore, S. (2020). Design of Neuro PID Controller and State Feedback Controller for Magnetic Levitation System. Proceedings of the 2020 IEEE International Conference on Communication and Signal Processing, ICCSP 2020, 996–1001. https://doi.org/10.1109/ICCSP48568.2020.9182057

Shabir, S. (2016). A Comparative Study of Genetic Algorithm and the Particle Swarm Optimization. 9(2), 215–223.

Sharma, D., Shukla, S. B., & Ghosal, S. K. (2018). Modelling and state estimation for control of magnetic levitation system via a state feedback based full order observer approach. IOP Conference Series: Materials Science and Engineering, 377(1).https:// doi.org/10. 1088/1757-899X/377/1/012156

Shu'aibu, D. ., Rabiu, H., & Shehu, N. (2017). Efficient fuzzy logic controller for magnetic levitation systems. Nigerian Journal of Technological Development, 13(2), 50. https://doi.org/10.4314/njtd.v13i2.2

Singh, B. K., & Kumar, A. (2018). Backstepping Approach based Controller Design for Magnetic Levitation System. 2018 5th IEEE Uttar Pradesh Section International

Conference on Electrical, Electronics and Computer Engineering, UPCON 2018, 1–6. https://doi.org/10.1109/UPCON.2018.8596885

Suebsomran, A. (2014). Optimal control of electromagnetic suspension EMS system. Open Automation and Control Systems Journal, 6(1), 1–8.https://doi.org/10.2174/187444430 1406010001

Sun, Y., Wang, S., Lu, Y., & Xu, J. (2021). Gaussian process dynamic modeling and backstepping sliding mode control for magnetic levitation system of maglev train. Journal of Theoretical and Applied Mechanics, 49–62. https://doi.org/10.15632/jtam-pl/143676

T. Rasheed, L., & K. Hamzah, M. (2021). Design of an Optimal Backstepping Controller for Nonlinear System under Disturbance. Engineering and Technology Journal, 39(3A), 465–476. https://doi.org/10.30684/etj.v39i3a.1801

Talukdar, R. P., & Talukdar, S. (2016). Dynamic Analysis of High Speed Maglev Vehicle-guideway System Using SIMULINK. Procedia Engineering, 144, 1094–1101. https://doi.org/10.1016/j.proeng.2016.05.069

Tambe, A. T. (2018). Introduction & Overview of Magnetic Levitation (MAGLEV) Train System. 3(2), 703–708.

Teja, K. Y., Narayana, K. M. L., & Sharon, G. M. (2021). Maglev Trains : An Application of Magnetic Levitation. 4(12), 103–109.

Thornton, R. (2006). Linear synchronous motors for Maglev. Fedral Rail Road Administration, 54(9), 168–173.

Tsai, H. H., Fuh, C. C., Ho, J. R., & Lin, C. K. (2021). Design of optimal controllers for unknown dynamic systems through the nelder–mead simplex method. Mathematics, 9(16), 1–14. https://doi.org/10.3390/math9162013

Varshney, A., & Bhushan, B. (2020). Trajectory Tracking and Ball Position Control of Magnetic Levitation System using Swarm Intelligence Technique. Proceedings of the International Conference on Electronics and Sustainable Communication Systems, ICESC 2020, Icesc, 29–35. https://doi.org/10.1109/ICESC48915.2020.9155772

Wang, D., Meng, F., & Meng, S. (2020). Linearization Method of Nonlinear Magnetic Levitation System. Mathematical Problems in Engineering, 2020(1).

https://doi.org/10.1155/2020/9873651

Wang, D., Tan, D., & Liu, L. (2018). Particle swarm optimization algorithm: an overview. Soft Computing, 22(2), 387–408. https://doi.org/10.1007/s00500-016-2474-6

Xu, J., Chen, C., Gao, D., Luo, S., & Qian, Q. (2017). Nonlinear dynamic analysis on maglev train system with flexible guideway and double time-delay feedback control. Journal of Vibroengineering, 19(8), 6346–6362. https://doi.org/10.21595/jve.2017.18970

Xu, J., Sun, Y., Gao, D., Ma, W., Luo, S., & Qian, Q. (2018). Dynamic Modeling and Adaptive Sliding Mode Control for a Maglev Train System Based on a Magnetic Flux Observer. IEEE Access, 6(c), 31571–31579. https://doi.org/10.1109/ACCESS.2018.2836348

YAVUZ, M. N., & ÖZTÜRK, Z. (2021). Comparison of conventional high speed railway, maglev and hyperloop transportation systems. International Advanced Researches and Engineering Journal, 5(1), 113–122. https://doi.org/10.35860/iarej.795779

Zhao, S., Liu, Y., Long, Z., Wang, S., Xu, M., & Xie, X. (2019). Research on Control System of Maglev Train Based on Fuzzy PID. Proceedings - 2019 Chinese Automation Congress, CAC 2019, 4422–4427. https://doi.org/10.1109/CAC48633.2019.8996477

Zhou, W., & Liu, B. (2013). Backstepping Based Adaptive Control of Magnetic Levitation System. 1, 435–438. https://doi.org/10.2991/icsem.2013.83

Zhou, X., Wang, P., & Long, Z. (2020). Parameters Optimization for suspension system of maglev train via improved PSO. Proceedings - 2020 Chinese Automation Congress, CAC 2020, 2197–2202. https://doi.org/10.1109/CAC51589.2020.9327899

APPENDICES

APPENDIX A

A.1 MATLAB code for open loop response of the nonlinear model

```
function nonlinear open loop
global a g R k
a= 2.1807e-6; g= 9.81; R= 1.2; k= 3.053e-3;loop=20000; h=0.0001;t=0;
x10= 10/1000;  x20= 0; x30= x10*sqrt(g/a); u0= R*x30;
x0= [x10;x20;x30];x=x0;
buf= [t x' 1];
for i= 1:loop
   u=1;
   x= RK4(@plant,t,x,u,h);
   t= t+h;
   buf= [buf;t x' u];
end
t= buf(:,1); y= buf(:,2);
plot(t,y,'k','linewidth',2);
xlabel('t(sec)'),ylabel('y(mm)')
axis([0 2 0 20])
title ('Open-loop response of the nonlinear model')
function xdot= plant(t,x,u)
global a g R k
xdot= zeros(3,1);
xdot(1)= x(2);
xdot(2)= -a*(x(3)/x(1))^2+g;
xdot(3)= x(3)*x(2)/x(1)-R*x(3)*x(1)/k+u*x(1)/k;
```

A.2 MATLAB code for open loop response of the linearized model

```
function linearized open loop
global a g R k a21 a23 a31 a32 a33
```

```
a= 2.1807e-6; g= 9.81; R= 1.2; k= 3.053e-3;loop=20000; h=0.0001;t=0;
x10= 10/1000;  x20= 0; x30= x10*sqrt(g/a); u0= R*x30;
x0= [x10;x20;x30];x=x0;
a21= 2*a*x30^2/x10^3;a23= -2*a*x30/x10^2;a31= -x20*x30/x10^2-R*x30/k+u0/k;
a32= x30/x10;a33= x20/x10-R*x10/k;buf= [t x' 1];
for i= 1:loop
    u=1;
    x= RK4(@plant,t,x,u,h);
    t= t+h;
    buf= [buf;t x' u];
end
t= buf(:,1); y= buf(:,2);
plot(t,y,'k','linewidth',2);
xlabel('t(sec)'),ylabel('y(mm)')
title ('Open-loop response of the linearized model')
function xdot= plant(t,x,u)
global a21 a23 a31 a32 a33
xdot= zeros(3,1);
xdot(1)= x(2);
xdot(2)= a21*x(1)+a23*x(3);
xdot(3)= a31*x(1)+a32*x(2)+a33*x(3);
```

A.3 MATLAB code for obtaining the root locus

```
a= 2.1807e-6; g= 9.81; R= 1.2; k= 3.053e-3;
x10= 10/1000;  x20= 0; x30= x10*sqrt(g/a); u0= R*x30;
x0= [x10;x20;x30];x=x0;
a21= 2*a*x30^2/x10^3;a23= -2*a*x30/x10^2;
a31= -x20*x30/x10^2-R*x30/k+u0/k; a32= x30/x10;
a33= x20/x10-R*x10/k;
A= [0 1 0; a21 0 a23; a31 a32 a33];
B= [0; 0; x10/k];C=[1 0 0];D=0;
rlocus(A,B,C,D)
```

APPENDIX B

B.1 MATLAB code for proposed control system

```
function BS
global a g R k m
a= 2.1807e-6; g= 9.81; R= 1.2; k= 3.053e-3; m= 700;
k1=33.5416;k2=   33.6734  ;k3= 31.1596;
x10= 10/1000; x20= 0; x30= x10*sqrt(g/a);
yr= 10/1000;
t= 0; x= [x10;x20;x30]; u0= R*x30; h= 0.001; loop= 2000;
buf= [t x' u0 yr 0];
for i=1:loop
   yr= 12/1000;
   yrd= 0; yrdd= 0; yrddd= 0;
   e1= yr-x(1);
   e2= x(2)-yrd-k1*e1;
   e1d= -e2-k1*e1;
   w1= k1*e1+yrd;
   q= (1/a)*(g-yrdd+e2*(k1+k2)-e1*(1-k1^2));
   w2= (yr-e1)*sqrt(q);
   e3= x(3)-w2;
   e2d= (-a/(yr-e1)^2)*(e3^2+2*e3*((yr-e1)*(sqrt(q)))+((yr-e1)^2)*q)+g-
yrdd+k1*(e2+k1*e1);
   w2d= (yrd-e1d)*sqrt(q)+((1/(2*a*sqrt(q)))*(-yrddd+e2d*(k1+k2)-e1d*(1-k1^2))*(yr-
e1));
   u1= w2d-k3*e3+(((a*e2)/(yr-e1)^2)*(e3+2*(yr-e1)*(sqrt(q))))-
(((e2+yrd+k1*e1)*(e3+(yr-e1)*(sqrt(q))))/(yr-e1));
   u= u1*(k/(yr-e1))+R*(e3+(yr-e1)*(sqrt(q)));
   % Calls the plant system
   x= RK4(@plant, t, x, u, h);
   t= t+h;
   buf= [buf;t x' u yr e1];
end
```

```
y=buf(:,2)*1000;t=buf(:,1);
plot(buf(:,1),buf(:,2)*1000,'b','linewidth',2);
plot(buf(:,1),buf(:,6)*1000,':r','linewidth',1);
axis([0 h*loop 10 13]) %up
function xdot= plant(t,x,u)
global a g R k
xdot= zeros(3,1);
xdot(1)= x(2);
xdot(2)= -a*(x(3)/x(1))^2+g;
xdot(3)= x(3)*x(2)/x(1)-R*(x(3)*x(1))/k+u*x(1)/k;
```

B.2 MATLAB code for LQR controller

```
function SimLQR
global a g R k m
a= 2.1807e-6;
g= 9.81; R= 1.2; k= 3.053e-3;m=700;
t= 0; h= 0.001; loop= 2000;  yr= 12/1000; ee= 0; z= 0;
x10= 10/1000;  x20= 0; x30= x10*sqrt(g/a); u0= R*x30;
x0= [x10;x20;x30]; x= x0;
a21= 2*a*x30^2/x10^3;
a23= -2*a*x30/x10^2;
a31= -x20*x30/x10^2-R*x30/k+u0/k;
a32= x30/x10;
a33= x20/x10-R*x10/k;
A= [0 1 0 0; a21 0 a23 0; a31 a32 a33 0;1 0 0 0];
B= [0; 0; x10/k;0];
Qm= diag([0.1 0.1 0.1 8e+7]);  Rm= 0.0001;
K= lqr(A,B,Qm,Rm);
buf= [t x' u0 yr 0];
for i= 1:loop
   e= yr-x(1);
   z= z+0.5*h*(e+ee);
   ee= e;
```

```
    u= u0-K(1:3)*(x-x0)+K(4)*z;
    t= t+h;
    buf= [buf;t x' u yr e];
end
t= buf(:,1); y= buf(:,2)*1000;
plot(t,y,'k','linewidth',2);
xlabel('t(sec)'),ylabel('Setpoint & Output')
axis([0 h*loop 9 13])
plot(buf(:,1),buf(:,5),'k','linewidth',2);
xlabel('t(sec)'),ylabel('Control input')
axis([0 h*loop 0 35])
function xdot= plant(t,x,u)
global a g R k
xdot= zeros(3,1);
xdot(1)= x(2);
xdot(2)= -a*(x(3)/x(1))^2+g;
xdot(3)= x(3)*x(2)/x(1)-R*x(3)*x(1)/k+u*x(1)/k;
```

B.3 MATLAB code for the PSO algorithm

```
function TuneMaglevBS
options = optimoptions('particleswarm');
options.PlotFcn= 'pswplotbestf';
options.InertiaRange= [0.2,0.9];
options.SelfAdjustmentWeight=2;
options.SocialAdjustmentWeight=2;
options.MaxIterations= 30;
options.SwarmSize= 20;
nvar= 3;
LB= [0.0001 0.0001 0.0001];
UB= [38 75 75];
[x,fval]= particleswarm(@EvalObj,nvar,LB,UB,options)
```